Microfluidic Platforms for Chemical and Electrical Signaling in Whole Retina Tissue

By

Kirsten Heikkinen Dodson

Dissertation

Submitted to the Faculty of the

Graduate School of Vanderbilt University

in partial fulfillment of the requirements

for the degree of

DOCTOR OF PHILOSOPHY

in

Mechanical Engineering

August, 2016

Nashville, Tennessee

Approved:

Deyu Li, Ph.D.

Rebecca M. Sappington, Ph.D.

Haoxiang Luo, Ph.D.

Yaqiong Xu, Ph.D.

Leon Bellan, Ph.D.

This dissertation is dedicated to my family and friends who have been with me through everything I have accomplished.  To my husband Stephen, who has loved me and encouraged me through this roller coaster of an experience.  To my parents Daven and Bonnie, who encouraged me and taught me so many things throughout this life for which I am forever grateful.  To my grandparents Bill and Barbara, who have always supported me and given me countless wonderful opportunities in this life.  To my brother Greg, his wife Megan, and my niece Addison, who have brought me so much joy in the best ways.  To the rest of my family and friends, who have consistently stood with me through difficult times and helped me over every obstacle.  Without each and every one of them, I would not be the woman I am today.  Thank you for your encouragement and love throughout my life.

# ACKNOWLEDGEMENTS

TABLE OF CONTENTS

LIST OF FIGURES

CHAPTER 1

**INTRODUCTION**

**1.1 Background**

Over the past two decades, the field of microfluidics has developed into an attractive option for cell and tissue culture by greatly reducing costs while opening doors of opportunity for many interesting biological assays that were not feasible previously[1–4]. In contrast to traditional culture techniques, the small channels and chambers in microfluidic devices provide a cost-effective approach for cell culture by using less media and fewer cells. More importantly, the capability of precise spatiotemporal control of cell microenvironments enables new assays to probe the physiological and pathological behavior of cells and tissues[4–6]. The ability to design devices to fit a broad range of needs provides opportunities for biologists to study phenomena in environments that cannot be achieved in a traditional petri dish. A wide variety of platforms have been designed to facilitate these needs in cell cultures, and more recently, some progress has been made to extend microfluidic culture to tissues or even organs[6–8]. The term tissue culture may be applied to two types of research, the formation of tissue from basic cell types, also known as tissue engineering, or the study of existing tissue via various interrogation methods. For studying tissue, the integration of advanced sensing technologies with microfluidic culture platforms allows researchers to probe or detect phenomena within the tissue. In this chapter we survey an assortment of devices and technologies including their significance in the fields of microfluidics and biology as well as their importance toward our own research. As the

biological research object of this dissertation, we also introduce the basic anatomy and physiology of the retina along with our motivation for studying it.

## 1.2 The retina

Some legends claim that the eyes are the windows to the soul, but in science they are considered a doorway to understanding the brain. In many ways, the retina is a better option to study brain activity rather than the brain itself. Pushed out from the brain into the eye during development, the retina is a part of the central nervous system and thus contains neurons, the cells responsible for processing and transmitting information throughout the body. Its simplicity, accessibility, unique trait of light sensitivity, and highly ordered structure have allowed researchers to delve deeper into understanding the nervous system.

*Neurons and the Nervous System*

Neurons are a specific type of cell with the base functions of receiving, processing, and sending information throughout an organism[9]. The information flow begins with sensing at a specific microenvironment and passage of the information along a pathway. This is followed by information processing in the brain that finally leads to a behavioral response. Simply put, these signaling and processing functions are the neuron's responsibility in the body. The basic structure of a neuron includes a cell body or soma, one or multiple axons, and dendrites as shown below in Figure 1.1[10].

As discussed above, neurons communicate via highly specialized cell-cell junctions called synapses, which are structurally composed of pre- and post-synaptic terminals. Dendrites receive synaptic inputs from other cells whereas axons send synaptic outputs to the next cell along the signaling chain. The two types of synaptic transmission, chemical and electrical, both require the passage of molecules from one neuron to the other but the methods are quite

different.  Chemical synaptic transmission occurs via the release and uptake of molecules at a synaptic cleft between a pre-synaptic and post-synaptic terminal.  In contrast, electrical synapses form a gap junction, a type of pore-to-pore connection between cell membranes, allowing for molecules to be freely exchanged between cells.  In more basic terms, chemical synapses pass molecules through extracellular space while electrical synapses pass molecules through intracellular space.  Note that because of this distinction, the information transfer in a chemical synapse is typically unidirectional while an electrical synapse can be bidirectional.
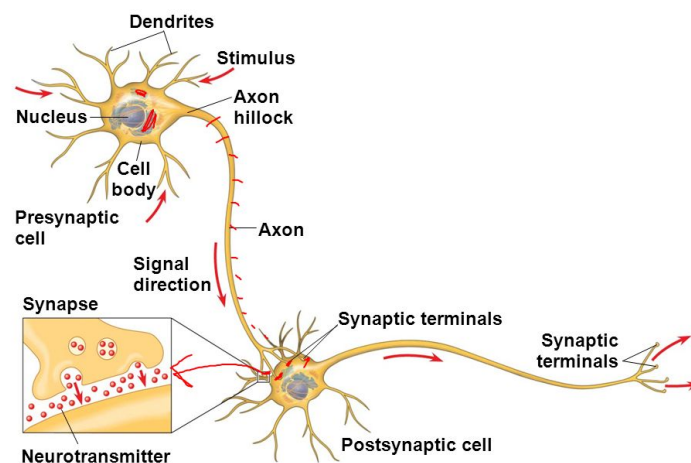
Figure 1.1 – Basic structure of a neuron[10]

Even though the two types of synaptic transmission differ in many ways, both depend on the exchange of electrically charged molecules to and from one another or the surrounding environment.  At rest, the membrane potential, or the voltage difference across the cell membrane, is typically between -40 and -90 mV for most neurons.  As cells communicate and ionic fluxes occur at the membrane, the potential changes accordingly.  If the potential is less negative due to an influx of positive ions, the neuron experiences depolarization, but if it is more negative (outflow of positive ions), the neuron undergoes hyperpolarization.  With this signaling ability, the cell membrane can be thought of as an electrical circuit containing a resistor and

capacitor, both resisting ion flow and storing charge.  When a neuron is dramatically depolarized past a certain threshold, an action potential is created and sent from the cell body along the axon to a synapse with another cell.  Between different parts of the body, neurons communicate by continuing this signaling pathway via synapses.  Like every other part of the central nervous system, the retina contains neurons that pass vital information along synaptic transmissions to the brain to be processed as images.  Later, we will discuss how we were able to record extracellular signaling in whole retina tissue.

*Structure, Function, and Relation to the Brain*

Although dissimilar in structure and function, the retina and brain are both considered parts of the central nervous system partially due to their common origin in the neural tube. During early development in the embryo, retina are formed from cells called neuroblasts which later differentiate into a range of retinal cells[11].  As the single layer of neuroblasts begins to transform into other cell types, they migrate and create multiple layers at the back of the eye. How neuroblasts become certain types of retinal cells and how they migrate is still not well understood, but research has shown evidence of some order in the process.  The first cells to differentiate and migrate to their final position are ganglion cells, a type of neuron within the retina.  These retinal ganglion cells (RGCs) form a layer closest to the vitreous, a watery substance that fills the eye supporting its rounded shape.  Other cells follow this process of specification and positioning until the layers of the retina are complete and synaptic connections begin forming.  Microglia on the other hand are a type of glial cell that act as the primary immune defense in the central nervous system.  These macrophages move freely throughout the layers of the retina whereas the RGCs and other neurons are relatively immobile.  Figure 1.2 below depicts the layered cells of the retina[12].  Figure 1.3 gives a general layout of the eye

including the retina, vitreous, and optic nerve, which connects the eye to the brain as an information pathway[11]. Note that the inner limiting membrane in Figure 1.2 separates the retina from the vitreous humor in Figure 1.3.
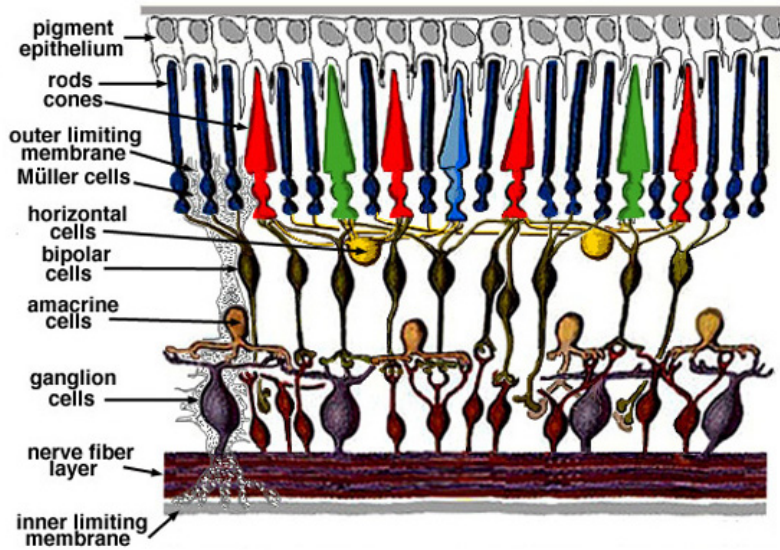


Figure 1.2 – Layers of the retina[12]
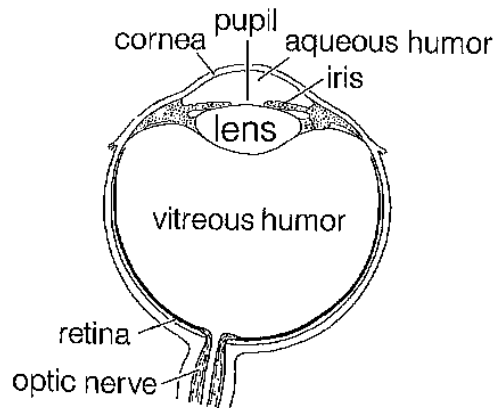


Figure 1.3 – Basic organization of an eye[11]

As discussed above, the retina is organized in layers by cell type each with its own function contributing to the overall tissue performance. The most unique trait of the retina is its

light sensitivity. This specific characteristic allows for very simple stimulation of the signaling pathway from eye to brain. Briefly, light enters the eye and passes through the transparent retina to the last layer of neurons called the photoreceptors, designated by the rods and cones in Figure 1.2. Transmission of light begins outside the eye and passes successively through the lens, vitreous humor, and inner limiting membrane to reach the retina. The rod and cone photoreceptors initiate a signaling process through the layers of the retina to the innermost layer or ganglion cell layer. The dendrites of RGCs collect signals from all layers of the retina and act as the output neurons of the eye. The information is processed in the RGC soma and sent as an action potential through RGC axons to the rest of the central nervous system via the optic nerve as depicted in Figure 1.3. From there, the brain receives the signal and processes the information into an image.

Unfortunately, signaling processes throughout the body can break down due to decay, accidents, or unknown causes. Though some pathways have the ability to rebuild themselves or fight off deterioration, others can lead to catastrophic losses. Cell death in the retina, specifically in RGCs, has been linked to loss of sight as observed in glaucoma patients. Similarly, other neurodegenerative diseases, like Alzheimer's, Parkinson's, and Huntington's, are also characterized by neuronal death. Aging is the highest risk factor for most neurodegenerative diseases though genetic predisposition also plays a role. Although we cannot prevent aging, further research into degeneration of the central nervous system could lead to preventative treatments or therapeutic advances. One devastating type of neuronal disease exhibits a phenomenon called spreading depolarization. Described as a wave of depolarization in neurons throughout the brain, spreading depolarization has been linked to severe brain trauma including ischemic stroke[13]. Beginning from a single point, one injured neuron can cause surrounding

neurons to depolarize which then progresses until a large region of neural tissue is damaged. Researchers in the field have utilized point application of noxious stimuli to study the propagation of this widespread neuronal degeneration[14–16]. While progress in the research is ongoing, it could greatly benefit from devices that can test neuronal degeneration in controlled microenvironments. In this dissertation, we discuss the design, fabrication, and experimentation of a device to study localized chemical and electrical signaling processes within the retina. By studying real-time pathological conditions at minuscule levels, we can take one step closer to better understanding these types of degeneration in the entire nervous system.

## 1.3 Microfluidic platforms for cell and tissue cultures

Cell culture is defined as the growth of cells in an artificial environment after removal from a body. This simple definition only reaches the tip of the iceberg of the actual activities that occur in real biological labs. Though keeping the cells healthy and growing over a period of time is vital for almost all experiments, cell culture goes far beyond this basic function. Although *in vitro* cell culture has existed for over one-hundred years[17], to date, most cell biologists still employ culture techniques that lack spatiotemporal resolution and control over the cellular microenvironment. Microfluidics challenges these typical culture techniques by introducing innovative methods and schemes for broader opportunities and more specialized testing.

Before the emergence of microfluidic culture techniques, most cell and tissue cultures were relegated to petri dishes or well-plates and required excessive quantities of media. Microfluidics miniaturizes the culture or examination space as microscale channels and chambers, which allows biologists to drastically reduce the number of cells used along with the amount of media vital to keep the cells healthy. In addition to cost reduction, microfluidics also

7

offers the opportunity to better control the microenvironment of the cultured cells or tissues. Biological processes in cells and tissue occur at minuscule scales, which can be controlled and probed in microfluidic devices through manipulating the media flow and with integrated sensing mechanisms. As described previously, neurons utilize synaptic transmission to pass information along a signaling pathway and although we focus on neurons and the retina in our studies, all organisms contain cells and tissues that communicate via the transfer of charged molecules. Therefore, utilizing microfluidic culture platforms with integrated electrical potential detection schemes, we can achieve a better understanding of the physiological and pathological conditions while saving time and money. In this section, we will discuss existing and emerging technologies that delve deeper into identifying and investigating various biological processes by employing microfluidic platforms in cell and tissue cultures.

*Cell Culture Platforms*

As a pioneer in the field, Whitesides recognized the importance of microfluidics in pharmaceuticals and bioanalysis while also pointing out that progress must be made in commercialization[1]. While there are companies producing microfluidic devices out of glass and plastic[2], these materials are not well-suited for low-cost biocompatible applications whereas polydimethylsiloxane (PDMS) has emerged as the preferred choice[18–20]. In this section, we focus on cell culture systems fabricated with PDMS, a low-cost, transparent, biocompatible elastomer, as the base structural component.

Although progress has been made in microfluidic culture with several excellent reviews published covering the basics of microfluidic cell culture[4,5,17,19,21,22], the opportunities for customization and advancement are still far from fully explored[1]. Miniaturization of a functional lab assay via microfluidics can drastically reduce the amount of required resources as well as

exponentially increase efficiency. As quantified by Dittrich and Manz, microfluidics allows for faster reactions and lower consumption at very high throughput in comparison to traditional laboratory techniques[23]. One type of application that has benefited greatly from this miniaturization by microfluidics is single cell culture and analysis toward drug discovery.

Single cell culture provides the advantage of studying cell behavior without averaging effects but the microfluidic techniques involved can be quite challenging. In order to culture, manipulate, or investigate a single cell, it must first be trapped or controlled within a small space. Methods for trapping a single cell in microfluidic culture generally fall into one of three categories: droplet encapsulation, fluid focusing, or optical manipulation. Droplet encapsulation provides the opportunity to not only isolate a single cell but also conduct tests on the cell within its own microenvironment. As possibly the first to employ droplet encapsulation of live cells, Martin et al. demonstrated the use of a T-channel to embed fluid segments with bacteria cells that exhibit continued growth and division[24]. Lagus and Edd later presented a review of the basic physics and fluid mechanics required for droplet creation in detail for both flow-focusing nozzles and T-junction geometries[25]. To achieve high throughput of up to 10 kHz, single cells were encapsulated into a droplet of water in oil as the carrier fluid via specialized channel geometry[25,26]. Although there is abundant interest in droplet encapsulation for enhanced analysis of single cells, the probability of capturing just one cell per droplet is imperfect, especially at high frequencies. Edd et al. has increased this probability of trapping a single cell by adjusting flow rates and order to create self-organized encapsulation[27]. While many authors have focused on individual droplet encapsulation and manipulation approaches, one group has combined the latest technologies into a fully integrated, high throughput workflow to determine viability and cytotoxicity of mammalian cells[28]. The device includes four steps in the workflow for a

complete experiment on one device: droplet coding/labeling, droplet merging, incubation, and fluorescence measurements. This 'lab-on-a-chip' device provides a great example of the applicability of the droplet encapsulation method toward pharmaceutical research.

In addition to droplet encapsulation for high-throughput single cell analysis, fluidic cell focusing has also been used to trap and investigate cells individually. This approach of single cell trapping allows for multiple experiments to be performed in succession to test viability in drug discovery studies. By utilizing channel geometry and laminar flow characteristics, cells can be captured in small compartments. Focusing the fluid flow around these compartments allows for single cells to be trapped and analyzed in the same view field. For example, drain channels on the sides of a compartment exploit the stagnation point of a T-junction to capture a single cell[29]. Another example used U-shaped PDMS pillars within a large chamber to trap single cells[30]. Empty pillars obstruct the laminar flow causing pockets of circulation that helps to capture a spherical cell and with a cell trapped, the flow characteristics favor the path of least resistance around the obstacle, leaving the cell in place for future analysis. Similarly, single cells can be trapped by laminar flow on opposite sides of a wall with an adjoining microchannel to create a co-culture between two cells[31]. Once a single cell or individual cells have been captured, minute volumes of reagents may be applied and removed in steps to probe the cell response under various conditions.

Optical manipulation such as using optical tweezers has also been successfully implemented in microfluidic devices for single cell trapping. Fiber bundles positioned as four prisms within a microfluidic device were able to capture single cells for fluorescence analysis and Raman spectroscopy[32]. Optical tweezers were also used to trap, inject, and position a single cell into a mechanical trap as shown by Hellmich et al.[33]. While single cell culture provides

10

promising opportunities for pharmaceutical testing and drug discovery, analyses at larger cell population is also needed due to the importance of cell-cell communication in physiological and pathological conditions.

The anatomy and physiology of tissue can be quite complex, and cell-cell interactions are extremely important in cell function, which cannot be readily studied with single cell analysis. Therefore, microfluidic platforms have been developed to culture populations of single or multiple cell types, which often integrate capabilities to control or manipulate the cell microenvironments in order to better understand cellular function in population. A brief survey of this very active research field is as follows with a focus on platforms using PDMS.

Although culturing and analyzing cells can be a lengthy and complicated procedure, many microfluidic platforms for single cell types are actually quite simple. One basic microfluidic device for culturing cells is a single chamber where cells are loaded and analyzed by adding reagents or imaging. Modifications with other functions integrated into the single chamber device have enabled many interesting studies. For example, a group from the University of Tokyo employed a stir bar and semi-permeable membrane within a single chamber device to monitor and culture a population of cells as a simplified model of intestinal tissue over two weeks[34]. Utilizing laminar flow characteristics has also been combined with the single chamber platform for additional control. Strategically placed pillars in a microfluidic channel were built to create a single chamber in the center of the device with media perfusion around the sides to provide nutrients to the cell culture[35]. Cells were cultured between the two lines of pillars while media flowed outside the pillars. Similarly, branched networks of microchannels generate a gradient of soluble factors by laminar flow mixing to perfuse through a cell culture allowing researchers to study chemotaxis, cell migration in response to the cue of

chemoattractants[36,37]. Many researchers expanded upon the single chamber device by including multiple cell chambers, wholly or partially connected, in a single device[38–42]. Microgrooves connecting two chambers were used to isolate axons from the cell bodies of neurons[43] or allow for co-culture of neurons and glia[44]. By adding a pressurization chamber on top of the device, the microgrooves can be pushed down to injure the axons for neuron regeneration studies[45] or allow for dynamic but isolated stimulation of two cell populations on either side of the barrier[46].

In addition to the microcompartment approach, surface patterning has also been realized for coating proteins or chemoattractants on a substrate for cell cultures/co-cultures. The device is assembled via reversible bonding, reagents are added to the microchannels to attach to the substrate, and the PDMS construct is removed to leave a pattern of molecules on the surface, to which specific cells preferentially attach. As early as 1998, Folch and Toner introduced a simple and cheap way to culture or co-culture cells via application of a protein template to a variety of substrates[47]. Just two years later, Folch et al. described the fabrication of PDMS stencils with the capability of cell co-culture on nonplanar surfaces[48]. Another advancement by Chiu et al. incorporated three-dimensional microfluidic structures for complex patterning of a substrate, i.e. nested spirals of proteins for co-cultures[49]. Similarly, an intricate pattern of cell co-culture was created by sequentially aligning arrays of PDMS microchannels for attachment within microwells[50], which has also been demonstrated to replicate basic tissue functions for drug development[51]. Note that all of the above methods result in two-dimensional cell cultures. Again, while these studies are advantageous for certain assays, real tissue is a three-dimensional (3D) environment and to better understand biological processes, 3D cell culture is preferred.

3D cell culture includes the effects of structure and organization, characteristics vital in real tissue, more closely mimicking *in vivo* conditions. A key component of 3D culture is the

extracellular matrix (ECM), essentially a natural scaffold structure for cells to grow on, migrate along, and interact with. One pioneering group employed ECM in a 3D culture to create a complex biomimetic arterial structure of cells and matrix in layers[52]. Vickerman et al. described another approach for a 3D cell culture by embedding cells into a collagen gel solution at an array of pillars to mimic native ECM[53]. Researchers have also utilized 3D cell culture to imitate tissue such as the retina[54] or the intestine[55] to better understand tissue function; however, the field is still in infancy and lacks the technology to form fully functional tissue. Taking another step forward, creating tissue from the combination of cell types readily employs the concepts of 3D cell cultures. Many groups have published a variety of 3D cell culture studies that strive toward tissue engineering for kidney[56], heart[57], breast cancer[58], lung[59], liver[60], and even efforts to mimic entire organ systems[61–67]. Overall, microfluidic cell culture provides limitless opportunities for novel biological assays through a wide variety of techniques and methods from single cell cultures to 3D cultures.

While microfluidic cell culture platforms afford prospects of discovery in the field of cell biology, restrictions remain, which prevent better understanding of the anatomy and physiology of the human body. Studying interactions between two or more cell types offer comprehension of basic behavior but little can be inferred about overall tissue function. In order to better realize the full potential of microfluidics in biological research, platforms must go beyond cell culture and move closer toward *in vivo* conditions. Two options lie ahead for *in vivo* simulation within microfluidic platforms: tissue engineering and tissue culture.

*Tissue Engineering Platforms*

Tissue engineering is broadly defined as the science of repair or regeneration of tissue through the combination of cells, proteins, and biomaterials[68]. As stated above, cell cultures

have been used to imitate tissue function, but tissue engineering surpasses basic behavior and simulates full structure and function. Tissue engineering includes a broad range of technologies and several reviews provide excellent summaries of the field[68,69]. Microfluidic platforms, with the capabilities of controlling nutrient supply and waste removal along with high spatiotemporal probing of tissue, can be an effective approach to build or organize cells into tissue or even organs[62,70]. Microfluidics for tissue engineering goes beyond simple chambers and channels to culture cells and provide nutrients. Because tissue and organs are much more complex, microfluidic platforms with sophisticated designs have been created to be physiologically relevant. Here we present a brief survey in tissue engineering using microfluidics.

One major obstacle in tissue engineering is to incorporate a network of vasculature that transports and provides nutrients throughout the tissue. Due to the small size, biocompatibility, and option for customization, microfluidics is an obvious choice for vascular tissue engineering[71]. Stroock and Fischbach presented some of the engineering and biological design considerations required for microfluidic tissue engineering specifically for tumor angiogenesis, the formation of blood vessels within tumors[72]. One example of innovative implementation of these rules is to engineer vasculature using sacrificial sugar structures to create a random 3D fluidic network within a polymeric matrix[73]. A recent review by Tien described the current microfluidic technology utilized in vasculature engineering including sacrificial approaches, bulk biomaterial, and multiplexed vessels[74]. In addition to vasculature, microfluidics can be utilized to create other structures for tissue engineering, all of which contribute to the structure and function of tissue. By stacking polyurethane replicas of an array of microchannels, Folch et al. were able to mimic a variety of bone architectures[75]. In fact, several reviews have been published detailing a long list of innovative and exciting advances in the field of tissue

engineering provided by microfluidic technologies[62,68,69,76]. While numerous developments have been made in tissue engineering, microfluidic platforms are equally important for tissue culture with capabilities for maintaining healthy tissue and allowing for investigation of biological processes within whole tissue samples.

*Tissue Culture Platforms*

Advances in the field of microfluidics have greatly improved a variety of biological assays, including tissue culture. Even though the first brain slice culture was reported over one hundred years ago in 1907[77], little has changed in basic tissue culture techniques. Since those first experiments, numerous sets of protocols were developed to better adjust nutrients in media and health of tissue cultures, but the equipment has changed very little. Many labs still use petri dishes or well-plates for cell or tissue culture, which limits their abilities for spatiotemporal control of the microenvironment. While these protocols extend the lifespan of a tissue culture[78–82], microfluidics provides additional benefits with new functions, drastic reduction in resource consumption, and the opportunity for spatiotemporal probing. Here we will briefly survey the technologies that utilize the advantages of microfluidics for tissue culture experiments.

In 2003, Passeraub et al. first demonstrated the use of microfluidics for brain slice tissue culture using micro-fabricated pillars[83]. By situating the slice on the pillars, media was perfused through the chamber beneath the slice while warm oxygen was blown over the top. Importantly, while perfusion of the brain slice improved long-term health of the tissue, the platform also included the option for electrophysiological recordings via a port in the lid as shown in Figure 1.4A. Just two years later, a slice of spiral ganglion tissue was explanted into a PDMS microfluidic chamber to assess neurite growth preference under a laminar flow concentration gradient[84]. When a piece of tissue was added to the trapezoidal placement region, budding

neurites were exposed to two distinct environments created by laminar flow through microchannels (Figure 1.4B). One more scheme tried to enhance media perfusion to both sides of the tissue by employing a micro-post array within a three-dimensional PDMS structure[85]. A flap on the top of the device allowed for a brain slice to be placed into a specially designed chamber. An opening at the end of the device provided space for electrophysiological recordings of spontaneous activity in the nerve roots of the brain slice. Due to the layout of the posts, the device also offered the capability to expose part of the slice to a flow-focused reagent. By applying a neural activity blocker to one side of the device, half of the brain slice was shown to continue spontaneous activity while the exposed region's activity was suppressed (Figure 1.4C). As another option, pillars within a device may be utilized as the media perfusion system as demonstrated by Choi et al[86]. A brain slice was placed onto hollow micro-needles fabricated by laser-ablating vertical channels in pillars. As shown in Figure 1.4D, oxygenated media was perfused into the tissue through the micro-needles for up to 4 hours of viability. It is worth nothing that even though the system was able to perfuse media to inner layers of tissue, the trauma from needles rupturing the tissue is unknown. These four microfluidic devices were among the first developments for microfluidic tissue culture from 2003 to 2007.
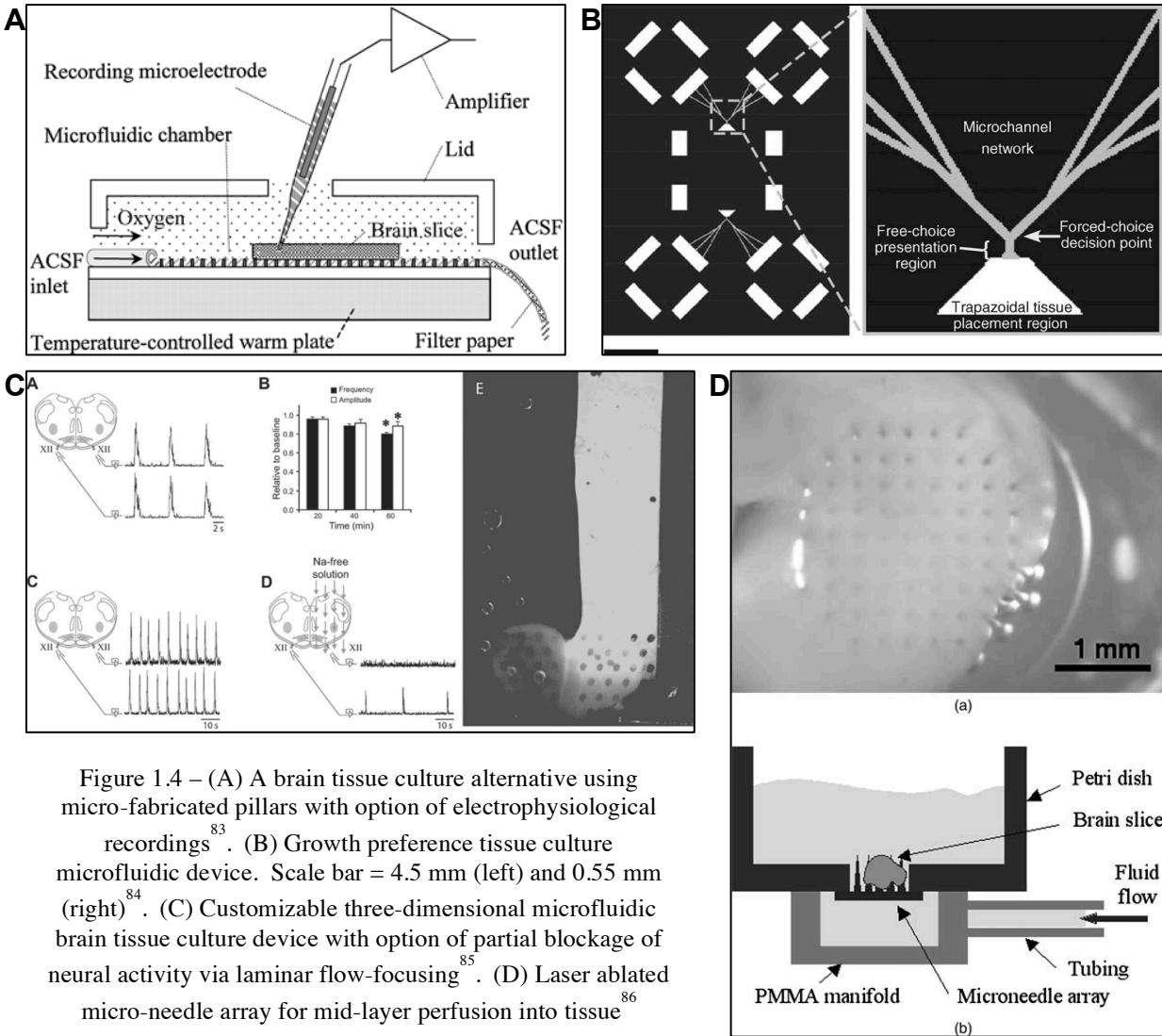
Figure 1.4 – (A) A brain tissue culture alternative using micro-fabricated pillars with option of electrophysiological recordings[83]. (B) Growth preference tissue culture microfluidic device. Scale bar = 4.5 mm (left) and 0.55 mm (right)[84]. (C) Customizable three-dimensional microfluidic brain tissue culture device with option of partial blockage of neural activity via laminar flow-focusing[85]. (D) Laser ablated micro-needle array for mid-layer perfusion into tissue[86]

From 2008 to 2015, continued efforts were made in microfluidic tissue culture with at least eleven journal articles published that discuss microfluidic perfusion platforms for tissue or organ culture. Bakmand et al. described an open fluidic system that allowed for the simultaneous culture of six brain slices with open air flow above and media flow underneath the tissue[87]. To better understand neural pathways, two brain slices were cultured in neighboring chambers interconnected by micro-channels[88]. The co-cultures of different regions of the brain showed attempts to create functional relationships by growing axons toward one another through

17

the channels. Another article even described a device for the culture of a whole zebra-fish, a physiologically simple organism used for modeling drug discovery[89]. On a smaller scale, a group from the University of Hull utilized a micro-port fitting as a tissue biopsy holder on top of perfusion channels[7,8]. The simple and adjustable design provided the opportunity for immediate investigation of the tissue sample as well as long-term culture up to 3 days[7]. Similarly, a microfluidic transwell insert was assimilated with a standard 6-well plate to create gradients in a conventional cell culture platform[90]. With this add-on type of device, biologists can easily apply a gradient to any tissue or cell culture in a familiar 6-well plate for a variety of experiments. Barkefors et al. held a piece of tissue between two perfusion channels inside a section of 3D collagen gel to study gradient-driven and directional angiogenesis, the formation of blood vessels[91]. Hydrogels have also been used to culture cells and tissues within the same device as shown by Sivashankar et al[92]. Pieces of liver tissue were sandwiched between 3D hydrogel structures with mesothelial cells cultured on the surface for improved health over a period of twelve days.

In addition, microfluidic channels were placed on top of a breast cancer tissue slice for personalized cancer therapy diagnostics[93]. By applying different therapeutic biomarkers to a variety of channels, an immunohistochemistry assay was formed on a single tissue slice, helping to reduce cost and tissue consumption while increasing efficiency. To better understand the underlying mechanisms within small blood vessels, researchers placed a 1.5 mm section of artery in a microfluidic channel[94]. With perfusion through the center and optional drug delivery from the exterior, the platform enabled biologists to study and assess resistance artery function and response. Although not typically used for gas exchange, one group created a microfluidic add-on for standard perfusion chambers which allows for oxygen exchange through a thin PDMS

membrane from underneath the tissue slice[95]. Similarly, researchers fabricated a perfusion system specifically for human skin biopsies where one side received a reagent through a porous membrane above microfluidic channels while the opposite was exposed directly to air[96]. Thus far, the microfluidic devices discussed have opened doors to innovation in the field of tissue culture, but little has been researched past basic perfusion systems. Even though some of the previously described microfluidic tissue culture systems demonstrated integration of electrophysiology or fluid focusing for localized stimulation and detection, most have not attempted to control and target specific discrete areas of the tissue slice for interrogation via microfluidic techniques. The advantages of miniaturization and laminar flow characteristics offer spatial and temporal resolution and control over local microenvironments. Why not utilize these aspects of microfluidics in tissue culture experiments?

While many of these platforms have shown novelty and assessed a demand in biological applications, signaling and diagnostic techniques must be integrated past simple perfusion for improved understanding. A variety of important physiological activities are triggered at a point within tissue, not a widespread stimulus. As such, spatial and temporal resolution in controlled microenvironments within tissue is certainly required to investigate these types of events. Next, we will survey a wide range of technologies, including microfluidics, designed for localized stimulation of cells and tissue.

## 1.4 Technologies for sensing and probing tissue

In all organisms, action and reaction are constantly occurring. Muscles stretch and flex using energy created by a chemical reaction from the consumption of nutrients. The brain accepts information from neurons throughout the body as electrical signals and sends a response back in the same way. Many of these reactions simply require signaling information through

cells and tissues. As described earlier, cells communicate with one another by the passage of ionic molecules to form signaling chains through tissue and the entire body. Failure to respond properly to a signal or stimulus can cause severe repercussions throughout an organism. Here we will discuss technology created to investigate a body's reaction or inaction to stimuli along with biological signaling.

*Devices for Cell and Tissue Signaling*

Throughout the body, cells communicate with one another by accepting and dispelling molecules that are needed for a variety of functions. Many of these molecules transferred between cells are electrically charged ions and thus are able to be detected using electrical approaches[97]. Patch clamping is a well-known and highly regarded method for electrophysiology recording in brain slices[98,99]. Although significant improvements to the method were made in 1981[99], patch clamping has a bad reputation for its low success rates and time consuming operation.

To perform patch clamping, a glass pipette with a tip the size of a few microns is filled with electrolyte solution and attached to a micromanipulator. The tip of the pipette is lowered onto a cell and suction is applied to create a seal with the cell membrane. Depending on the type of test, the suction might be increased suddenly or the pipette removed to rip away a small piece of the membrane. These methods allow for an electrode within the pipette to sense the signaling from a single ion channel with a current measuring around a few picoamperes. Note that although this procedure does not sound intricate or difficult on paper, there are a variety of challenges to surmount. If the cell is not perfectly healthy or a slight excess of suction is applied to the pipette, the cell dies and the experiment fails. Due to ionic molecules in the surrounding environment within tissue or cell culture, distinguishing the signal from a single cell from noise

can also be problematic. Many researchers take weeks to learn and practice the technique only to give up due to the frustrating circumstances accompanied by patch clamping.

Similar to this renowned method, reviews have been published discussing a variety of electrode-enabled devices fabricated to detect signaling in cells and tissue[100–104]. Strong emphasis has been shown to interface these technologies specifically with neuroscience due to their electrical parallels[6,105–107]. While electrical biosensors have a wide range of applications in detecting biological response, other technologies have instead focused on stimulation of cells and tissue. This section will focus on describing biosensors, stimulation, and probe technologies relevant to the original research presented here in this dissertation.

Mechanical stimulation[107] has been reviewed as well as chemical stimulation through drug delivery techniques[108]. Several reports have partially focused on localized chemical stimulation in brain slice cultures using microfluidic technologies. In 2008, a group from the University of Illinois published a microfluidic add-on for standard electrophysiology chambers to allow local chemical application from underneath a brain slice[109]. Sip and Folch improved upon this technology by fabricating a valving mechanism to control the release of chemicals for use in non-microfluidic cell cultures[110]. In contrast to the valving mechanism, Tang et al. created a combined injection and suction port for confined chemical application in brain slices[111]. In addition to the above technologies, various designs of micro-fabricated probes have been utilized as both sensors and stimulants[112]. Many of these probes have microscale protruding structures that create electrical or chemical interfaces with tissue at specific sites. Though the previously mentioned devices claimed a localized application of reagent, very few have included results of the size of the affected region. Sip and Folch included diffusion results related to the pressure required to apply fluid to the control area, but the smallest region was about 200 μm diameter.

Later, we will describe our own attempts at localized chemical probing of whole retina tissue with the option of a 100 μm diameter or less stimulus point. In addition to chemical or mechanical stimulation within tissue, electrical signaling is also an interesting and widely researched topic in microfabricated devices.

Due to advances in microfabrication technology, the ability to electrically record and stimulate cells has also been widely demonstrated and extensively published[97]. A large amount of studies have been devoted to developing microelectrode arrays for cell cultures and specifically for recording neuronal activity[113,114]. Moving forward, researchers have begun using tissue instead of cell culture as more relevant studies in biology and medicine. The addition of microfluidic capabilities allows for improved tissue health over a longer investigation period. In 1998, a group from Germany demonstrated one of the first devices to both culture and record organotypic brain slice activity in a single platform for four weeks[115]. Since then, multiple groups have demonstrated innovative methods for the culture and documentation of organotypic brain slice activity using microelectrode arrays[116,117]. In addition, research has also been completed to create devices for electrophysiology studies of tissue. By leaving the top or side of a device open, stimulation and recording electrodes can be inserted into the tissue to document activity. Cheah et al. described a microfluidic device for maintaining heart tissue for electrochemical monitoring studies for up to five hours[118]. Blake et al. created a device that held an organotypic brain slice between two sets of microposts with a side opening for penetrating electrode access[119]. As described above, most of these technologies focused solely on one type of localized stimulation. In the body, electrical stimuli can produce a chemical response or vice versa. Only one group thus far has attempted combined electrical and chemical signaling capabilities in a single microfluidic device[117], but electrical detection is limited to the region of

chemical exposure.  To better understand biological functions at distinct points in tissue, we present our own novel microfluidic device that combines localized chemical stimulation and high-resolution electrical detection over the entire retina in Chapter 3.  Interestingly, implants are another type of advanced technology that provide and receive a variety of signaling cues with surrounding tissue via electrical or chemical means.  Our project goals focus on *ex vivo* signaling studies instead of implantation, but many implants employ similar methods for stimulation and detection thus the following survey of technologies.

*Electrical and Chemical Signaling via Implants*

Electrical or chemical stimulation of tissue is an important approach for studying cell signaling in the central nervous system (CNS), which controls all activities in the body.  As stated previously, the retina is made of neurons and is a part of the central nervous system. These neurons communicate via the transfer of electrically charged molecules allowing for electrical detection or stimulation.  Using an implant as a replacement step in the signaling process, a broken chain of information transfer can be repaired.  Here we discuss a few of the interesting and groundbreaking advancements in central nervous system implants.

Recently, a group from Melbourne developed a diamond-integrated circuit for electrical signaling as a retinal prosthesis for patients with degenerative eye diseases[120,121].  Though the implant provided high-resolution electrical arrays to bridge gaps in neuronal signaling, the surface of the substrate was flat and did not conform to the rounded tissue of the retina.  To create an implant more suitable for living tissue, carbon nanotubes were used in a microelectrode array on a variety of flexible support layers like medical adhesive tape for neuronal stimulation and recording[122].  As another approach toward a retinal implant, Chen et al. fabricated a

graphene-based microelectrode encased in PDMS for flexibility and biocompatibility, both vital characteristics for acceptance into live tissue[123].

Another option for an implant that has been somewhat overlooked is chemical stimulation of tissue instead of or in combination with electrical. Cells communicate via the passage of ionic molecules, thus the process can be considered both electrical and chemical. Inayat et al. performed tests of glutamate injections into retina to investigate the feasibility of a chemical prosthesis as an alternative approach to replace current electrical devices[124]. For joint signaling studies, Gao et al. described a combination device with a passive release microfluidic channel integrated with a microelectrode array for future development as an implant[125]. Although the device provided a controlled amount of fluid for passive release into tissue, there is no containment area and the reagent may affect unintended regions. In our own research, we combine local, defined chemical stimulation of tissue with high-resolution electrical detection of cell signaling into one device for *ex vivo* studies. While an implant can be considered a type of long-term solution to bridge gaps in cell signaling, other options like micro-probes exist for short-term electrical or chemical signaling.

*Microfabricated Probes for Temporary Signaling*

Probes, generally built using microfabrication techniques, may be used to introduce drugs or soluble factors into a specific area of tissue or to stimulate and record electrical activity. While needles and electrodes have long been used to probe tissue chemically or electrically, here we will focus on microfabricated probes. To enhance localized delivery of drugs or chemical stimulants, needles must be miniaturized to distribute discrete volumes within tissue. In 2000, Mcallister et al. reviewed some of the earliest micro-needles for drug discovery[126]. To study single cells within whole tissue, a group from MIT described a microfluidic device for restricted

cell lysis, or rupture of a cell's membrane, without disrupting the surrounding environment[127]. Another microfluidic device created by Queval et al. contained six apertures on one microprobe allowing for a variety of simultaneous chemical injections and aspirations on the surface of tissue[128]. Although microfluidic channels are valuable tools for drug discovery, some groups have focused strictly on probes for electrical stimulation and recording. Du et al. devised various configurations of a neural probe for high-density, low noise electrophysiology with up to 64 recording sites in just one of the designs[129]. To increase the opportunity for joint signaling, microelectrodes can be integrated with a microfluidic probe for instantaneous electrical recording after chemical stimulation. Lee et al. published results from a multi-functional probe containing microfluidic channels integrated with an iridium microelectrode array for combined drug delivery and recording of neural activity[130]. While microprobes provide the opportunity for less invasive temporary signaling within tissue, more development is required before these technologies reach clinical application due to the severity of brain surgery.

As discussed throughout this section, a wide variety of devices have been fabricated and tested for the stimulation and recording of biological functions. Due to constant cell communication via electrically charged molecules, microelectrode arrays have been employed as a simple way to record activity while microfluidic channels provide drug delivery as a possible stimulus. Some of these devices attempt to combine electrode arrays and microfluidics for simultaneous stimulation and recording, but most do not specifically address localized changes in microenvironments within live tissue. In this dissertation, we describe our efforts to design and build a single device for localized high-resolution chemical and electrical signaling in whole retina tissue.

## 1.5 Overview of dissertation

Beginning with a review of the physiology of the retina and neurons, Chapter 1 provided a setting for this dissertation by including a thorough examination of current technological advances in the fields of microfluidic cell and tissue culture. While great progress in this research field has offered innovative and powerful opportunities for biologists, there are still unmet needs for many biological/pathological studies. In this work, we describe our own efforts to close this gap through the design, fabrication, and testing of microfluidic platforms for tissue culture, specifically for localized stimulation and probing. Chapter 2 will discuss the first project: a three-piece device for spatially isolating and chemically probing a discrete region of whole retina tissue, which allows for point application of specific reagents to a 100 μm diameter area on the inner surface of the retina. To extend the abilities of this device, Chapter 3 describes the second project: a preliminary design and study of graphene integration with a microfluidic platform for localized chemical and electrical signaling in whole retina tissue. Before full integration of graphene with the platform, we first investigate the capability of the single-layer material to record electrical signals within live tissue. As with all microfabrication, difficulties were encountered in the development of this device that will be discussed in depth in Chapter 4. Thin-film PDMS molding techniques, such as sandwich molding, are examined including the pitfalls as well as alternative options such as laser cutting microscale holes. Finally, we conclude this dissertation with a summary of the work completed and a brief discussion of future plans to continue the research.

CHAPTER 2


**RETINA-ON-A-CHIP PLATFORM**


**2.1 Motivation**

As discussed previously, a variety of microfluidic platforms have been designed for tissue culture and investigation, mostly for brain slices. Many of these have demonstrated chemical signaling or electrical recording, but to date the approaches lack precise, simple, and effective spatial control of stimulation. Although a few groups have demonstrated some spatial resolution with brain slices, none could achieve well-specified local stimulation[109–111]. Most relevant to the current study, Mohammed et al. characterized a microfluidic add-on for electrophysiology in brain slices[109]. In this device, channels underneath the tissue were used to provide fluid at a via-hole to the entire thickness of the tissue via passive pumping from inlet to outlet. As quantified in the article, 80% of the dye spread to a radius of about 200 μm from the center of the via-hole. Similarly, Sip and Folch presented a valving dispenser but the smallest affected region reported resulted in a 200 μm diameter stimulant bolus[110]. Tang et al. utilized the combination of an injection and suction port to attempt localized stimulation of brain tissue, but the affected region is again at least 300 μm in diameter[111]. Note that due to a layer of dead cells in brain slices resulting from the trauma of dissection and slicing, these studies required larger stimulation regions which allow for the stimulant to reach deeper into the tissue where cells are still living[111]. However, the reported platforms cannot scale down the stimulation region easily because the affected region is also determined by diffusion and flow processes in the media. As such, they lack the precision control required for studies with smaller stimulation regions. For example, in

contrast to brain slices, the layers in the retina do not experience the same type of extreme trauma during dissection; thus there is much less immediate cell death. Instead of cutting through cells as in brain slices, the retina tissue is kept as a whole without major damage, and in the explanted retina, the first layer of cells (RGCs) is alive and available for probing after dissection.

Although brain tissue is the ultimate choice for studying neuronal activity, retina is often used as a preferred substitute. Difficulties in studying brain tissue include slice thickness, dissection trauma, oxygen consumption, complicated organization, and inconvenient location. In contrast, while retina tissue still requires oxygen for long-term health, many of the disadvantages in using brain slices do not apply. One issue with studying retina is its inherent curved profile, which could pose significant challenges to imaging. However, effective approaches to flatten retina without damaging it have been achieved, but this is an important issue to consider in the design of platforms targeted at studying retina. The most desirable traits of the retina are its *in vivo* accessibility and light sensitivity allowing for easy stimulation for a variety of important and interesting studies. Seeing the great opportunities that microfluidics could provide toward studying retina, here we describe a novel microfluidic platform for culture and localized chemical stimulation to a 100 μm diameter affected region, of whole retina tissue with confocal imaging compatibility.

## 2.2 Design and fabrication

The overall design of the microfluidic platform incorporates three comprehensive goals: (1) flatten the retina for imaging capabilities without damage, (2) provide media to the retina for long-term health and culture, and (3) allow for point application of a reagent to the surface of the retina. To achieve these goals, innovative design and fabrication techniques must be utilized.

The design consists of three structural components while the fabrication includes a thin-film PDMS technique and plastic molding as well as laser cutting. This chapter represents a first step toward full electrical and chemical characterization of neuronal tissue by focusing solely on localized chemical stimulation of whole retina tissue.

*Design of Structural Components*

The microfluidic platform consists of three structural components that all contribute toward accomplishing the three goals stated previously. A thin-film PDMS layer bonded to a glass coverslip is the cornerstone of the overall design. This layer contains sets of 50 μm tall, 300 μm wide microfluidic channels in a 100 μm thick PDMS film with 100 μm diameter open through-holes above the channels. A second design, aimed at reducing the layer thickness, decreased the height of the channels and total PDMS thickness by half to give 25 μm tall channels in a 50 μm thick layer. Note that no major differences were discovered between the two designs. One channel, designated as the suction channel, is used to pull the retina into contact with the rest of the thin-film layer via an array of through-holes by applying a negative pressure to the channel. A set of twelve separate channels, deemed the access channels, allows for point access delivery of reagents to the surface of the retina at the through-hole in each channel. Note that these access channels are separated into four quadrants of three access points each (bisected by the suction channel) thus providing twelve distinct chemical stimulation regions within a 3 mm by 3 mm area of tissue. The combination of the suction and access channels in a single thin-film PDMS layer helps to achieve two of the three stated goals above, i.e., to maintain the retina in a flattened form and to provide point access reagent delivery. Figure 2.1 presents a detailed view of the thin-film layer.
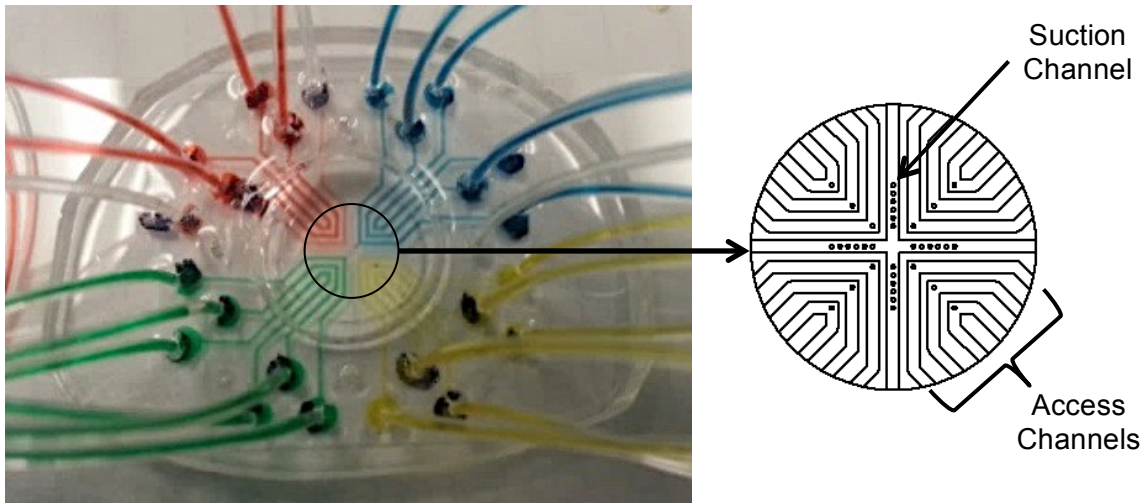
Figure 2.1 – Retina-on-a-Chip platform with media cylinder removed and mock PDMS retina in place. Dye was added to all 12 of the access channels for improved viewing while the suction channel remains empty

The second part of the platform, named the tubing support layer, provides handiness and an alignment guide for the user. Though it does not directly address any of the earlier stated goals, without it, the device would be incredibly difficult to operate. The tubing support layer is a 1-1.5 mm thick piece of bulk PDMS with one large hole in the center for alignment of the retina over the through-holes and 28 holes around the edge for tubing connections to the thin-film layer.

The third and final piece of the device, the media cylinder, includes three components of its own, a glass cylinder, agar gel, and retina well. The combination of these three parts fits inside the large central hole in the tubing support layer and acts as an explant platform and media perfusion system for the retina. A thin piece of PDMS in the shape of a washer, named the retina well, is attached to the bottom of a 10 mm glass cylinder. Agar gel is then placed into the cylinder and pushed through to abut the top of the retina well. The assembled media cylinder is inverted for explant of retina into the PDMS well onto the agar gel, which provides a slightly sticky surface to allow for temporary flattening of the retina. Note that the RGC layer of the

retina is facing out and opposite the agar gel after explant. Once the retina has been unfolded onto the agar gel from its naturally curved shape, the media cylinder is flipped and placed with the retina side down into the large hole in the tubing support such that the RGC layer of the retina is now in contact with the thin-film PDMS layer. Media added to the top of the cylinder slowly perfuses through the agar gel to deliver a constant supply of fresh nutrients to the tissue throughout experiments. The weight of media on top of the agar gel subtly provides extra pressure to further flatten the tissue. Thus the media cylinder helps to achieve two of the three previously stated goals: (1) holding the retina flat from its naturally curved state and in-place over the through-holes and (2) maintaining tissue health during testing by dispensing a constant supply of media. Together, these three components are integrated into a fully functional but simple device to accomplish the three challenging goals.

*Basic Fabrication of Components*

The fabrication of the Retina-on-a-Chip platform follows some standard soft lithography techniques but also employs unique techniques including sandwich molding thin-film PDMS, plastic molds, and laser cutting. Here we will discuss how each of the pieces in the platform are fabricated and assembled to create the final device. Note that multiple fabrication techniques were tested throughout the reiterative design process to find the most efficient solutions, especially for the thin-film layer. In-depth thin-film PDMS layer fabrication techniques will be later discussed in Chapter 4, as this chapter will instead focus on the assembly of the Retina-on-a-Chip platform.

Before the device itself was fabricated, a silicon mold with SU8 features was crafted in a clean room via photolithography. First, a 50 μm (or 25 μm) tall layer of negative SU8 photoresist was spun onto a clean silicon wafer that was then pre-baked and exposed to UV light

under a mask to cross-link the channel regions.  Next, the wafer was post-baked on a hotplate and the features developed using SU8 developer solution.  Once developed, a 100 μm (or 50 μm) tall layer of SU8 was spun onto the wafer and pre-baked.  Using alignment marks, a mask was aligned and exposed to light to cross-link the through-holes and tubing connection regions at the ends of the channels.  Again, the wafer was post-baked and the features developed.  Finally the wafer was cleaned using a quick wash of acetone and isopropyl alcohol.  To ensure solid features and dissolve any leftover alcohol, the wafer was baked a final time on a hotplate.  Note for all pre-baking and post-baking steps, the wafer was placed on a 65°C hotplate for a short period of time (about 1 to 2 min) to gradually increase the temperature before baking on a 95°C hotplate (time varies depending on SU8 thickness).

With the SU8 mold ready, two options are available: fabricate a thin-film PDMS layer using the SU8 mold directly or create a plastic replica mold for thin-films.  Plastic replica molding was developed by a group at the Massachusetts Institute of Technology for replacement and improvement to SU8 molds traditionally used in microfluidics[131].  The advantages of plastic molds over SU8 molds include ease of use, sturdiness and strength, and high-aspect ratio features.  To create a plastic mold, two commercially available liquid polyurethane parts (Smooth-Cast 310, Macungie, PA) are mixed in equal volumes, poured over a PDMS piece, and cured at room temperature.  Though the plastic begins to harden within five minutes of mixing the two parts, full cure occurs around two hours depending on the thickness and size of the plastic piece.  For ensured strength, a second cure at higher temperature for four hours is optional.  Note that for different components, the PDMS pieces over which the plastic is poured are either from a SU8 master mold or cut by hand using a scalpel and hole punches.  For our purposes, we created two plastic molds for rapid production of the devices: (1) a replica of the

two-layer SU8 mold to create the thin-film PDMS layer with microchannels and (2) a tubing support mold created from a hand-punched PDMS piece.  In contrast to the SU8 molds for the thin-film layer, the aspect ratio of cylindrical features in the tubing support plastic mold were close to 2:1 at approximately 1.5 mm tall and 0.75 mm thick.  While high-aspect-ratio features are a distinct advantage over SU8 features, the plastic molds are also capable of micron-sized features as shown by Desai et al.[131] and the plastic replica of our SU8 mold.

As microfluidic devices become more complex, PDMS fabrication techniques are continuously improving.  In 2000, Jo et al. reported a sandwich-molding process to create thin-film layers of PDMS with open channels for assembly into three-dimensional devices[132].  Four years later, Hsu et al. improved upon the process by utilizing a fluoropolymer-coated polyester (PE) sheet for transferring the PDMS thin-film from the SU8 mold to a glass substrate[133].  To allow for confocal microscopy imaging of retina, we combined these techniques and optimized the process (as discussed in Chapter 4) to fabricate a PDMS thin-film layer with open through-holes above microchannels.

For final assembly of the device, the PDMS thin-film layer was bonded via oxygen plasma treatment to a thin glass coverslip before very carefully removing the fluoropolymer-coated PE sheet.  To form the tubing support layer, liquid PDMS was poured into a plastic mold, degassed, and cured for about four hours.  Both the tubing support and thin-film PDMS layers were then exposed to oxygen plasma, aligned at the tubing connections, and bonded together.  Pieces of tubing were inserted into each of the connections with needles added to the outlet tubings.  To build the media cylinder, PDMS was spun onto a fluoropolymer-coated PE sheet at approximately 200 RPM with a target thickness of about 200 μm.  After curing for four hours, the thin PDMS was cut into the shape of a washer, 10 mm for the outer ring and 5 mm for the

inner. The PDMS washer or retina well was glued to the bottom of a 10 mm glass cylinder using liquid PDMS. Once cured, a piece of high gel-point agar gel (3.5% w/v) was added to the cylinder on top of the retina well. Figure 2.2 depicts the platform in its individual components.
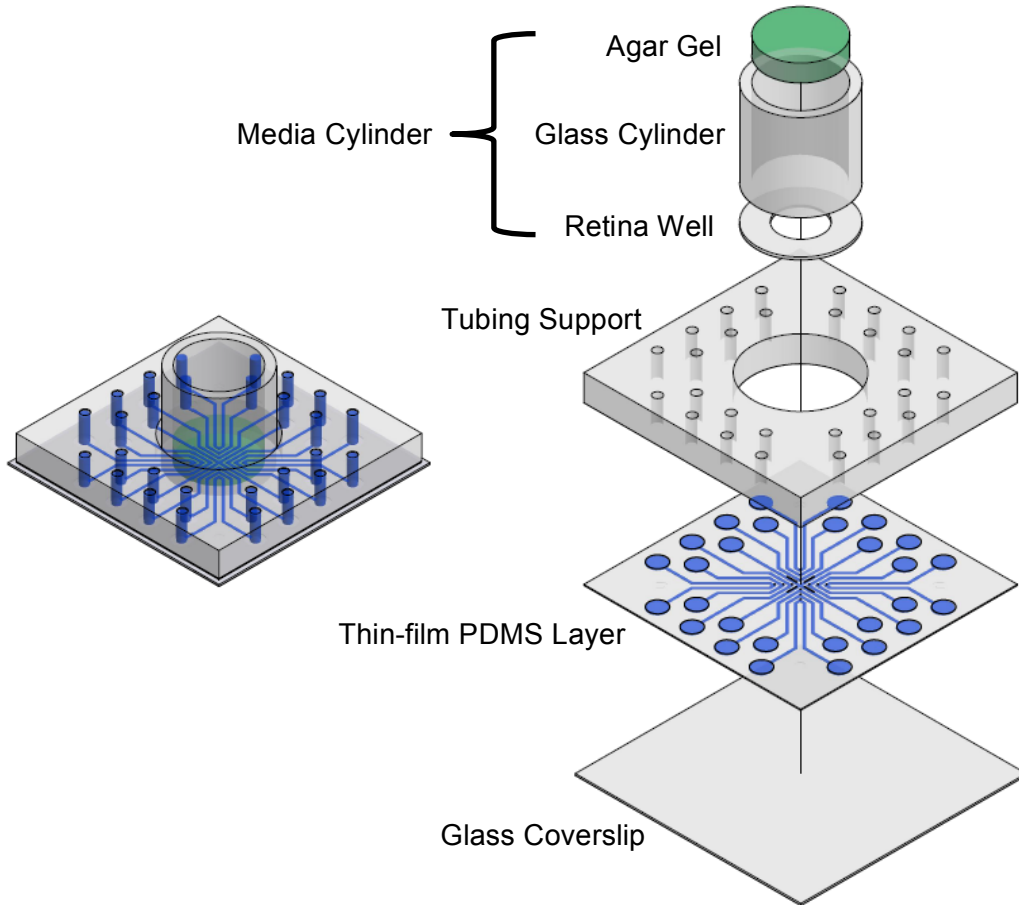


Figure 2.2 – Retina-on-a-Chip platform in assembled and exploded views. Blue coloring was applied to the channels for better visibility of the intricate structures. Agar gel was tinted green to distinguish it from the PDMS pieces

As previously described, the retina was explanted onto the agar gel within the retina well and the media cylinder inverted and placed inside the tubing support layer atop the channels in the thin-film layer. Figure 2.3 depicts an explanted retina on the platform with the optic nerve head and vasculature easily visible as evidence to its healthy condition.
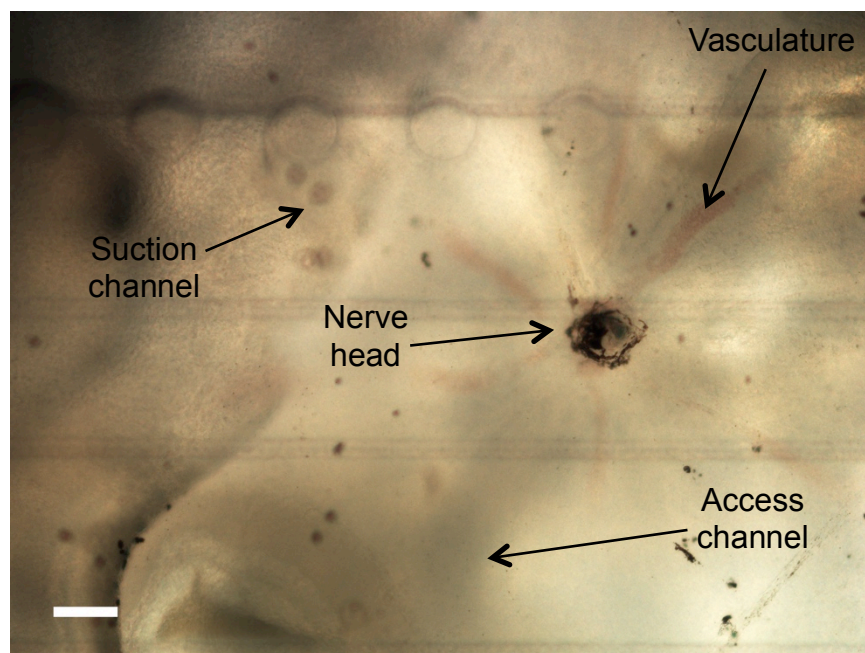
Figure 2.3 – Explanted retina on device with vasculature and nerve head visible demonstrating sound health. One access channel and part of the suction channel are also visible underneath the transparent retina. Scale bar = 100 μm

## 2.3 Experimental analysis of the Retina-on-a-Chip platform

To test the viability of the Retina-on-a-Chip platform, a set of experiments was conducted including localized staining and cell signaling studies inside the retina. Before we enter into discussion of physiologically relevant results, we will explain and demonstrate effective operation of the device. As described earlier, the device has a specific protocol to be followed for successful point application of reagents to the surface of the tissue.

*Negative Pressure Operational Protocol*

Point application of reagents is by no means a novel idea in the field of biology. Drug delivery or stimulation to specific areas of tissue is crucial for a wide range of treatments and therapies. By focusing and controlling drug delivery to a confined area, we can study signaling events that cascade from the origin of application. A few groups have attempted to create microfluidic platforms for this purpose, but none have reported well-controlled localized delivery

of reagents to the surface of tissue. Here we demonstrate how a straightforward design and innovative operation contribute to effective point application of a reagent to whole retina tissue.

Below in Figure 2.4, a cross-section of a through-hole is illustrated to better demonstrate the device operation. Note that the schematic applies for through-holes in both the suction and access channels since both experience negative pressure.
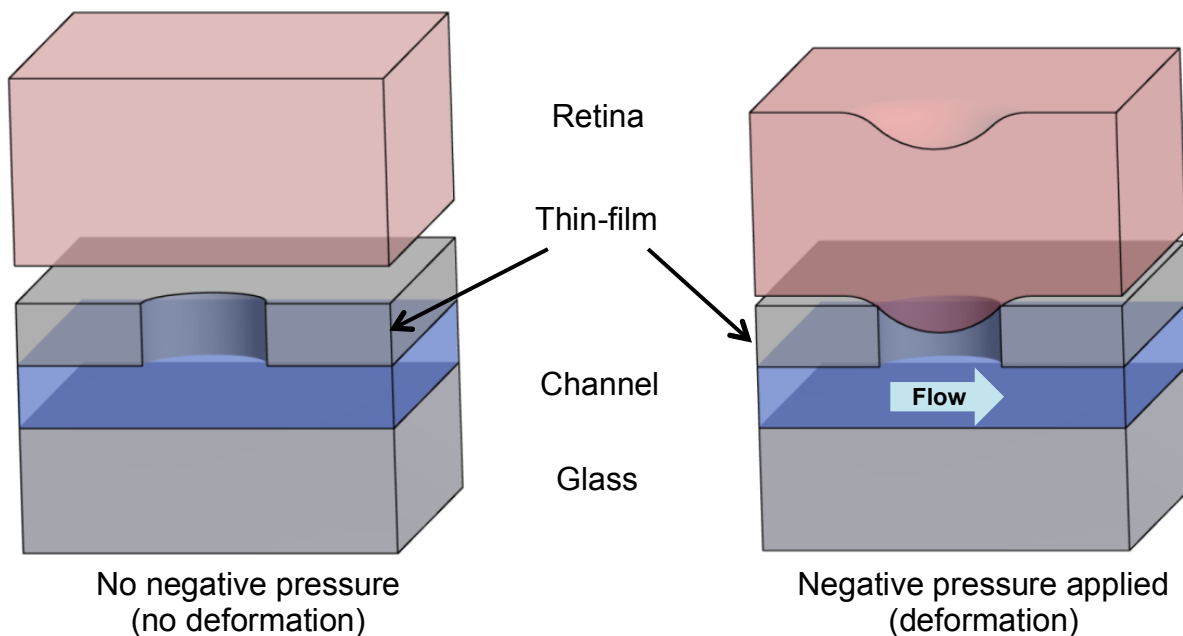


Figure 2.4 – Schematic cross-section of through-hole before and after negative pressure is applied to the suction or access channel via a syringe attached to the outlet tubing

After explant of the retina onto the platform, media was introduced to the media cylinder to provide a slow but steady supply of nutrients to the tissue through the agar gel. Before reagents are delivered to the access channels, the suction channel must be activated to further flatten the retina from its naturally curved structure into contact with the thin-film PDMS layer. Tubing from one of the four outlets of the suction channel was connected to a needle and syringe while the other three connections were sealed at the tubing support with PDMS to prevent leakage. Slowly a negative pressure of about 7 kPa was applied to the syringe causing the retina to deform into the suction channel through-holes. A clamp was added to the tubing to hold the

pressure steady within the channel. Pressure within the device was measured using a pressure gauge connected to the tubing at a T-connector. Evidence of tissue deformation is shown in Figure 2.5. Fluorescent imaging of retina from CX3CR1-GFP mice, microglia expressing GFP under the CX3CR1 promoter, revealed the capability to isolate a single microglial cell at one of the suction through-holes without disrupting its relationship to the surrounding tissue.
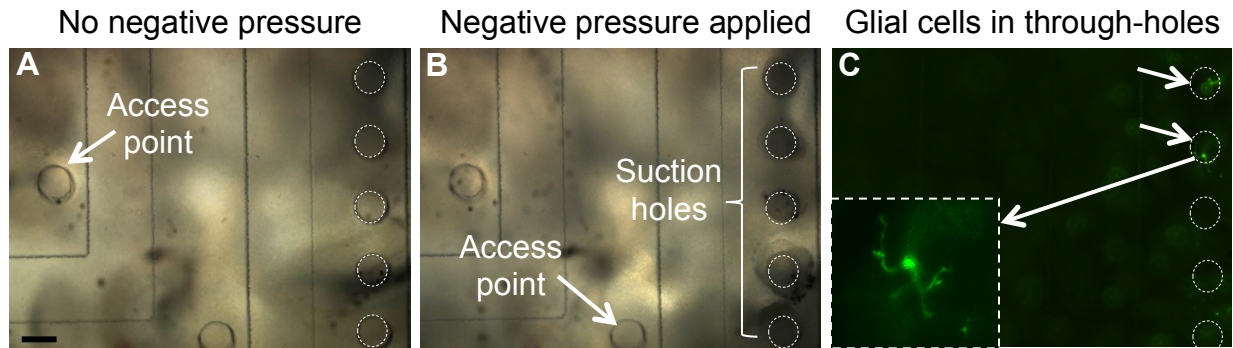


Figure 2.5 – (A)-(B) Visual demonstration of the effect of negative pressure on the retina tissue at the suction channel through-holes. (C) Glial cells are found at the focal plane of the through-holes while the surrounding tissue rests above at a different focal plane. Scale bar = 100 μm

By employing a negative pressure in the suction channels, the retina was fully secured and flattened within the device before attempting reagent delivery to the access channels via a similar protocol. A needle and syringe were attached to the outlet tubing of one of the access channels while the inlet tubing was inserted into the desired reservoir. Gently, a negative pressure of about 6 kPa was applied to the syringe causing the retina to deform into the access channel through-hole. Once the tissue had fully sealed the through-hole, fluid from the reservoir began to flow through the tubing, into the microchannels within the device, and out the second tubing toward the syringe. Depending on the type of reagent delivered, the tubing was either clamped to permit long-term contact with the tissue up to 24 hours or the reagent was replaced with media via the same negative pressure protocol by simply switching reservoirs at the inlet tubing. All of the above operations may be performed on a confocal microscope to permit real-

time imaging if desired. Figure 2.6 illustrates the addition of histological stain toluidine blue (Sigma, St. Louis, MO) to an access channel and subsequently replaced with media after the dye has sufficiently stained the tissue. Incorrect operation of the device by using positive pressure to apply a reagent to the access channel can lead to significant leakage out of the through-hole onto the tissue as demonstrated in Figure 2.6C. Severe negative pressure upward of 23 kPa can lead to rupture of the retina tissue causing fluid to escape the through-hole region as well. The reported focal fluid delivery techniques using positive pressure result in a similar widespread and uncontrolled leakage over tissue. In contrast, as shown in Figure 2.6B, proper use of the Retina-on-a-Chip platform provides a spatially controlled region of affected tissue at the through-hole region of about 100 μm in diameter, at least a 50% drop from other reported chemical stimulation attempts. Importantly, with today's microfabrication capabilities, our approach should be easily scaled down with smaller through-holes even to single-cell level (~10 μm diameter through-holes). As such, we believe that this approach could be a general technique for point application of reagents. The current size of point application allows for simultaneous stimulation of only a few cells within the surface of tissue, specifically RGCs and glial cells, in contrast to the deep and widespread regions as shown in the devices developed for brain slices.
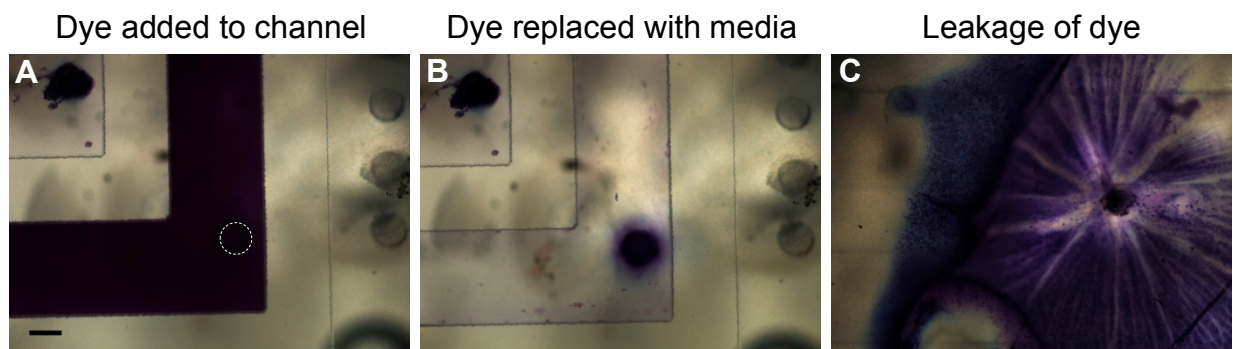


Figure 2.6 – (A)-(B) Visual demonstration of the addition and replacement of dye to an access channel through-hole to contact the retina. (C) Incorrect device operation can cause widespread leakage of dye across the tissue. Scale bar = 100 μm

*Physiologically Relevant Applications*

With effectiveness of the device proven, we move on to demonstrating physiologically relevant applications made possible by the Retina-on-a-Chip platform. To show the usefulness of the device in biological applications, three studies were completed based on chemical signaling of cells, which focus on two major goals: (1) maintaining tissue health over an extended time period, and (2) investigating physiologically significant phenomena originating at a spatially isolated microenvironment. As described in Chapter 1, culturing tissue is required for a variety of biological experiments to assess long-term effects and health. Throughout much of our study of the retina, we elected to focus specifically on RGCs due to the relatively high stress experienced after explant, which requires complete transection of the axons at the optic nerve head (ONH). Later, we will also explore the response of microglial cells in the RGC layer due to induced localized inflammation in the tissue.

To begin, we will demonstrate short-term health of the retina on the platform by probing the RGCs with a neural tracer over 24 hours. Cholera toxin beta subunit (CTB; Invitrogen) was applied to the retina tissue via the access points using the above protocol after successful explant from CX3CR1-GFP mice. Before applying CTB to the access points, the suction channel was activated and media cylinder filled with fresh media. CTB is an active uptake, active transport neural tracer that is primarily taken up by RGCs in the retina. Given that both uptake and transport of CTB requires active endocytosis by RGCs, CTB labeling indicates viability of the cell. When exposed, healthy RGCs uptake CTB into their cell somas and transport it along their axons through the optic nerve to their axonal terminals in the brain[134]. After explant of the retina onto the platform, a 1% solution of CTB in culture media was added to an access channel. The tubings were clamped and the entire platform was cultured under standard conditions for 24

hours.  The CTB in the channel was then replaced with culture media and the retina was imaged

under confocal microscopy.  Uptake into the cell somas was visible as well as transport along

axons thus validating retina health on the device and confinement of fluid delivery to the region

of tissue at the through-hole.  Figure 2.7 depicts the results of the CTB application to an access

channel under 24 hour culture conditions.  Note that zoom-in images of the tissue at the through-

hole is shown as a progression from left to right with red CTB RGCs and green GFP microglia.
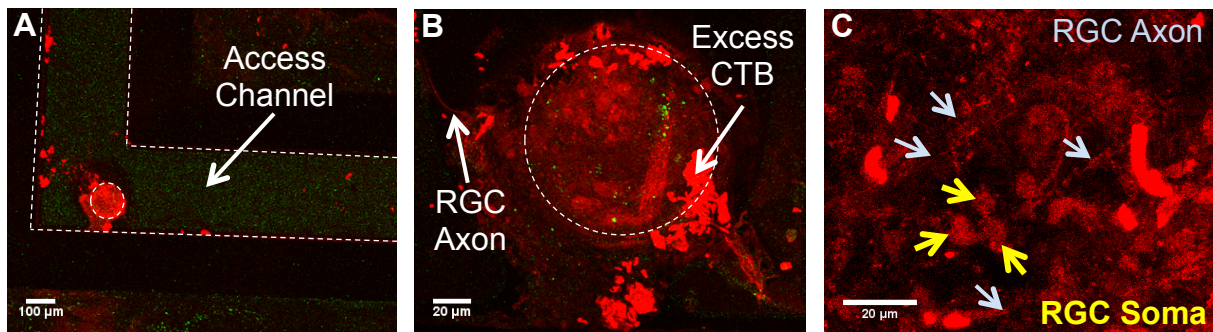


Figure 2.7 – (A) Point access delivery of CTB with media rinse after 24 hour culture (B) Some excess CTB
was found attached to the edge of the through-hole though most was washed away.  (C) RGC somas and
axons are visible demonstrating healthy conditions

To establish long-term health of the retina in the device, we performed a similar trial by

culturing the tissue over a period of four days.  Retina from C57BL/6 mice were explanted onto

the media cylinder and inverted into the platform.  The suction channel was activated and a fresh

supply of media was added to the cylinder before the entire platform was placed into an

incubator.  After four days of culture, CTB conjugated to Alexa Fluor 594 (CTB-594) was

introduced to the media cylinder while CTB conjugated to Alexa Fluor 488 (CTB-488) was

applied to access channels.  Thus the entire retina tissue was exposed to red CTB-594, but only

regions of tissue at access through-holes were subjected to green CTB-488.  The device was

cultured overnight (16 hours) under the same standard conditions before the access channels

were rinsed with media. Confocal imaging revealed that the entire retina took up CTB-594 while CTB-488 was restricted to tissue at the through-hole regions as shown in Figure 2.8.
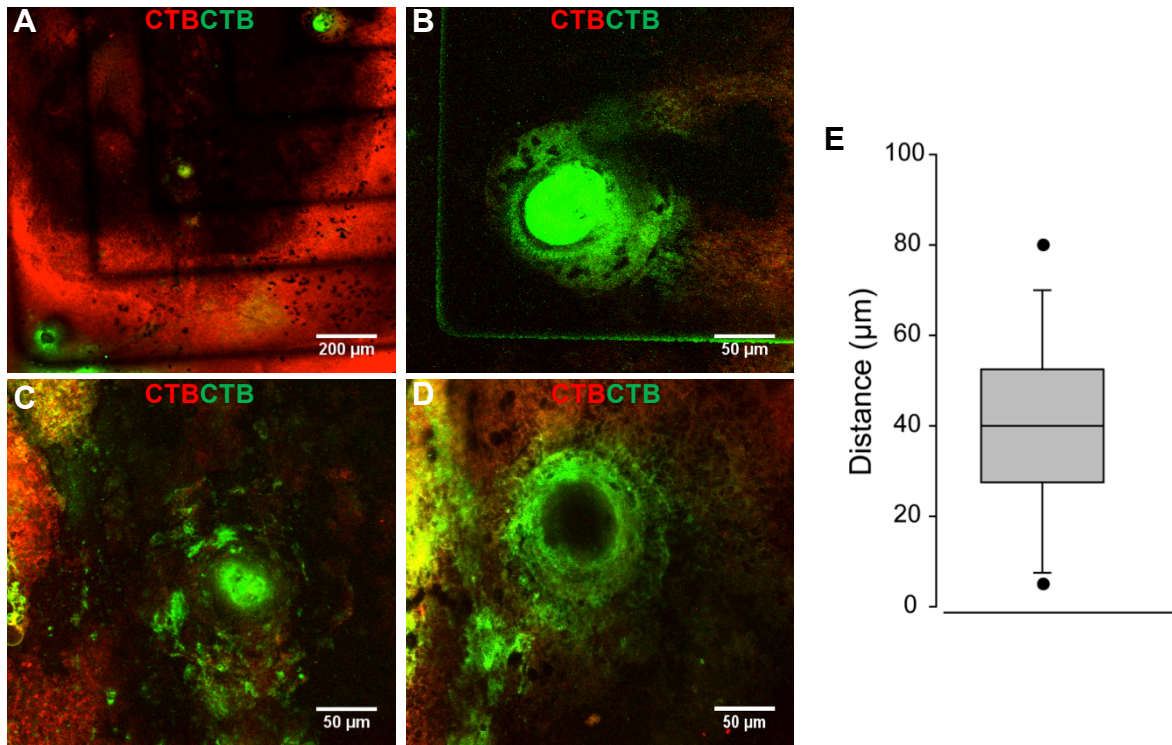


Figure 2.8 – Four days into culture, the entire retina was exposed to red CTB added to the media cylinder while tissue at the through-holes only took up green CTB added via the access channels. (A) Point application of green CTB at three through-holes. (B)-(D) Three regions of tissue at through-holes with green CTB uptake. (E) Diffusion over 16 hours averaged 39 μm with a standard deviation of 19 μm

These results imply that RGCs in the retina were healthy enough after four days in culture to actively uptake CTB. Due to successful introduction of CTB-488 to the through-holes, we also show that the suction channel held steady pressure for up to four days as well. Note that even though CTB-488 was restricted to uptake in the immediate vicinity of the through-holes, some diffusion occurred during the overnight culture. However, the diffusion of CTB-488 past the edge of the through-holes averaged only 39 μm with a standard deviation of 19 μm as plotted in Figure 2.8. Using Fick's law, the diffusion length from a single point is directly proportional to the square root of the product of the diffusion coefficient and time as shown in Equation (1).

$$L \propto \sqrt{Dt} \tag{1}$$

A quick estimation with 0.26 μm²/s as the diffusion coefficient D for CTB-488[135] yields a diffusion length L of about 120 μm over 16 hours. As this value is three-fold of the observed length, we believe that media perfusion through the retina from the cylinder offset the diffusion process due to the negative pressure in the access channel. Together, these CTB experiments verify the ability of the platform to maintain retina health over a period of four days and deliver reagents to a restricted region of the tissue. Thus we have confirmed the capability of the Retina-on-a-Chip platform for both long-term culture of whole retina tissue and local application of a chemical to the surface of the tissue.

To examine the applicability of the device to investigate real-time cellular activity and physiologically relevant phenomena, we shifted our focus from studying the integrity and health of RGCs to stimulating response from microglia in the retina. As described in Chapter 1, microglia are part of the primary immune defense in the central nervous system and have the ability to move freely within layers of tissue unlike neurons, which are primarily stationary. Lipopolysaccharide or LPS is a bacterial endotoxin well known for instigating robust inflammation by activating glial cells, specifically microglia[136–138]. Other groups have shown that microglia respond to LPS by activation and migration between 6-48 hours after exposure[139–143]. However, in contrast to our point application technique, these studies introduced LPS to tissue via a bath or intravenous injection into a live animal resulting in widespread and uncontrolled delivery to entire parts of the tissue or body. We found only one group that microinjected LPS *in vivo* into the corpus callosum of a mouse and observed microglia reactivity after six hours, but the authors did not report on the region size of the affected tissue region, only the size of the needle[143]. Here we will describe our own efforts to further understand the

physiological behavior of microglia by examining their early spatiotemporal response to localized delivery of LPS.

For this study, 2.5 ng/μL LPS was applied via through-holes on the device to retina from CX3CR1-GFP mice. Within one minute of delivery, we witnessed an immediate response from microglia by migration toward the access point (Fig. 2.9D,E). Over the period of thirty minutes, microglia were observed to continue migrating into the through-hole area and from outside the field of view (Fig. 2.9F). In contrast, culture media added to an access channel resulted in no observable migration toward the through-hole but simply migration through layers of the retina without regard for the location of the through-hole, evidence of normal microglia activity (Fig. 2.9A-C). Thus, with localized delivery of LPS to retina tissue, microglia distinctly responded by migrating toward the point of inflammation.

Hand-counting cells at and around the through-hole quantified migration of microglia induced by LPS. To complete this analysis, images from three time-points were sectioned into four regions centered at the access point with the first region signifying the through-hole. Next, regions 2 and 3 were represented as concentric circles about region 1 with corresponding diameters of 200 and 300 μm. The remainder of the view field was defined as region 4. GFP-expressing microglia were counted five times in each region before averaging. The results of the analysis are found in Figure 2.9G with the total number of cells for each time point in the legend. As described previously, immediate migration was witnessed after one minute of exposure via the migration of cells toward the access points as quantified by an increase in number of microglia in regions 1 and 2. Thirty minutes later, we found microglia had continued to migrate in toward the through-hole as quantified by the increase in total number of cells in the view field as well as a distinct increase in cells at regions 3 and 4. Also note that microglia can migrate in

all 3 dimensions, thus cells from other layers of the retina may be moving toward the point of inflammation at the surface of the tissue, especially after 30 minutes of exposure.
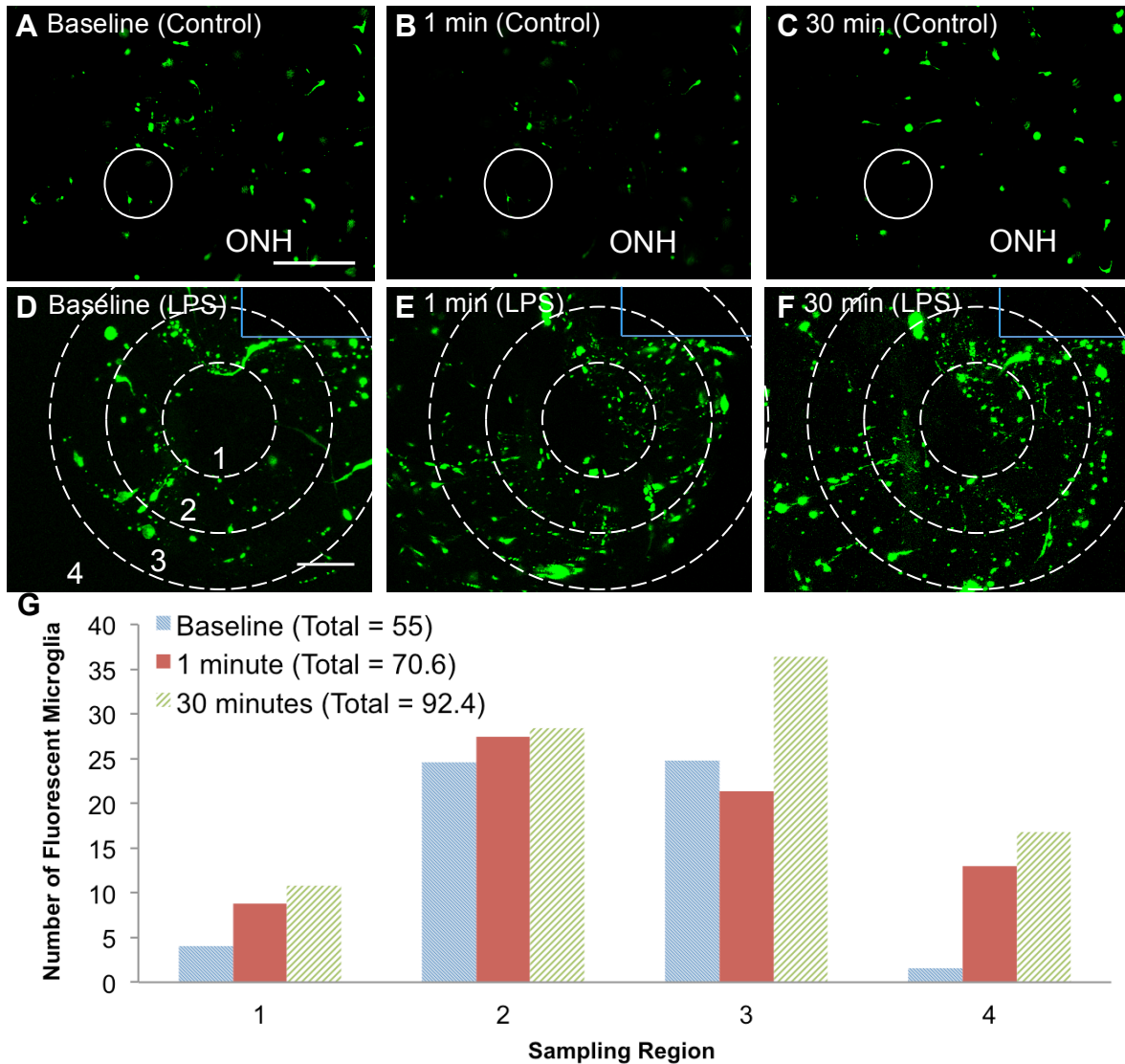


Figure 2.9 – (A)-(C) Culture media applied to an access point exhibits no observable microglia migration over 30 minutes although some cells move in and out of the focal plane. Scale bar = 200 μm. (D)-(F) LPS applied to an access point induces immediate and prolonged microglia migration after one and thirty minutes. Scale bar = 50 μm. ONH represents the optic nerve head. Blue lines depict a channel edge. (G) Migration analysis was quantified by hand-counting microglia in four regions of the view field. Total number of cells for each time point is given in the legend

From these three sets of data, we validate the success of the Retina-on-a-Chip platform to achieve controlled spatiotemporal resolution of directed reagent delivery to whole retina tissue for real-time confocal imaging of biological phenomena in discrete microenvironments.

**2.4 Summary**

The Retina-on-a-Chip platform was designed with three main components to provide localized reagent delivery to a discrete area of retina tissue via a point access through-hole. Fabrication of the device requires typical soft lithography techniques though plastic molding and laser cutting methods were also employed. Once assembled, a specific but straightforward operational protocol is required utilizing negative pressure applied via a common syringe. To determine the validity of the platform, retina was cultured for up to four days in the device. After one day, application of CTB to a through-hole revealed tracing in RGC somas and axons confirming tissue health and drug delivery confined to the access point. Four days in culture found similar results but slight diffusion at the through-holes occurred during the overnight CTB exposure. To examine physiological relevance of point application of reagents, LPS was introduced to access points to investigate microglia reactivity and chemical signaling. Results of the assay demonstrate immediate microglia activation and migration within one minute of LPS delivery, in contrast to previous findings, and prolonged signaling over the course of 30 minutes. Thus, the Retina-on-a-Chip platform was verified as a viable tissue culture and point access chemical stimulation tool with the opportunity for a variety of *ex vivo* tissue studies.

CHAPTER 3


**GRAPHENE-INTEGRATED MICROFLUIDIC PLATFORM**


**3.1 Motivation**

As described in Chapter 1, cell signaling processes are completed via the transfer of charged molecules, which can be probed by two different methods, chemical or electrical. Chapter 2 described a microfluidic platform specifically for localized chemical stimulation of cells in whole retina tissue. By applying a drug or reagent at a confined point in the tissue, we studied how cells respond and signal to one another from that initial local stimulation. While Chapter 2 focused solely on chemical stimulation, we aim to improve upon the platform by integrating graphene-based sensors to allow for electrical signaling detection. As a light-sensitive organ, the retina can be easily stimulated by exposing the tissue to flashing light, which could lead to electrical responses for detection and investigation. Later in this chapter we will demonstrate how we use our graphene-integrated device to record cell responses induced by flashing light as well as the ability to identify the specific cell types by the response.

Over the past decade or so, graphene has become a well-known and highly regarded material due to its incredible physical characteristics and exceptional electrical properties[144,145]. Based on its many unique properties, researchers have attempted to utilize graphene in biomedical applications like tissue engineering and implants[146–148]. Here we utilize the extraordinary optoelectronics properties of graphene to detect electrical response of cells and signaling within whole retina tissue.

For electrical response studies within cells, patch clamping has been a commonly used electrophysiology technique since its introduction by Neher and Sakmann in 1976[98]. Briefly, a glass pipette with a recording electrode creates a seal with a single cell to study membrane potential at an ion channel. Even though many improvements to the method have been made[99], patch clamping remains a difficult and time consuming technique. Earlier in Chapter 1, we discussed in-depth the challenges of patch clamping as well as a few documented alternatives to the technique. To overcome the obstacles inherent to patch clamping that have plagued biologists for years, researchers have attempted to utilize graphene[123,149,150], microelectrode arrays[151–153], and voltage-sensitive dyes[154–157] as alternative electrophysiology techniques. In our research toward a powerful electrical sensing scheme, we integrate graphene transistors with our existing Retina-on-a-Chip platform to provide the opportunity for combined localized chemical and electrical probing of whole retina tissue. Though full integration of graphene devices with the Retina-on-a-Chip platform is still in progress at this point, we have conducted experiments and obtained preliminary results demonstrating the feasibility of using graphene-based scanning photocurrent microscopy to probe the electrical response of retina.

## 3.2 Design, fabrication, and experimental setup

The first step to integrate graphene into the Retina-on-a-Chip platform is a preliminary study to determine if graphene is able to detect electrical signals from the retina. To achieve this goal, we have prepared a simplified design that allowed us to record electrical signaling in whole retina with graphene. In future work, we will introduce a more complex microfluidic design to combine chemical and electrical signaling capabilities in a single device (Figure 3.1).
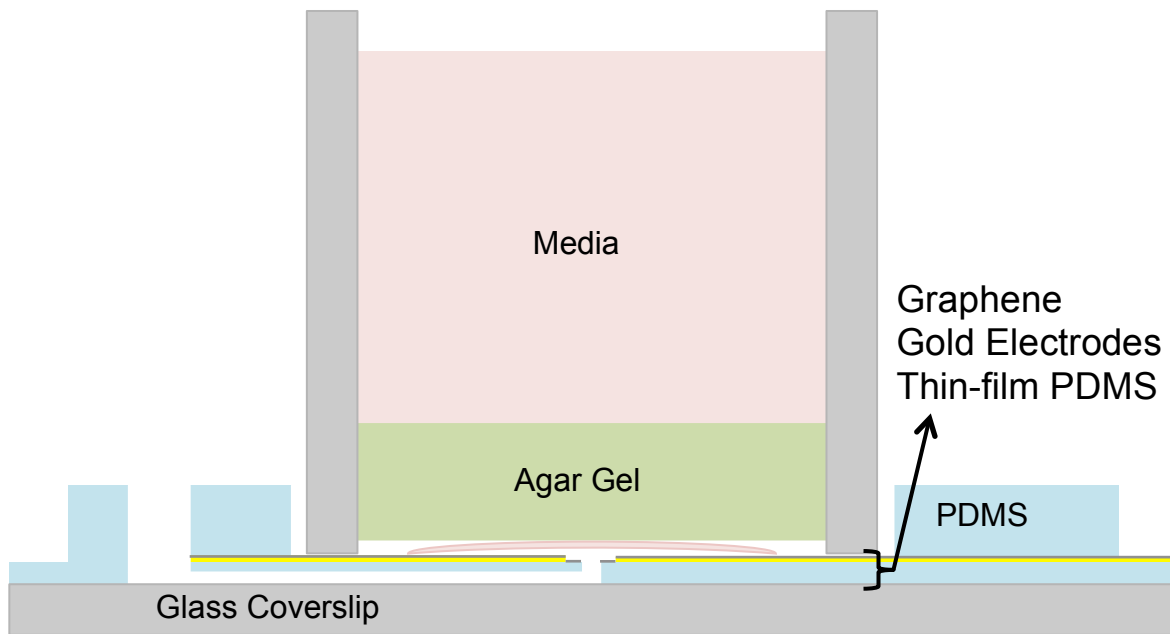
Figure 3.1 – Schematic of the graphene-integrated Retina-on-a-Chip platform. On the left side, one access channel in the thin-film PDMS layer is shown. The retina is shown in the color pink under the agar gel. The simplified version simply eliminates the thin-film PDMS layer and tubing connections. Not to scale

*Basic Design and Fabrication*

The design of the simplified platform involves two separate fabrication processes, one for electrical recording and one for handling and placement of the retina tissue. To create the electrical recording portion of the device, first a lift-off process was implemented. Positive photoresist was spun onto a glass coverslip and photolithography was used to create a pattern for the electrodes. Gold pellets were thermally evaporated onto the coverslip and the portion on top of the photoresist was removed through the lift-off process. Next, single-layer graphene was synthesized via chemical vapor deposition onto copper foil using methane as the reactive gas. The graphene was then covered by spinning a layer of polymethyl methacrylate or PMMA and placed into a plastic boat of copper etchant overnight. Once the copper was dissolved, the etchant was replaced with deionized (DI) water and the graphene was taken out of the boat using the glass coverslip onto the gold electrodes. Finally the PMMA was removed with acetone to

reveal a single-layer graphene sheet on top of the glass and gold electrodes. To determine the quality of the graphene, Raman spectroscopy was performed before further processes.
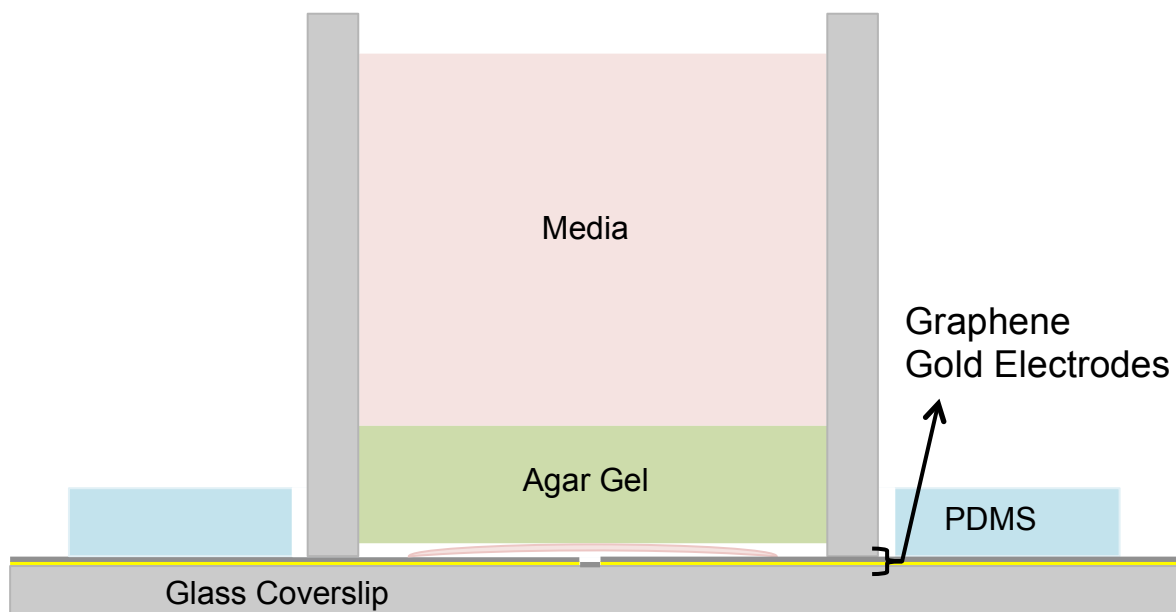


Figure 3.2 – Schematic of the simplified version of the graphene-integrated Retina-on-a-Chip platform. The retina is depicted in the color pink under the agar gel. Note that the only difference is the thin-film PDMS layer and tubing connections. Not to scale

To provide for handiness and alignment of the retina tissue onto the graphene, parts of the Retina-on-a-Chip platform were modified. Since complex microfluidic handling for chemical stimulation is not yet required, the thin-film PDMS layer was dismissed, as were the tubing connections in the PDMS tubing support layer. The large hole in the center of the tubing support layer remained for alignment of the retina in the media cylinder. Thus, the tubing support layer no longer required a mold for fabrication, but instead only a scalpel and hole punch to create a 1.5 mm thick ring from bulk PDMS. The PDMS retina well was also dismissed in order to allow the retina to flatten as much as possible without the restriction of the well thickness. A design schematic of the fully integrated device is shown in Figure 3.1. Note the simplified platform as shown in Figure 3.2 without the thin-film layer and tubing connections. It is worth noting that without the thin-film layer, no suction channels exist to flatten the retina into contact with the

substrate.  Without this part of the device, the retina does not easily conform to the flat substrate thus causing some operational challenges.

*The Contact Issue*

Contact between the tissue and substrate is crucial for acquiring photocurrent signaling, but with the simplified platform, we have encountered difficulties in achieving perfect contact between the retina and graphene.  As shown in the retina structure, between the ganglion cell layer and the vitreous humor, there exists a layer of extracellular matrix called the inner limiting membrane (ILM), which has the function of preventing retinal detachment.  The thickness of the ILM in embryonic chicks was measured to be about 400 nm using atomic force microscopy[158].  For mice, the thickness was estimated to be less than 500 nm from electron micrograph images of the retina[159].  Unfortunately this thin and fragile membrane cannot be easily removed from the retina without severely disrupting the structural integrity of the tissue.  Instead, researchers have utilized an enzyme wash to soften this membrane such that it can be moved aside for patch clamping of RGCs[160].  This procedure is not easily compatible with our explant procedure so we have focused some of our measurements at the optic nerve head (ONH) because the ILM does not exist in this region of the tissue.  For some of our experiments, we have attempted a brief enzyme wash before placement into the device, but unfolding the retina after the wash can be difficult.  In addition, to resolve the issue caused by the ILM in regions outside of the ONH, we etched posts into the glass under the graphene using buffered oxide etchant for about 7 minutes.  These posts are intended to puncture the ILM to allow the graphene to better reach and contact the RGCs directly.

In addition to the ILM, an electric double layer could exist between the tissue and graphene formed by ions in the culture media.  An electric double layer is defined as a build-up

of counter ions on the surface of a charged substrate. Although well-developed theory has presented a clear description of this phenomenon[161,162], it is difficult to accurately determine the thickness of the layer known as the Debye length due to one unknown variable – the extracellular ionic concentration. Assumptions can be made to obtain an estimate of the Debye length, but this will not resolve the problem at hand. Essentially, this electric double layer can shield the electrical interactions between the retina and graphene thus inhibiting detection of the full signal.

To resolve these contact issues, we attempted a variety of approaches in the explant procedure. The first attempt was to implement extra manipulation of the explanted retina without changing the media cylinder design. As described in the introduction, the ONH is composed of RGC axons, which must be cut during explant. Due to this bundle of severed axons, the ONH protrudes from the inner surface of the retina such that the surrounding areas are incapable of contact with the graphene. By cutting out the entire ONH during the explant process, the tissue is no longer restricted from contact by the protrusion and sits flat under the media cylinder for better contact with graphene. Unfortunately, the trauma experienced during this procedure decreases the longevity of the tissue. Without the need to further flatten the tissue with the protrusion removed, media may simply be added to the cylinder allowing for a supply of fresh nutrients to the rapidly drying retina. The second attempt compensated for the loss of the suction channel by removing the PDMS retina well from the media cylinder and applying a gentle pressure from the top of the retina for flattening. We found that adding a smaller PDMS-filled 6 mm cylinder into the 8 mm cylinder provided gentle and even pressure to the top of the agar gel, and hence the retina. As a third attempt, the media cylinder and PDMS ring were removed altogether and the retina was explanted directly onto a small glass coverslip. Although this allowed for pressure to be easily applied from the top of the glass using a small weight, the

retina was found to dry very quickly without a fresh supply of media. All three attempts are depicted in Figure 3.3.

Option 1:
Fill cylinder with media
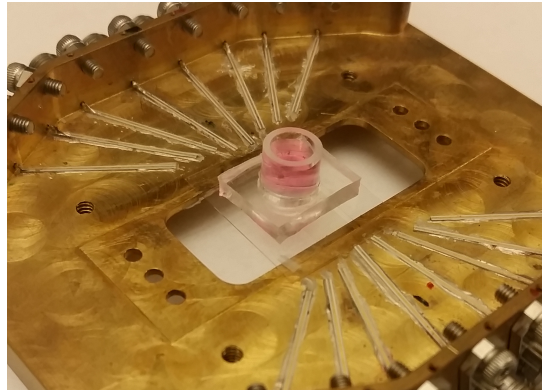
Option 2:
Apply pressure cylinder
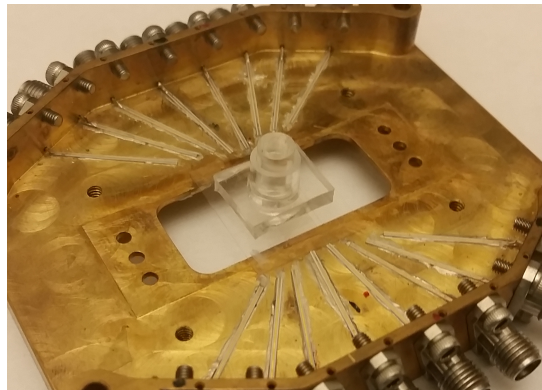
Option 3:
Explant onto glass coverslip
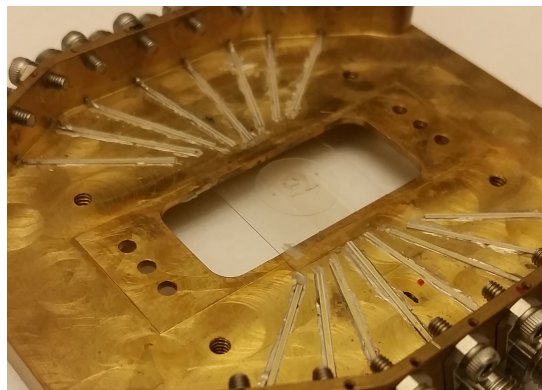
Figure 3.3 – Three attempts for improved contact between retina tissue and graphene

Thus far in our attempts, we have not determined the best solution yet but each option provides its own distinct advantages. The first option delivers media to the tissue for better long-term health while the third option provides firm but even pressure without media supply. As a sort of middle ground, the second option provides for gentle pressure and a little bit of moisture

from the agar gel to keep the retina alive during experiment. The first option is useful for electrical detection of signal in areas outside the ONH, possibly even single cell. In turn, the second is advantageous for extended experimental periods with a focus on detection of signaling within the ONH, while the third option may be used for short-term experiments probing around the ONH. Although we have not yet verified which of these options provides the best signal detection, we have recorded some signals from the retina thus far.

*Experimental Setup*

To assemble the device for the first two options, the PDMS ring was aligned over the graphene and gold electrodes. The whole retina tissue was explanted and unfolded onto the agar gel within the media cylinder. Excess pieces of the vitreous humor were removed, as was the thin membrane on the surface of the retina surrounding the ONH. For the first option, the ONH was carefully cut out of the whole retina tissue. The cylinder was then inverted and fit snugly into the PDMS ring. Media was added to the cylinder for the first option while a 6 mm cylinder filled with cured PDMS was lowered into the 8 mm cylinder for the second option. During experiment, if the retina is not in contact with the graphene, a micromanipulator was used to apply more pressure through the 6 mm cylinder as shown in Figure 3.4. As for the third option, the retina was explanted directly onto the glass coverslip and inverted for placement onto the graphene without the PDMS ring. A weight may be applied to the top of the coverslip for additional pressure if needed.
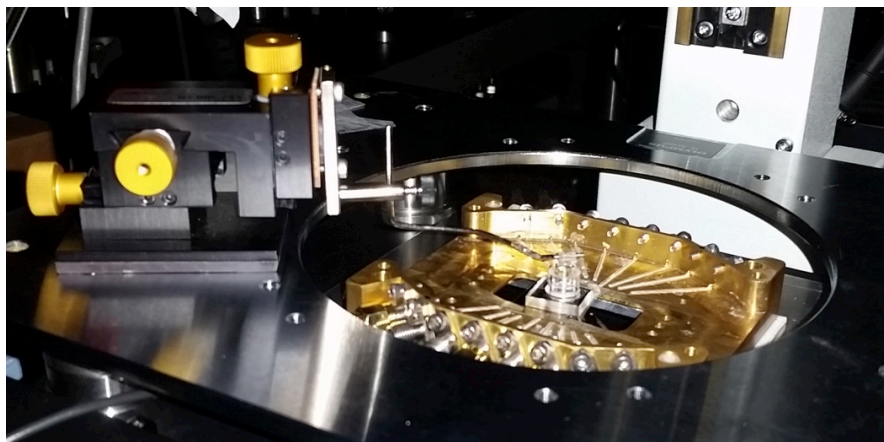
Figure 3.4 – Experimental setup of option 2 with micromanipulator for scanning and temporal photocurrent microscopy in whole retina tissue with simplified design

To demonstrate the validity of graphene for electrophysiology measurements of retina tissue, we utilized scanning and temporal photocurrent microscopy with the general setup shown in Figure 3.4. For our experiments, the graphene acts as a field effect transistor with the gold as source and drain electrodes. As the laser strikes the graphene, it excites electron-hole pairs that separate and travel to two gold electrodes under the effects of local potential thus inducing localized photocurrent[163]. At the graphene-gold interface, the bended band structure of graphene allows for efficient separation of the electron-hole pairs. In regions with graphene only, there is no bending in the band structure, thus the electron-hole pairs recombine easily. As previously described, cell signaling is characterized by the exchange of charged molecules between cells and across membranes. When retina is placed on graphene, the exchange of these molecules through ionic channels in the cell membrane creates a local electric field causing bending in the band structure and photocurrent signal.

This cell communication can be recorded over a region to create a map through scanning photocurrent or over a time period through temporal photocurrent at a single point. To achieve a higher success rate, at the initial stage we chose to focus most of our photocurrent testing at the

ONH of the retina.  This area of the retina (if not removed) contains the highest concentration of RGC axons and makes the closest contact with the graphene due to the protrusion in the tissue thus providing an opportunity to capture the strongest signals.  Moreover, to explore the feasibility of single cell signaling detection, we also conducted photocurrent tests on single cells outside the ONH.

Although we have found some signaling without perfect contact, we will continue to research our options to resolve this contact issue.  We expect that these contact issues will be resolved in the full device by flattening the retina using the suction channel in the thin-film layer.  With this capability, we expect much better contact between the tissue and graphene layer, thus stronger signal and easier manipulation.  In the following, we describe our obtained results in validating the graphene-based assay as a promising approach for electrophysiology through both scanning and temporal photocurrent microscopy based on the simplified platform and retina tissue.

### 3.3 Measurement results

As stated previously, photocurrent measurements may be recorded over a region of graphene or at a single point during a certain time period.  Retina from B6129SF2/J and CX3CR1-GFP mice were injected *in vivo* with Alexa Fluor-594 CTB two days before sacrifice for full RGC uptake and axonal transport.  Thus far, we have not found any evidence that the type of mouse has an impact on the photocurrent microscopy results.  As discussed in Chapter 2, CTB is an active uptake, active transport neural tracer specifically for RGCs.  When exposed, healthy RGCs uptake the CTB into their somas and transport the tracer along their axons to their axon terminal in the brain if intact.  During explant, the axons were severed at the optic nerve head and the bulk of the vitreous humor was detached and discarded.  With the vitreous humor

entirely removed, the structure and organization of the RGC layer and ONH was easily visible

after explant and placement into the device as shown in Figure 3.5.
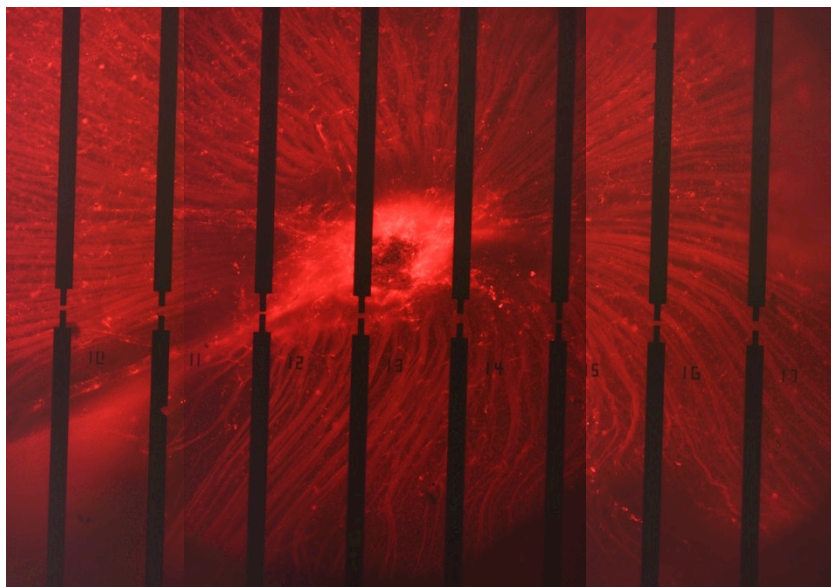


Figure 3.5 – Fluorescent imaging compilation of retina injected *in vivo*
with CTB after explant onto the device. Lateral distance between
electrodes is 200 μm

With the ONH and RGCs fluorescently labeled, comparisons can be made between our

CTB images and scanning photocurrent microscopy. First, we focused our studies at the ONH

where both the CTB and scanning photocurrent images produced strong signals. Again, retina

from B6129SF2/J mice were injected *in vivo* with CTB two days before sacrifice and explanted

onto a device before imaging. Note that no light stimulation was provided to the retina during

scanning photocurrent microscopy. All experiments were completed in a dark room unless

otherwise stated. As shown in Figure 3.6, we found strong scanning photocurrent signal with an

amplitude of about 1 nA that correlates with the region of the ONH as shown in the bright field

and fluorescent images. While with scanning photocurrent, we mapped a large electric field

generated by the ONH, with temporal photocurrent, we can focus at one point and detect

photocurrent over a time period to examine local electrical potential and how it changes with

time. From these tests, we may be able to pinpoint single cells and further investigate their behavior, much like the patch-clamping method.
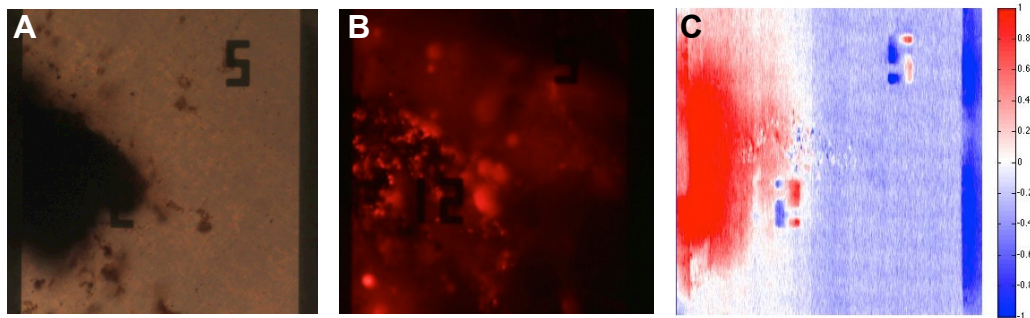


Figure 3.6 – (A) Bright field, (B) fluorescent, and (C) scanning photocurrent microscopy of the optic nerve head. Lateral distance between electrodes is 200 μm. Photocurrent scale is nA

For temporal studies of the retina, researchers patch-clamp a cell and expose the tissue to a variety of lighting conditions for stimulation. The response to light stimulation is then recorded via the electrode inserted into the patch-clamping pipette. Depending on the type and strength of electrical response, it is possible to classify the cell type. Hartline first distinguished the three major types of RGC response to light stimuli in 1938[164]. During experiments, he found that some of the RGCs exhibited bursts of activity to light onset, some to light offset, while others to both on and offset. These bursts of activity or outputs are categorized into three groups: ON, OFF, and ON-OFF cells[12]. It was also discovered that these RGCs are tiled throughout the ganglion cell layer, ON cells surround OFF and vice versa[165]; as well as one type of ON-OFF cell, called local edge detectors, is responsible for spatial detail recognition[166]. In addition to white light, mice are particularly sensitive to light with wavelengths less than 600 nm thus green, blue, and ultraviolet but not red, yellow, or infrared[167]. As such, mice retina produce a similar ON and OFF response to green and red light, respectively, as they do for onset and offset of white light. By exposing the retina to red and green light, we may find a different response than that observed in white light onset and offset similar to that from other probing techniques[168].

57

If we look at the input to the three types of RGCs, some receive signals from other light sensitive cells like photoreceptors while others are intrinsically light sensitive and need no input. In the non-light sensitive RGCs, light detected in photoreceptors is passed on as a signal through a synapse with amacrine or bipolar cells that then input the signal to the RGCs[169]. On the other hand, melanopsin-containing RGCs are light sensitive neurons that have shown sustained ON response to light stimulation for up to 10 hours[170]. While dyes or morphology have been utilized to determine the RGC type[171–175], recording the output signals via electrophysiology is the most widely accepted approach. Since the discovery by Hartline in 1938, numerous groups have applied electrophysiology recordings from patch clamping[176–180] or microelectrode arrays[181,182] to determine the type of RGCs based on the response from light stimulation. Tian et al. was able to determine ON, OFF, and ON-OFF RGC response to light stimulation with a readily-available microelectrode array[152]. Overall, determining a cell type can be quite complicated within the retina due to the wide variety of cell response and signaling cascades.

For our purposes we will focus on the immediate response to red and green light onset and offset in an attempt to categorize cell types. Note that graphene responds to all wavelengths of light, but responds at a much lower level to red and green light than white light. Thus for our temporal photocurrent microscopy experiments, we stimulated the retina with red and green light in order to better distinguish retina response from graphene's intrinsic photo-response. For this experiment we focused our attention just outside the nerve head and chose a point with strong scanning photocurrent for our temporal studies. Results of two test points from one retina are shown below in Figure 3.7. For this retina, we chose to utilize option 3 to provide good contact with graphene in the experimental setup.
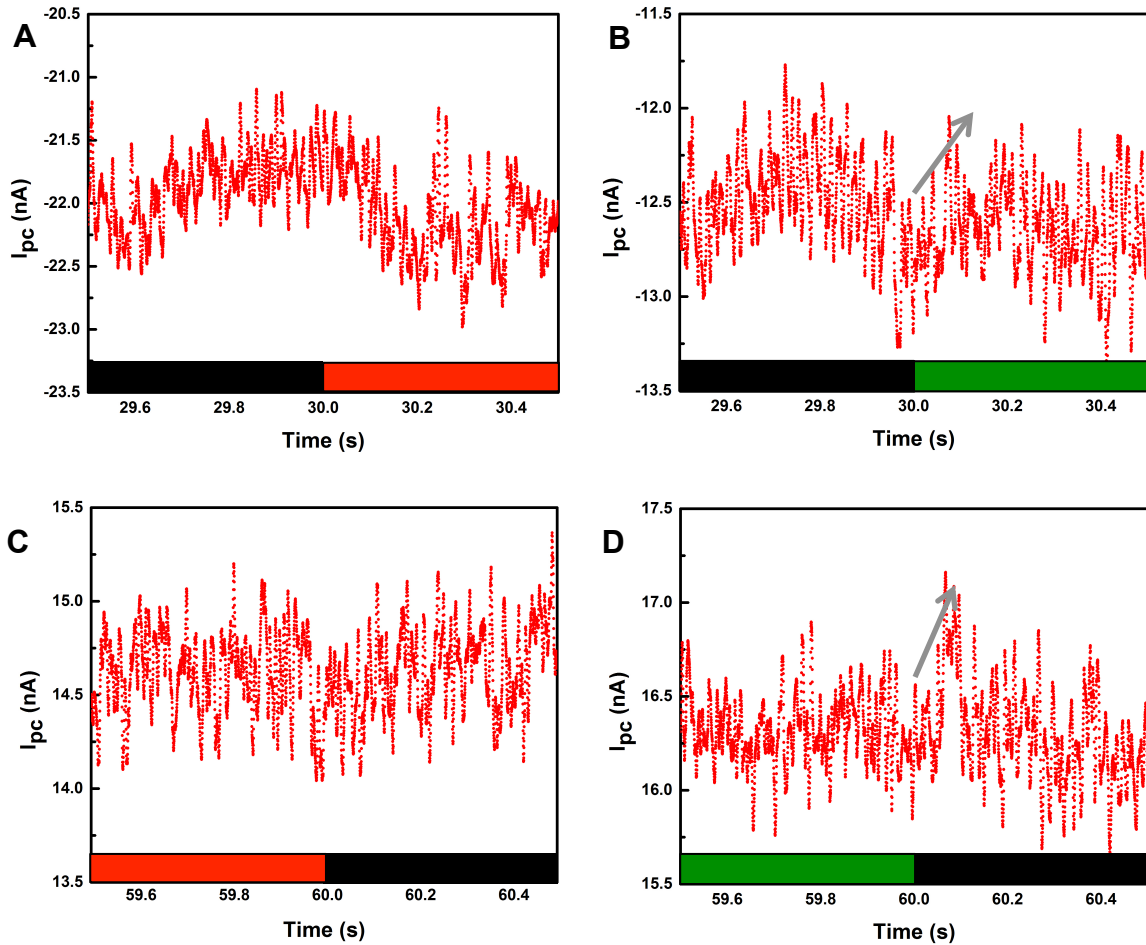
Figure 3.7 – Temporal photocurrent during light stimulation due to the onset and offset of red or green light as depicted by the bars at the bottom of the graphs. Note that mice are only sensitive to green light and not red light. (A)-(B) Point 1's response shows no obvious change in photocurrent at the onset of red light compared to a slight increase in current due to the onset of green light. (C)-(D) Point 2 shows a response to the offset of green light, but no response to the offset of red light. Grey arrows depict trends in photocurrent response after green light onset or offset

As shown in Figure 3.7, the response changes at different points due to red or green light onset and offset. Figure 3.7A shows no immediate change in the photocurrent activity due to red light onset as expected since mice are not sensitive to red light. Subtle, but random dips in the photocurrent activity are due to noise and drift in the system and do not correspond with the onset of red light. Figure 3.7B, however, suggests that we evoked a response due to an immediate change in activity when the retina was exposed to the onset of green light. Note that the negative scale in Figure 3.7A&B is caused by the inversion of current between the two

electrodes surrounding the stimulation point. Similarly at a second point we also see a response to the offset of green light in Figure 3.7D, but no response to the offset of red light in Figure 3.7C. Due to the immediate response to green light onset and offset, we believe that the first point is signal from an ON cell and the second is from an OFF cell. One setback in the experiment that we have encountered is inconsistency in responses from a single point. Without perfect contact between tissue and graphene, we suspect that multiple cells may be contributing to these points causing a mixture of responses. More recordings and data processing may give us the opportunity to better narrow down the exact cell types we are probing. But before we continue we must investigate whether or not these responses are actually coming from the tissue.

To ensure our scanning and temporal photocurrent results were due to cell signaling in the live tissue, we also tested a retina from a mouse perfused with fixative. Fixing the retina causes cross-linking between the fixative and proteins thus stabilizing the structures and functions, essentially the tissue is frozen in time allowing for long-term manipulation or imaging[183]. After a lethal dose of sodium pentobarbital, mice were transcardially perfused with 50-100 mL of 1X PBS followed by 100 mL of 4% paraformaldehyde (PFA). Following perfusion, eyes were enucleated and stored in 4% PFA at 4°C until use. Utilizing the same procedure as live retina, the fixed retina was removed from the eye and flattened onto the agar gel. Relief cuts were made for better flattening of the tissue onto the graphene.

Scanning photocurrent microscopy was performed over two regions of the ONH, which was split due to the relief cuts as shown in Figure 3.8. Temporal photocurrent was performed at a point within the ONH at each of the two regions with light and dark intervals. As shown in the figure, no significant scanning or temporal photocurrent signal was detected in the fixed retina. Due to cross-linking during fixation of the tissue, no cell signaling occurred at the ONH thus the

lack of scanning photocurrent mapping. As light was turned on and off for temporal testing, the fixed retina showed no obvious changes in activity, only slight drifts in the background noise of the system. Note the large difference in the baseline temporal photocurrent scale between live tissue at over 10 nA and fixed tissue at only 10 pA.
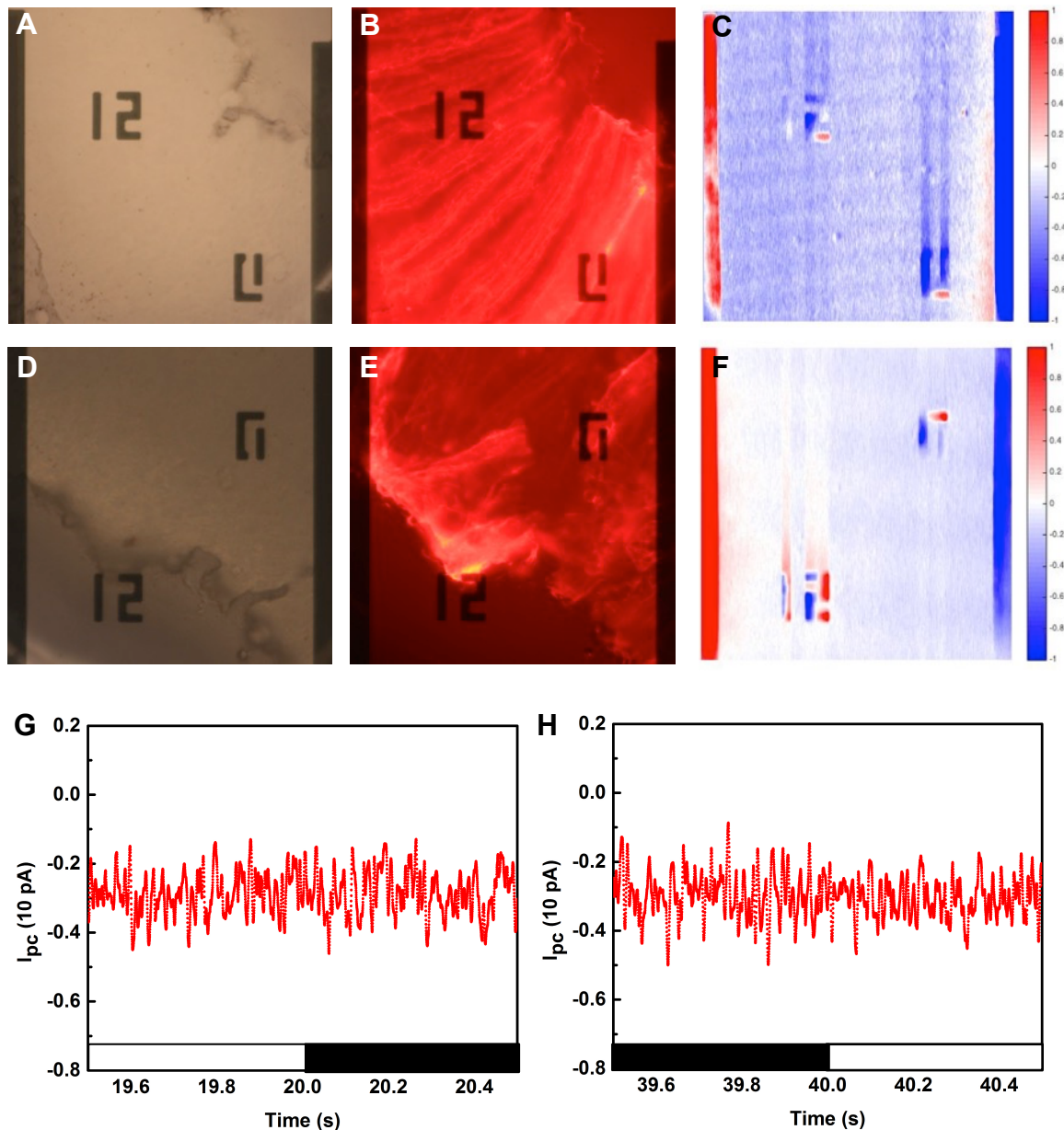


Figure 3.8 – (A) Bright field, (B) CTB, and (C) scanning photocurrent at one part of the nerve head. (D) Bright field, (E) CTB, and (F) scanning photocurrent at another section of the nerve head. Lateral distance between electrodes is 200 μm. Scanning photocurrent scale is nA. (G) and (H) Two temporal photocurrent signals from points within the fixed retina nerve head due to light onset and offset

Comparison between the live and fixed retina demonstrates that the photocurrent detected was from cell signaling within the live tissue. Overall, these samples provide promising evidence and a first step toward photocurrent microscopy using a single-layer graphene-based optoelectronic probe.

**3.4 Summary**

Our motivation for integrating graphene into the Retina-on-a-Chip microfluidic platform provides the opportunity for localized chemical and electrical stimulation and sensing within a single device. Although we are still in the initial stage of design and implementation, the successful photocurrent detection already demonstrates strong potential as a promising technology for neuroscience. Our initial results show the ability to map photocurrent signal at the optic nerve head as well as probe cellular response through temporal photocurrent tests. Though more results and samples are required for full validation of the platform and technique, we believe that the unique advantages of this technology could lead to a powerful tool for exploring the important neurobiological processes in the brain and retina.

CHAPTER 4


**THIN-FILM LAYER PDMS TECHNIQUES**


**4.1 Motivation**

Over the years, imaging capabilities have slowly and steadily improved, providing opportunities to better visualize minute details and processes. Advanced optical imaging techniques, however, have limited working distances, which pose strict limitations to the design of microfluidic platforms that need to be compatible with high-resolution imaging. For example, it is necessary that the microfluidic construct is thin enough such that the biological processes of interest occur within a couple of hundred microns from the objective lens. In fact, since confocal microscopy not only allows for high-resolution imaging of a single cell but also 3D visualization by compiling stacks of horizontal sections, thinner microfluidic constructs allow for a larger probing depth. Confocal microscopy is widely used in biology including studies of retina by visualizing cell morphology throughout the layers of the retina. Therefore, in order to better utilize confocal microscopy for retina studies, we must adapt our microfluidic platforms for high-resolution imaging by reducing the thickness of the microfluidic layers.

In addition to meeting the requirements for confocal microscopy, thin PDMS layers have a variety of applications in microfluidic devices. For example, thin PDMS layers with open channels or holes have been aligned and stacked to create intricate 3D geometries including knots[184]. In this chapter, we describe our efforts to create thin PDMS constructs necessary for confocal imaging of our platforms. First, we discuss some of the current methods for creating thin PDMS layers along with methods for revealing open channels or holes.

In 2000, two separate research groups published methods for fabricating thin PDMS layers for three dimensional microfluidic devices. Jo et al. described the first sandwich molding method including approximately 100 μm wide channels[132]. Briefly, liquid PDMS is added to a mold followed by a transparency film. The assembly is placed under pressure using a clamp before curing in an oven. Once cured, the transparency film with PDMS attached can be removed from the mold. The PDMS is then bonded to glass or another PDMS piece and the transfer film removed to reveal open channels. Complex three-dimensional microchannels can be formed in a single device by aligning and stacking more thin PDMS layers. Similarly, Anderson et al. was able to create three-dimensional geometries but instead utilized molds with alignment guides to sandwich the liquid PDMS[184]. This technique also allowed for fabricating thin PDMS layers with molded features on both sides as well as open holes. Later in 2004, Hsu et al. improved upon the sandwich molding methods by including a fluoropolymer polyethylene sheet as the transfer film[133]. As they report, the surface adhesion between the sheet and PDMS is stronger than that between the PDMS and mold, but not as strong as that adhesion between PDMS and glass after oxygen plasma treatment. Hsu's sandwich molding method is depicted in Figure 4.1[133].
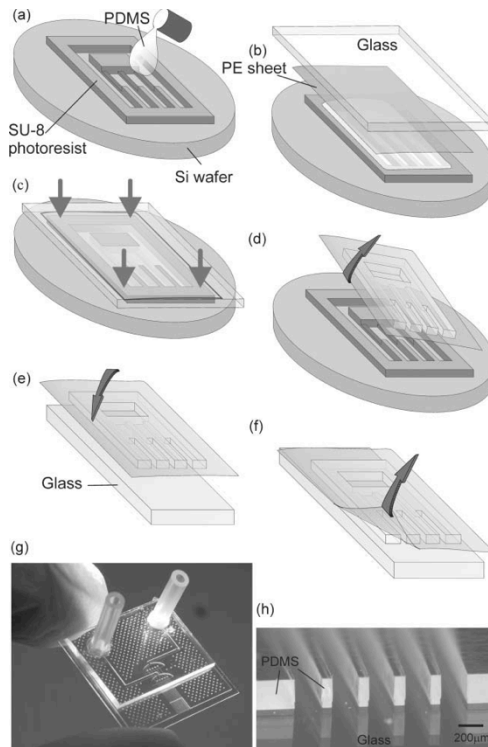
Figure 4.1 – Step-by-step fabrication of thin-film PDMS layers from Hsu et al.[133] A silicon wafer with SU8 features is used as the mold and a fluoropolymer-coated polyester sheet is used to transfer the thin-film layer

As shown by these three articles and Figure 4.1h, the sandwich molding method is able to reveal open channels or holes, but they are not the only techniques to achieve this. Other reported options for creating thin PDMS layers with open features include spin-coating and selective ripping. Kartalov et al. first described the spin-coating technique as adding liquid PDMS to a mold which was then spun to a layer shorter than the features[185]. Similarly, two other groups followed with their own utilization of spin-coating thin PDMS layers[186,187]. However, this technique does have a downfall as recognized by all three authors: the spun PDMS frequently covers the tall features intended to create open through-holes in the PDMS layer. Kartalov et al. simply repurposed this thin membrane above the channels as a septum, a type of 'destructive engineering' that fails under too high of a pressure[185]. Kang et al. in turn removed

65

excess PDMS covering the features by blowing gas at the mold, but this technique is fairly low-throughput[187]. Other techniques instead focus on removal of PDMS after curing to reveal open features like selective ripping or patterning. Childs and Nuzzo first demonstrated this technique by ripping away the top layer of a PDMS piece that had been attached to glass or bulk PDMS to reveal open PDMS features on the substrate[188]. Thangawng et al. expanded on this idea by forming a PDMS stamp to selectively remove bonded regions of a thin PDMS membrane from a substrate[189]. Similarly, Mosadegh et al. used a PDMS stamp to selectively rip a thin PDMS membrane but with the added option to reveal open through-holes above microfluidic channels at high-throughput[190]. Although the mechanical failure of PDMS allowed for open channels or through-holes, the remaining features had defects and irregularities due to the unpredictable nature of tearing.

Is there a technique that consistently and efficiently reveals clean and open through-holes in thin PDMS layers on the scale of approximately 100 μm? In this chapter we will explore novel fabrication techniques for this purpose. As described in Chapter 2, we first employed the sandwich molding method for fabrication of the thin-film PDMS layer, which contains the microfluidic channels with open through-holes. Unfortunately, we encountered some pitfalls when fabricating thin-film PDMS using this method, specifically the lack of revealing clean open through-holes. The problem was examined and analyzed, and solutions were investigated to provide more efficient and repeatable results. Our attempts, which will be outlined and discussed in this chapter, included drilling, punching, and laser-cutting holes in the thin-film PDMS layer. Note that these options for creating microscale holes in thin PDMS layers are not well documented. In addition to exploring solutions for thin-film PDMS fabrication, we also studied the physical phenomenon that causes these complications.

## 4.2 Basic fabrication

As mentioned previously, Jo et al. introduced the idea of sandwich molding PDMS into thin-film layers with open channels[132], and Hsu et al. improved upon the technique by utilizing a fluoropolymer-coated PE sheet[133]. First we will describe how we used these techniques to produce a thin-film PDMS layer with the goal of revealing open through-holes above microfluidic channels. With the general fabrication technique covered, we will then delve into some of the problems that were encountered using this method. Following a mathematical model of squeeze film flow, the complications are further analyzed in order to better understand the limiting factors.

*Sandwich-Molding Method*

Using either the SU8 or plastic mold for the Retina-on-a-Chip platform, a small amount of liquid PDMS was added to the center of the two-layered features and a piece of fluoropolymer-coated sheet was placed on top. The PDMS was degassed under vacuum for about 30 minutes. Any remaining bubbles under the sheet after that time were removed by gently pushing the bubbles to the edge of the mold using a flat edge. Next, a glass slide was pressed down atop the sheet over the features by adding weights and the entire assembly was baked for about six hours at 70°C. Once cured, the PDMS layer attached to the sheet was gently removed from the mold and bonded via oxygen plasma treatment to a glass coverslip. To strengthen the bond, the coverslip with PDMS was baked for one more hour before very carefully removing the fluoropolymer-coated PE sheet.

*Difficulties Encountered*

Though the two groups referenced above have successfully revealed open channels of at least 100 μm wide, we stumbled upon difficulties in consistently yielding open 100 μm diameter

holes in thin-film PDMS. As shown in Figure 4.2, while some holes were opened after removal of the fluoropolymer sheet, others remained covered with an ultra-thin layer of PDMS. After further inspection, we found that all holes that were revealed open were torn at the edges. This indicates that the liquid PDMS was never fully squeezed out from between the mold and the fluoropolymer sheet during the sandwich molding process. Instead, an ultra-thin layer of PDMS cures between the two surfaces but is ripped away when the fluoropolymer sheet is removed. To resolve this layer, we attempted adjusting the parameters of the sandwich molding, but none were able to completely squeeze out the liquid PDMS. We estimated the thickness of this ultra-thin layer to be about 2-4 μm thick by measuring the distance between focal planes of the top of the PDMS and the top edge of the hole.
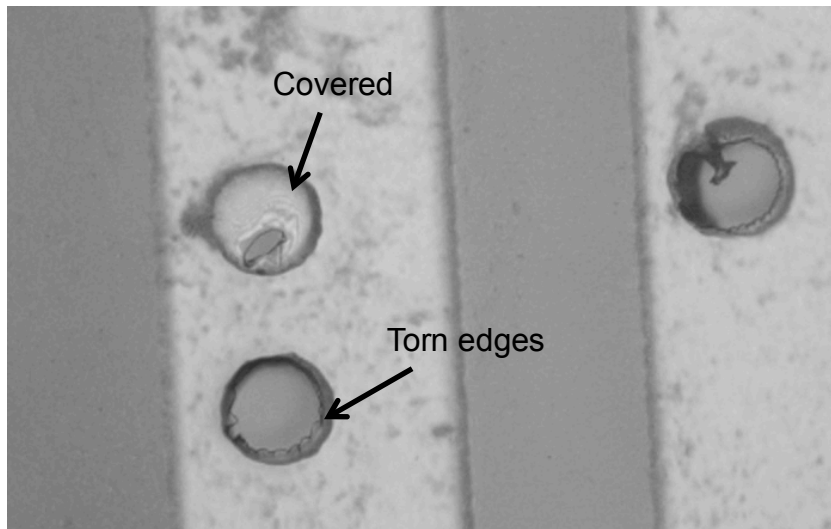


Figure 4.2 – Sandwich molding did not always reveal clean and open through-holes. Some holes were largely covered by a thin layer of PDMS while others showed tearing at the edges

To better understand our difficulties, a thorough literature survey of the sandwich molding method was conducted to determine if other groups struggled with this problem. Unfortunately, the literature search simply revealed wide discrepancies in the pressure applied and absolutely no mention of tearing a thin PDMS membrane covering through-holes. Although

it is unclear as to how they apply pressure to the assembly (via a clamp or weights), an article from the Whitesides group claims a very high pressure of 1000 kPa (100 g/mm$^2$) as sufficient to remove excess PDMS from between the molds[184]. Jeon et al. also utilized a sandwich molding method for PDMS but stated a pressure of only 1 psi (~6.9 kPa) as sufficient to squeeze out the PDMS from between the molds[191]. Interestingly, another article from Whitesides group declared 10-50 kPa as the pressure required[49]. Thus far, microfluidic fabrication literature has not addressed these inconsistencies of pressure values or the relationships that govern this squeezing action. In this following section we will analyze the sandwich molding technique and required pressures to resolve this gap in fabrication techniques.

*Squeeze Film Flow Modeling*

Below in Figure 4.3 is a depiction of our sandwich molding method with the problem area indicated by the red oval. As described by others, if an appropriate amount of pressure is applied to the assembly, the liquid PDMS from between the transfer film (PE sheet) and the tallest SU8 feature should be completely removed. The SU8 is shown as two layers in Figure 4.3, the channel layer and post layer, atop the silicon wafer. For simplification of modeling, we will assume the channel and posts are each 25 μm thick layers of SU8. Note that the cartoon is not to scale and only a local area is depicted.
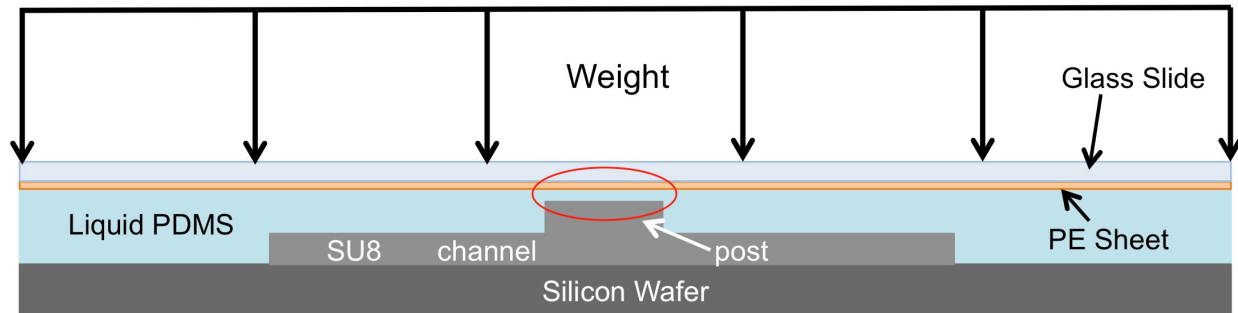
Figure 4.3 – Cartoon depiction of the sandwich molding method from side view. Liquid PDMS is applied to a silicon mold with SU8 features that is then covered with a fluoropolymer polyethylene (PE) sheet. A glass slide is added followed by weight to apply pressure. The assembly is then baked in an oven to cure the PDMS. The red oval indicates the problem area where liquid PDMS is not completely squeezed out from between the PE sheet and SU8 features. Not to scale

If we focus on the problem area and utilize the experimental dimensions and parameters, we can model this fluid flow as squeeze film flow. For squeeze film flow, the thickness of the fluid under normal pressure must be much smaller than the width. Here, our thickness is only 2-4 μm compared to the size of the through-hole post that is 100 μm diameter. The mathematical model begins as a simplification of lubrication theory. Note that for our experiments, there is no parallel velocity of the top plate relative to the bottom plate, only perpendicular velocity in the negative z-direction. The geometry of squeeze film flow is shown below in Figure 4.4.
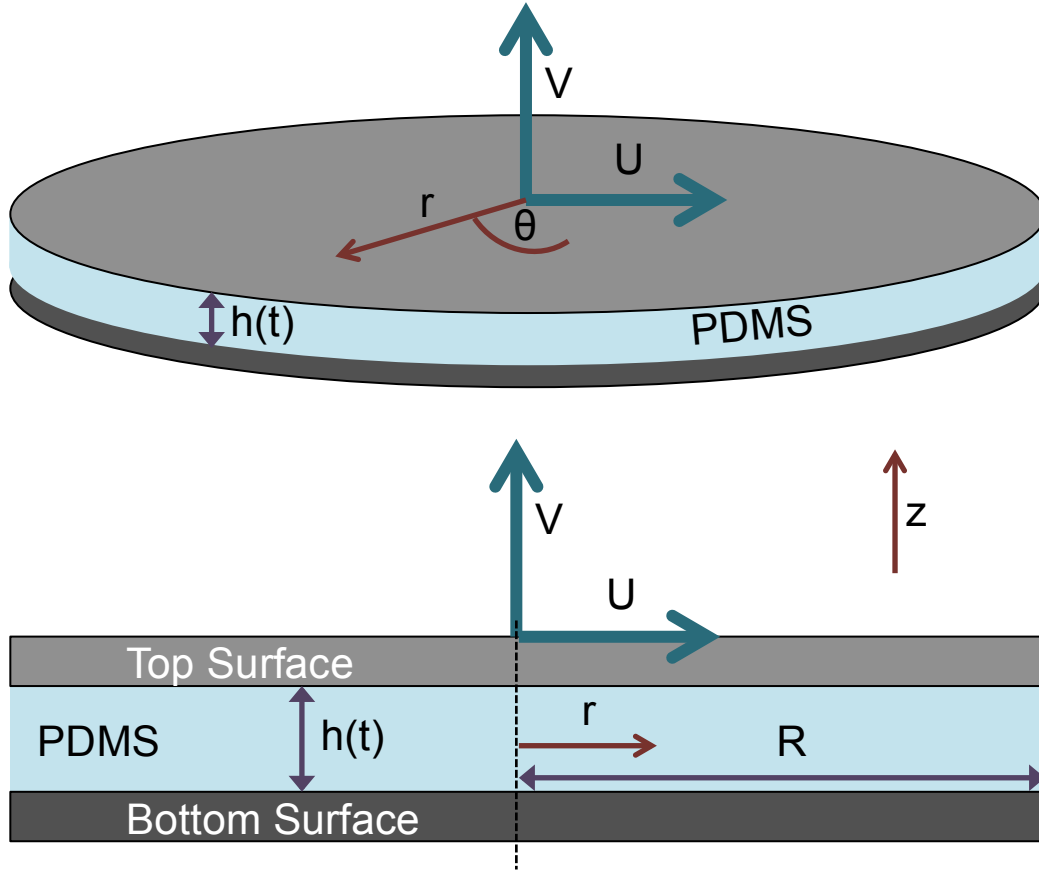
Figure 4.4 – Geometry of squeeze film flow. For lubrication theory to apply, the thickness of the fluid between two surfaces, h, must be much less than the width of the surfaces, R. Note that squeeze film flow assumes the surface only moves perpendicular to the opposite surface without a parallel velocity, thus U=0. For our purposes, the velocity of the top plate will only be in the negative z-direction or toward the bottom plate

Applying the continuity and Navier-Stokes equations, we can model the thin-film fluid flow using the Reynolds equation[192,193] as shown below.

$$\frac{\partial}{\partial t}(\rho h) + \frac{1}{2}\frac{\partial}{\partial x}(\rho h U) = \frac{\partial}{\partial x}\left(\frac{\rho h^3}{12\mu}\frac{\partial P}{\partial x}\right) + \frac{\partial}{\partial y}\left(\frac{\rho h^3}{12\mu}\frac{\partial P}{\partial y}\right) \quad (2)$$

Converting to cylindrical coordinates, assuming constant density, and setting the parallel velocity, $U$, to zero gives

$$\frac{1}{r}\frac{d}{dr}(rq_r) + \frac{dh}{dt} = 0 \quad (3)$$

where $q_r$ is the radial flow rate:

$$q_r = -\frac{h^3}{12\mu}\frac{dP}{dr} \qquad (4).$$

Note the assumptions made thus far: (1) incompressible, isoviscous, isothermal fluid; (2) velocities are steady; (3) inertial effects are negligible; (4) rigid, nonrotating plates; and (5) no air bubbles. At the radial boundaries, we assume fluid can freely flow outward. If we define

$$V = \frac{dh}{dt} \qquad (5)$$

and integrate Equation (3), we achieve a relationship for the radial flow rate:

$$q_r = -V\frac{r}{2} \qquad (6).$$

A second integration of $q_r$ with substitution of Equation (4) reveals a relationship for pressure across the radius of the plates:

$$P(r) = P_a - 3\mu\frac{V}{h^3}(R^2 - r^2) \qquad (7)$$

where $P_a$ is the ambient pressure at the plate boundary $R$. For our application, a force is applied to the top plate causing the squeeze film flow and can be given by

$$F = \int_0^R 2\pi r * \{P(r) - P_a\}\,dr \qquad (8).$$

Integrating with substitution of Equation (7) leads to a relationship for the force applied:

$$F = -\frac{3\pi\mu R^4}{2h^3}V = -\frac{3\pi\mu R^4}{2h^3}\frac{dh}{dt} \qquad (9).$$

To determine a final height due to the force applied, we can integrate again to achieve a relationship for the film thickness based on time, radius, force, and initial thickness $h_0$.

$$h = h_0\left(1 + \frac{4}{3}\frac{Fh_0^2}{\pi\mu R^4}t\right)^{-1/2} \qquad (10)$$

Note a few hypothetical situations that may be applied to Equation (10): as time approaches infinite, the film thickness $h$ should reach zero, but if the radius $R$ approaches infinite, the film thickness should remain at the initial thickness. Similarly a very large force should also resolve the film thickness between the plates. Before we can use this model to verify our own squeeze film flow results from experiment, we need to evaluate some of the parameters, specifically force and viscosity.

First, we examine the ratio of forces at different regions to determine which has the strongest effect on film thickness. We will designate three regions: the wafer (the blank areas of silicon wafer), the channels (the first layer of SU8), and the posts (the second layer of SU8). Assuming the film thickness at the post is 1 μm giving a thickness of 26 and 51 μm at the channel and wafer layer respectively. Using Equation (9), the ratios of force are

$$\frac{F_c}{F_p} = \frac{\dfrac{A_c^2}{h_c^3}}{\dfrac{A_p^2}{h_p^3}} \approx \frac{380000}{8100} \approx 47 \tag{11}$$

and

$$\frac{F_w}{F_p} = \frac{\dfrac{A_w^2}{h_w^3}}{\dfrac{A_p^2}{h_p^3}} \approx \frac{1.5 \cdot 10^8}{8100} \approx 1852 \tag{12}.$$

Thus, the force acting on the whole wafer is much larger than those acting on either the posts or the channels. To simplify our modeling, we will ignore the force effects of the channel since the wafer experiences a much stronger force than both the channels and the posts. In order to evaluate the film thickness at the post, we must determine a relationship between the force on the wafer and the force on the 36 posts. First, we know that the top surface moves at the same velocity for both the wafer and the post region:

$$\frac{dh}{dt} = -\frac{2}{3}\frac{h_p^3}{\pi\mu R_p^4}\frac{F_p}{36} = -\frac{2}{3}\frac{h_w^3}{\pi\mu R_w^4}F_w \qquad (13).$$

We can also assume that the total force applied to the system is split between the force on the posts and on the wafer

$$F_p + F_w = F_{total} = 4\ lb \qquad (14).$$

Using Equations (13) and (14), we find the forces at each region are dependent upon the film thickness at both regions as well as the radii:

$$F_w = \frac{F_{total}}{1 + 36\left(\frac{h_w}{h_p}\right)^3\left(\frac{R_p}{R_w}\right)^4} \qquad (15)$$

$$F_p = \frac{36\,F_{total}\left(\frac{h_w}{h_p}\right)^3\left(\frac{R_p}{R_w}\right)^4}{1 + 36\left(\frac{h_w}{h_p}\right)^3\left(\frac{R_p}{R_w}\right)^4} \qquad (16)$$

Note that the height of the wafer is simply the height of the post plus 50 μm. A simple calculation shows that the force at the post only balances the force at the wafer for a post film thickness of 5.3 femtometers. This means that the wafer carries the large majority of the force for the entire relevant range of the model. While the posts physically restrict movement of the top surface toward the wafer, the posts have little effect on the overall fluid flow between the transfer film and mold. Thus, we will focus our modeling on the film thickness above the wafer.

Now that we have a relationship for the applied force, we also need to determine a relationship for viscosity. Assuming a constant viscosity is unrealistic for our case because the viscosity of mixed PDMS increases with time as it cures. Given time points for viscosity, we can determine an equation for viscosity with respect to time. Additionally, the viscosity of PDMS may also be a function of shear rate. PDMS is a viscoelastic, non-Newtonian fluid and does not behave like Newtonian fluids under certain conditions, like varying shear rate. For low

molecular weight (MW) PDMS, the viscosity is largely constant with shear rates less than 10,000 $s^{-1}$. For high MW PDMS (>10,000 g/mol), the viscosity is constant until a critical shear rate is exerted. At this point, the PDMS demonstrates shear thinning behavior, or the viscosity decreases as the shear rate increases. As the MW increases, the critical shear rate decreases. To better model our thin-film thickness, we need to determine whether or not viscosity is dependent on shear rate for our PDMS.

Given the initial viscosity of mixed PDMS and density, we can determine the kinematic viscosity of PDMS. From this value, our mixture of PDMS is considered high MW, thus there is a critical shear rate[194]. Based on values provided by the manufacturer (Dow Corning, Auburn, MI), the critical shear rate can be estimated to be about 1,000 $s^{-1}$ at which point the PDMS transitions from constant viscosity to shear thinning. Now that we know the critical shear rate of PDMS, we must determine if our case actually reaches that value. To calculate shear rate, we first evaluate the average velocity of fluid exiting the region above one through-hole post.

$$V_{avg} = \frac{1}{2}\frac{R}{h}\frac{dh}{dt} \tag{17}$$

Assuming laminar flow, we can create a relation for the parabolic velocity profile

$$u(y) = 2V_{avg}\left(1 - \frac{y^2}{h^2}\right) = \frac{R}{h}\frac{dh}{dt}\left(1 - \frac{y^2}{h^2}\right) \tag{18}$$

where $y$ is the distance from the center of the film thickness. Taking the derivative with respect to $y$ gives

$$\frac{du}{dy} = \frac{dh}{dt}\frac{R}{h}\left(\frac{-2y}{h^2}\right), \tag{19}$$

which defines shear rate. By inspection, the shear rate reaches a maximum at the edges of the film thickness, $y = -\frac{h}{2}, \frac{h}{2}$. Substituting Equation (9) results in a linear relationship between maximum shear rate and film thickness:

$$\left|\frac{du}{dy}\right|_{max} = \frac{2}{3}\frac{F}{\pi\mu R^3}h \tag{20}.$$

Setting our maximum shear rate at 1,000 s$^{-1}$, we find that the PDMS viscosity is constant under a height of 67 μm. Note that for squeeze film flow, the film thickness height must be much less than the width of the feature, thus we can assume for our case, the viscosity is constant with respect to shear rate.

Although this greatly simplifies our model, the viscosity is still dependent on time and the curing effect must be taken into account. An accepted relationship for the curing effect models the viscosity as an exponential function with respect to time. Given the initial viscosity of mixed PDMS at 3500 cP and a pot life of 1.5 hr (the point at which the viscosity doubles), we can determine the best-fit equation:

$$\mu(t) = 3500 \exp\left(\frac{ln\,2}{5400}t\right) \tag{21}.$$

For simplicity, this equation is valid at room temperature. Additionally, our own fabrication attempts at room temperature revealed similar results (2-4 μm) as the oven-cured PDMS film thickness.

Now that we have an equation for force and viscosity, we can model our squeeze film flow. Since both force and viscosity are now dependent on time, we utilize numerical integration in MATLAB using the ode45 function to solve the following differential equation[195]:

$$\frac{dh_w}{dt} = -\frac{2}{3}\frac{h_w^3}{\pi}\frac{F_w}{\mu(t)R_w^4} \tag{22}.$$

Given an initial thickness between the top surface and wafer of 70 μm (20 μm at the post) and assuming 30 minutes of degassing before pressure is applied, the height of the film thickness is modeled as shown.
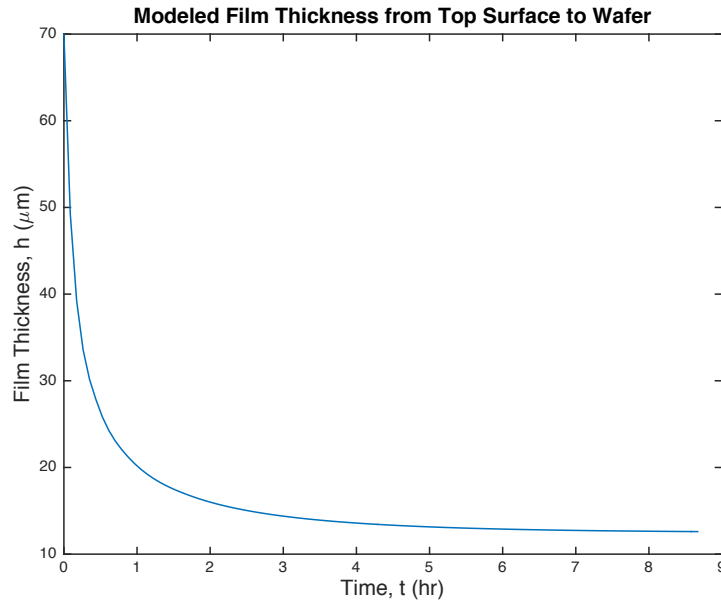


Figure 4.5 – Using Reynolds equation and numerical integration in MATLAB, the PDMS film thickness between the top surface and wafer is plotted as a function of time. Note that both force applied and viscosity are also dependent on time, thus the need for numerical integration. At about 7 hours the film thickness reaches steady state at a thickness of 12.6 μm

The modeling in Figure 4.5 shows that the film thickness actually decreases past the height of the post to about 12.6 μm. Essentially, if the post did not physically restrict the top surface, the PDMS film would reach about 12.6 μm within about 8.5 hr over the entire 3-inch wafer. So, why is there still a residual of PDMS film left over the post region?

PDMS is a viscoelastic, non-Newtonian polymer with long molecular chain lengths. As viscosity increases, the polymer chains begin to crosslink and may become entangled with one another. With increasing entanglement at microscopic levels, the PDMS film is less likely to be removed from between two surfaces under pressure, thus a residual is left. Although the

modeling here includes viscosity and force applied, the complex molecular phenomena are ignored. Through this analysis, we have shown that for our case, we cannot evaluate a force or a time at which the film thickness is completely resolved without accounting for the molecular physics of polymer chains.

However, we can make a few conclusions about the modeling and its relevance to our fabrication procedures. Within the first hour of pressure, the film thickness decreases to less than 25% of the original height. Thus, the limitation on time is dependent on complete curing of the PDMS, not film thickness. Similarly, the radius of the feature is a strong player in the model as shown by Equation (22). Because the radius of the wafer is so much larger than the radius of the posts, the wafer carries much of the weight applied. This is advantageous for long-term fabrication procedures to avoid severe degradation of the SU8 features. While this modeling has presented interesting fluid flow characteristics for our own fabrication, our initial problem still needs a solution. Thus, to further our own research endeavors, we must find a new technique for creating through-holes in thin-film PDMS.

## 4.3 Alternative approaches for through-hole fabrication

Now that we have examined the limitations of sandwich molding, we need to figure out an alternative approach to creating clean, open through-holes in the thin-film PDMS layer. A variety of solutions were tested as shown in Figure 4.6 including drilling holes using a very small bit, punching holes using a very thin needle, and laser cutting the holes. All three possible solutions were attempted on PDMS attached to transfer film and PDMS attached to a glass coverslip to find the best option. In Figure 4.6A, a covered through-hole is shown in the PDMS resulting from unsuccessful thin-film layer fabrication. This was used as a comparison for proper sizing and cleanliness of the options tested. Figure 4.6A also shows a hole, covered in

debris and jagged edges, resulted from drilling through the PDMS using a 75 μm drill bit (Performance Micro Tool, Janesville, WI).  Figure 4.6B depicts the resulting tears from punching through the PDMS using a 100 μm diameter carbide blank awl.  Thus far, the results do not seem promising for using micron-sized tools for creating clean through-holes in PDMS mechanically, so we attempted to cut the holes with a laser.  The HSE Kern laser-machining system available in the mechanical engineering department at Vanderbilt was tested as the first option for cutting holes in the thin PDMS layer.  As shown in Figure 4.6C, laser cutting provided cleaner, rounder through-holes than both punching and drilling.
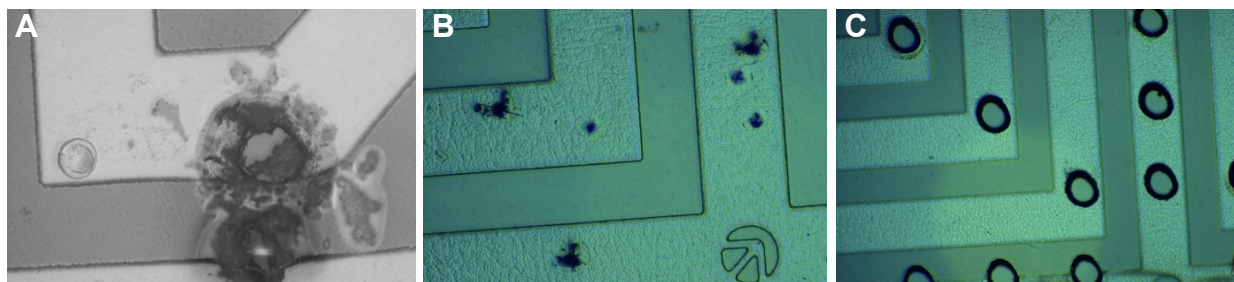


Figure 4.6 – (A) Hole drilled in thin-film PDMS layer with a 75 μm diameter bit left excessive amounts of debris in the channel.  (B) Holes punched in thin-film PDMS with a 100 μm diameter awl did not create clean holes, but instead tears in the PDMS.  (C) Holes cut by laser were fairly clean and completely through in contrast to drilling and punching.  Channel widths are 300 μm for scale

Although alignment was challenging, laser cutting was the best solution in our trials for producing relatively clean, round through-holes in the thin-film PDMS layer as seen in Figure 4.6C.  Note that optimal laser cutting was completed with PDMS attached to the transfer film. As seen in Figure 4.6C, the laser properties used in this trial did not result in 100 μm diameter holes but instead closer to 200 μm.  With laser cutting as the best option, further research and trials are required to determine optimal properties for laser cutting with better precision.

The Kern HSE-52 200W $CO_2$ laser system utilizes a variety of settings for a range of cutting and etching capabilities in metal, acrylic, wood, etc.  For our purposes, the power was set to very low values less than 0.2 W (1% of the total available power) due to the very thin

material. We also experimented with different values of hole diameter, nozzle air pressure, and scan speed. The resulting through-holes are shown in Figure 4.7. Although a variety of settings were tested, all had little to no effect on the overall size of the through-hole even though the drawn diameter was set as small as 1 μm. From these results, we realized some limitation exists in the system that prevents the laser from cutting holes smaller than approximately 200 μm. Further inspection of our system and comparison to a literature search revealed the nature of this setback.



Figure 4.7 – Demonstration of effect of a variety of laser settings. (A)-(C) Decreasing air nozzle pressure slightly reduced the amount of debris around the through-hole. (D) Percentage of total power ha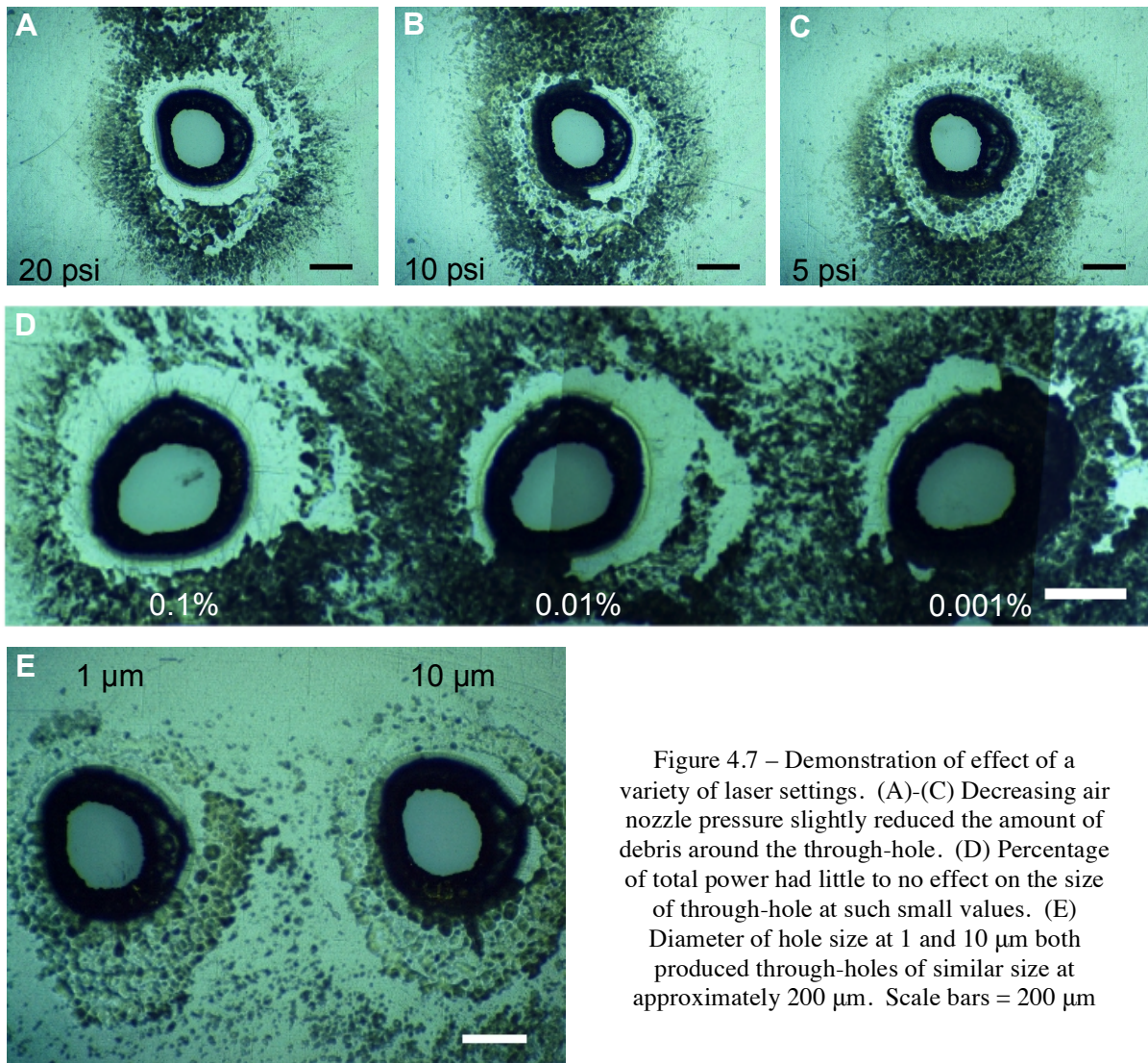d little to no effect on the size of through-hole at such small values. (E) Diameter of hole size at 1 and 10 μm both produced through-holes of similar size at approximately 200 μm. Scale bars = 200 μm

Although lasers are commonly available in many engineering fields, we found only two other groups that have attempted cutting PDMS with a $CO_2$ laser[196,197]. In 2009, Liu and Gong developed a rapid-prototyping laser-machining method for cutting and transferring PDMS without a template to create a microfluidic device[196]. In addition, they presented a variety of data from their own tests with laser cutting PDMS. Unfortunately there is a great contrast in laser tip and power between their trials and our own attempts. The maximum power of a laser determines the available power settings, theirs at only 30 W whereas ours is much stronger at 200 W. Liu and Gong also employed a high power density focusing optic (HPDFO) lens assembly that allowed for a laser spot of only 25 μm resulting in a channel width of 30 μm[196]. Similarly, Li et al. used a 30 W laser with a standard focusing lens that allowed for a laser spot of 50 μm[197]. The focusing lens for our laser cutter can only reach a focal spot of 127 μm, thus holes cut by the laser are much larger than the desired 100 μm diameter. Though power settings, scan speed, and air pressure can be tuned to create cleaner and smaller holes, there is a limit to the size due to the focusing lens. As demonstrated here, with the current departmental laser system we cannot cut small holes in thin-film PDMS, but other laser systems should be able to create the desired hole size with more accuracy. As such, we have tried out several other laser-machining systems.

The first option we tested was the Mira 900 laser system at Fisk University in Professor Richard Mu's lab. As shown in Figure 4.8A, while the laser cutter was able to burn the surface of the PDMS, the holes were not completely open. Alignment was also very difficult to achieve with the setup of the system, thus severely decreasing the efficiency of using this laser system to cut the through-holes.
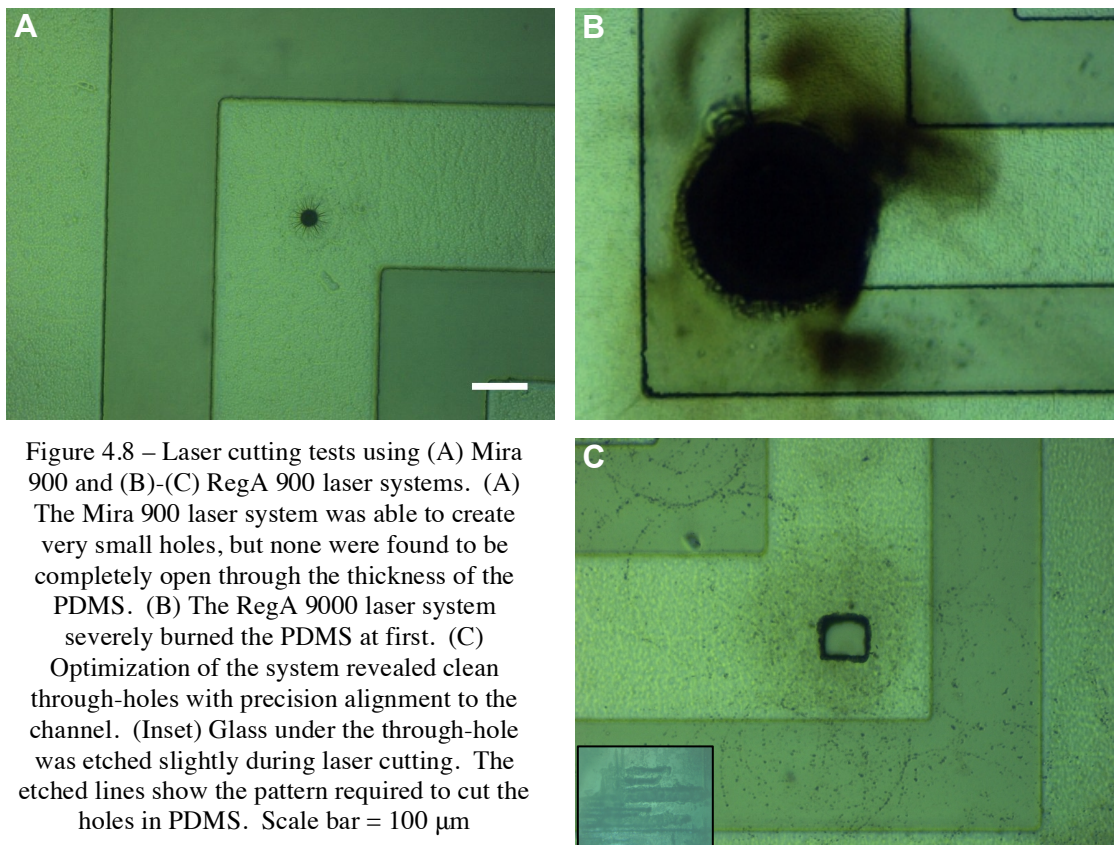
Figure 4.8 – Laser cutting tests using (A) Mira 900 and (B)-(C) RegA 900 laser systems. (A) The Mira 900 laser system was able to create very small holes, but none were found to be completely open through the thickness of the PDMS. (B) The RegA 9000 laser system severely burned the PDMS at first. (C) Optimization of the system revealed clean through-holes with precision alignment to the channel. (Inset) Glass under the through-hole was etched slightly during laser cutting. The etched lines show the pattern required to cut the holes in PDMS. Scale bar = 100 μm

The second option was testing the RegA 9000 laser system in the Center for Laser Applications at the University of Tennessee Space Institute (UTSI), specifically with the help of Dr. Alexander Terekhov. The results of testing are shown in Figure 4.8B,C. At first, we had difficulty finding the correct parameters to cut through the PDMS without severely burning the surrounding regions (Figure 4.7B). After multiple trials, we found that by immersing the substrate in water and setting the power to 150 mW with a laser pulse frequency and length of 250 kHz and 150 fs, respectively, we were able to cut the PDMS without burning. But further optimization revealed that cutting dithered lines (1-2 μm between lines) to create a 60 μm by 60 μm square allowed the laser to cut clean holes through the PDMS layer (Figure 4.8C). As shown in the inset to Figure 4.8C, the glass was etched slightly underneath the through-hole area revealing the dithering pattern used to cut the PDMS. After the setup and parameters had been

optimized, we found that we were able to cut fairly clean and well-aligned holes in the PDMS layer.  Due to the ability to visualize the substrate and locations before and after cutting without adjustment, alignment was very simple making the laser cutting more efficient than both the Kern and Mira 900 laser systems.

With the PDMS construct fabricated by the laser cutting process, we need to validate the laser cutting holes as a viable alternative to the sandwich molding method.  The goal of this test is to determine if the laser cut edges can create the same seal between the through-holes and tissue to prevent leakage from the channel.  Following the same assembly and protocols as described in Chapter 2 for the Retina-on-a-Chip platform, toluidine blue was added to the access channels.  As shown in Figure 4.9B, the toluidine blue was restricted to the region of the through-holes at three of the channels and successfully stained the tissue without leakage.
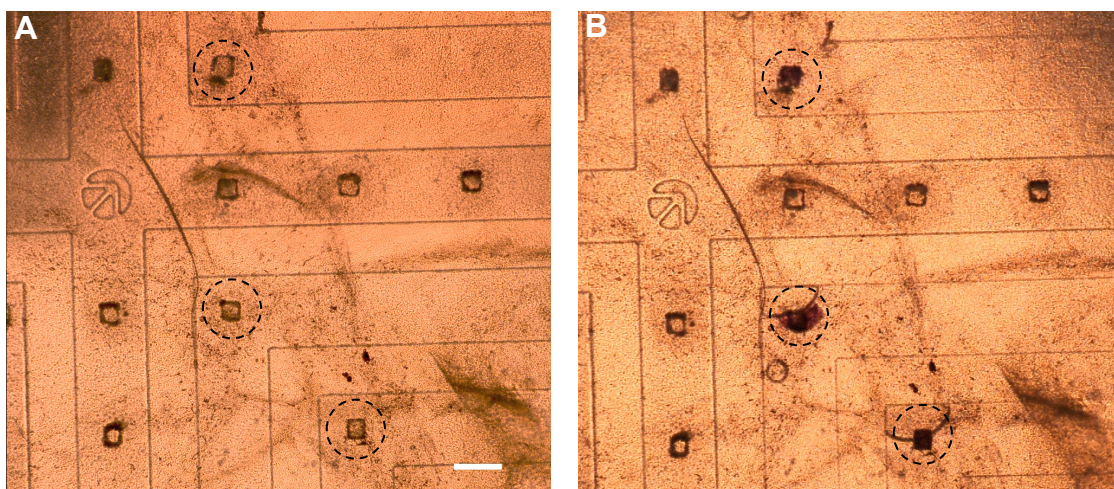


Figure 4.9 – The through-holes cut by laser were tested for comparison to the sandwich molding method.  The Retina-on-a-Chip device was assembled as outlined in Chapter 2 and followed the same protocols.  (A) The device is shown before dye is added to any of the channels.  (B) Toluidine blue was added to three access channels and rinsed with media to stain the tissue.  The three dashed circles indicate the three local deliveries of dye to the tissue.  Note that no leakage outside of the through-hole occurred.  Scale bar = 200 μm

Although we were able to cut fairly clean holes in the PDMS, we believe that with further adjustments a variety of hole sizes and shapes can be created, thus allowing for customization.

Validation of the laser cut holes was fairly successful as shown by the local application of toluidine blue to the surface of a retina.  Overall, laser cutting through-holes in thin-film PDMS was optimized using the RegA 9000 laser system and successful tests of staining a retina with toluidine blue indicate the tight seal achieved between the through-holes and the tissue surface.

**4.4 Summary**

In this chapter, we discussed current methods for fabricating thin-film PDMS layers as well as obstacles.  The sandwich molding method was described in depth as well as a study to expose the limitations of the method, specifically the lack of removing all liquid PDMS from between the mold and transfer film.  Discrepancies in literature show that a knowledge gap exists, and past research has not addressed this occurrence.  To fill that gap, we analyzed the issue through mathematical modeling and found that the problem is likely due to a molecular phenomenon, which occurs in thin liquid PDMS layers but not in bulk.

Revealing through-holes in the thin-film layers was challenging by the sandwich-molding method, thus other techniques were tested including punching, drilling, and laser cutting.  After testing three separate systems, laser cutting holes in PDMS with the RegA 9000 system produced the cleanest of the three options.  Finally, the Retina-on-a-Chip staining experiment showed that the through-holes cut via laser are equally effective in achieving a tight seal between the PDMS layer and the retina.

# CHAPTER 5

## SUMMARY

Microfluidics includes the design, fabrication, testing, and analysis of devices that contain microscale channels and chambers for precise manipulation of fluid flow. After two decades of development, microfluidics has become an attractive approach for biological assays and experiments, including neuroscience. The opportunity for customization in cell and tissue cultures allow for a reduction in time and cost, with potential high-throughput. In the field of neurobiology, microfluidics can be particularly useful; after almost a century of development, there are still large technological gaps to be filled. Much interest has especially been poured into the research of neurodegenerative diseases, like Alzheimer's, Huntington's, and Parkinson's. While most researchers have focused on utilizing microfluidics to study neurodegenerative diseases in the brain, here we present a microfluidic platform for retina.

Studying retina has a few advantages over studying brain slices: it is highly organized and easily accessible; it is part of the central nervous system; and it is uniquely light sensitive. Unlike the brain, the retina does not need to be sliced, thus every layer of neurons is alive and available for probing. Specifically in the retina, glaucoma has been linked to the degeneration of a layer of neurons called the RGCs. Although the exact cause is unknown, some types of neurodegeneration has been shown to start at a single point and spread like a wave. This phenomenon is known as spreading depolarization and can be studied by inducing localized damage to neurons and studying the subsequent effects. Using the microfluidic platforms developed in this dissertation, we were able to provide point application of a reagent to the

surface of the retina and observe the tissue's reaction, thus simulating spreading depolarization experiments. With the more complex design with embedded graphene sensors, we could simultaneously probe the retina, chemically and electrically, at a localized position and examine the effects.

Importantly, for our platforms to be compatible with current imaging technologies, specifically confocal microscopy, the microfluidic pieces must be thin. To allow for confocal microscopy, we employ a thin-film PDMS layer fabrication technique called sandwich molding. Though this is not a new technique, using this approach to fabricate small features in PDMS has not been widely studied and complications unfolded during our research. As such, the sandwich molding method was analyzed and modeled to better understand the limitations of the technique. In addition, to solve the risen challenges, new fabrication techniques were investigated and examined for their efficacy and viability. Here we summarize the completed work in this dissertation as well as future work for the Retina-on-a-Chip platform.

## 5.1 Summary of completed work

The overall goal of the microfluidic platforms developed in this dissertation is stimulation and detection of cell signaling within retina. The Retina-on-a-Chip platform was designed for localized reagent delivery to the RGC layer of whole retina tissue. Many unique soft-lithography fabrication techniques, such as plastic molding and sandwich molding, were employed to create this device. Using a thin-film PDMS layer designed with microchannels underneath and through-hole connections to the retina, we were able to flatten the retina and deliver reagents to well-defined points on the surface of the tissue without leakage throughout the device, which represents a significant improvement compared to current techniques, specifically tissue baths or pipetting. In order to provide a reagent to a point without leakage, a new negative pressure

operational protocol was utilized. This protocol limited exposure of the tissue to a well-defined area at the exposed region. With this platform, cells at the access points were targeted to demonstrate the health of the retina after long-term culture on the device as well as the ability to investigate physiologically relevant signaling events. For the long-term culture, media was fed to the retina via a cylinder with agar gel to provide a constant fresh supply to keep the retina healthy for five days *ex vivo*. To probe a signaling event, a neurotoxin was applied to an access point and the resulting immune response was observed through microglia reaction and migration toward the point of application within 30 minutes of exposure. Overall, the Retina-on-a-Chip platform was validated through successful long-term culture of the tissue and point application of a reagent to the surface layer of the retina.

By integrating graphene with the Retina-on-a-Chip platform, we incorporate new capabilities into the device. Neurons communicate with one another via chemical and electrical synapses, thus it is advantageous to create a device that can employ chemical and electrical stimulation and detect cellular response as well. As the first step, we embedded graphene transistors into a simplified version of the platform and obtained scanning photocurrent signals from the retina. By scanning the diffraction-limited laser spot over a region and focusing the laser spot at a single point over a period of time, we were able to record cellular signaling and examine the tissue's response to light stimulation.

Thus far, scanning photocurrent microscopy of retina tissue with single-layer graphene demonstrates strong signals at the optic nerve head while temporal photocurrent reveals the ability to isolate and detect electrical signal from cells stimulated by light. Both scanning and temporal photocurrent tests in live retina resulted in current on the order of about 1-10 nA. Throughout our experiments, contact between the RGCs and graphene was a challenge due to the

inner limiting membrane of the retina and possible development of an electric double layer. Attempts were made to resolve these contact issues including etching posts on the glass substrate, soaking the retina in an enzyme wash to break down the inner limiting membrane, and completely cutting out the optic nerve head during explant for better flattening. Note that we expect this issue might be resolved more easily with a thin-film PDMS layer in the full version of the device that would provide suction to pull the retina into contact with the graphene. Even though more results are required for full validation, initial testing of temporal photocurrent response appears to be capable of recording photosensitive signaling of the retina tissue while scanning photocurrent microscopy provides high-resolution mapping of electric signals within the live tissue.

Finally, we discussed the procedure and difficulties of current fabrication approaches for thin-film PDMS layers with small through-holes. The sandwich molding method was described and tested before analysis of the technique was performed. The Reynold's equation was utilized to determine the effect of viscosity and force applied on PDMS film thickness between two surfaces. Modeling provided a better insight into the physics of the fluid flow for this case, and a variety of tests were performed including mechanical punching and drilling as well as laser cutting PDMS with three different laser systems. By fine-tuning the laser cutting to optimal operation parameters, we were able to fabricate clean through-holes in thin PDMS layers. To validate laser cutting as a viable and efficient approach, toluidine blue was successfully applied to the surface of a retina in a staining assay.

Altogether, the performed experiments and obtained data demonstrate the strong potential of the Retina-on-a-Chip platform for studying whole retina tissue. Chemical stimulation and detection of biological responses was achieved with the Retina-on-a-Chip platform and the

feasibility of detecting electrical signals using scanning photocurrent microscopy was realized. While these advances pave the road toward a powerful technology for neuroscience via probing retina tissue under a well-controlled microenvironment, more research is required to solve encountered challenges and achieve full potential.

**5.2 Outlook**

Because of the challenges associated with the novel graphene-based biosensor scheme, the development of the graphene-integrated platform is still in its infancy. Although we have obtained a plethora of results, comparisons should be made with results from established methods like patch-clamping. Once scanning photocurrent microscopy for detecting electrical signaling in retina tissue is well developed, integration of the gold electrodes and single-layer graphene with the thin-film PDMS layer will be implemented. After graphene integration is accomplished, the capabilities of the platform must be tested for simultaneous stimulation and detection of chemical and electrical signaling within the retina. These trials will also include demonstrating health and integrity of the retina on the device. After further development, the Retina-on-a-Chip platform with embedded graphene sensors together with scanning photocurrent microscopy will be employed to study neurodegenerative phenomena like spreading depolarization, which may open doors to better understanding retina-related diseases like glaucoma.

# REFERENCES

1. Whitesides, G. M. The origins and the future of microfluidics. *Nature* **442,** 368–73 (2006).

2. Mitchell, P. Microfluidics--downsizing large-scale biology. *Nat. Biotechnol.* **19,** 717–721 (2001).

3. Weibel, D. B., Garstecki, P. & Whitesides, G. M. Combining microscience and neurobiology. *Curr. Opin. Neurobiol.* **15,** 560–567 (2005).

4. Paguirigan, A. L. & Beebe, D. J. Microfluidics meet cell biology: Bridging the gap by validation and application of microscale techniques for cell biological assays. *BioEssays* **30,** 811–821 (2008).

5. Walker, G. M., Zeringue, H. C. & Beebe, D. J. Microenvironment design considerations for cellular scale studies. *Lab Chip* **4,** 91–97 (2004).

6. Huang, Y., Williams, J. C. & Johnson, S. M. Brain slice on a chip: opportunities and challenges of applying microfluidic technology to intact tissues. *Lab Chip* **12,** 2103 (2012).

7. Webster, A., Dyer, C. E., Haswell, S. J. & Greenman, J. A microfluidic device for tissue biopsy culture and interrogation. *Anal. Methods* **2,** 1005 (2010).

8. Hattersley, S. M., Dyer, C. E., Greenman, J. & Haswell, S. J. Development of a microfluidic device for the maintenance and interrogation of viable tissue biopsies. *Lab Chip* **8,** 1842–6 (2008).

9. Levitan, I. B. & Kaczmarek, L. K. *The Neuron: Cell and Molecular Biology*. (Oxford University Press, 2002).

10. Urry, L. A. *et al. Campbell Biology in Focus*. (Pearson, 2014).

11. Dowling, J. E. *The retina: an approachable part of the brain*. (The Belknap Press of Harvard University Press, 2012).

12. Kolb, H. Simple Anatomy of the Retina. *Webvision* at <http://webvision.med.utah.edu/>

13. Dreier, J. P. The role of spreading depression, spreading depolarization and spreading ischemia in neurological disease. *Nat. Med.* **17,** 439–447 (2011).

14. Hossmann, K.-A. Viability thresholds and the penumbra of focal ischemia. *Ann. Neurol.* **36,** 557–565 (1994).

15. Leão, A. A. P. Spreading depression of activity in the cerebral cortex. *J. Physiol.* **7,** 359–390 (1944).

16. Leão, A. A. P. Further Observations on the Spreading Depression of Activity in the Cerebral Cortex. *J. Neurophysiol.* (1947).

17.    Meyvantsson, I. & Beebe, D. J. Cell culture models in microfluidic systems. *Annu. Rev. Anal. Chem.* **1,** 423–449 (2008).

18.    Beebe, D. J., Mensing, G. A. & Walker, G. M. Physics and applications of microfluidics in biology. *Annu. Rev. Biomed. Eng.* **4,** 261–286 (2002).

19.    Kim, L., Toh, Y.-C., Voldman, J. & Yu, H. A practical guide to microfluidic perfusion culture of adherent mammalian cells. *Lab Chip* **7,** 681–694 (2007).

20.    Sia, S. K. & Whitesides, G. M. Microfluidic devices fabricated in poly(dimethylsiloxane) for biological studies. *Electrophoresis* **24,** 3563–3576 (2003).

21.    El-Ali, J., Sorger, P. K. & Jensen, K. F. Cells on chips. *Nature* **442,** 403–411 (2006).

22.    Mehling, M. & Tay, S. Microfluidic cell culture. *Curr. Opin. Biotechnol.* **25,** 95–102 (2014).

23.    Dittrich, P. S. & Manz, A. Lab-on-a-chip: microfluidics in drug discovery. *Nat. Rev. Drug Discov.* **5,** 210–8 (2006).

24.    Martin, K. *et al.* Generation of larger numbers of separated microbial populations by cultivation in segmented-flow microdevices. *Lab Chip* **3,** 202–207 (2003).

25.    Lagus, T. P. & Edd, J. F. A review of the theory, methods and recent applications of high-throughput single-cell droplet microfluidics. *J. Phys. D. Appl. Phys.* **46,** 114005 (2013).

26.    Osborne, G. W. Recent advances in flow cytometric cell sorting. *Methods in Cell Biology* **102,** (2011).

27.    Edd, J. F. *et al.* Controlled encapsulation of single-cells into monodisperse picolitre drops. *Lab Chip* **8,** 1262–1264 (2008).

28.    Brouzes, E. *et al.* Droplet microfluidic technology for single-cell high-throughput screening. *Proc. Natl. Acad. Sci. U. S. A.* **106,** 14195–14200 (2009).

29.    Wheeler, A. R. *et al.* Microfluidic Device for Single-Cell Analysis. **75,** 16531–16536 (2003).

30.    Di Carlo, D., Wu, L. Y. & Lee, L. P. Dynamic single cell culture array. *Lab Chip* **6,** 1445–1449 (2006).

31.    Frimat, J.-P. *et al.* A microfluidic array with cellular valving for single cell co-culture. *Lab Chip* **11,** 231–237 (2011).

32.    Liberale, C. *et al.* Integrated microfluidic device for single-cell trapping and spectroscopy. *Sci. Rep.* **3,** 1–6 (2013).

33.    Hellmich, W., Pelargus, C., Leffhalm, K., Ros, A. & Anselmetti, D. Single cell manipulation, analytics, and label-free protein detection in microfluidic devices for systems nanobiology. *Electrophoresis* **26,** 3689–3696 (2005).

34.  Kimura, H., Yamamoto, T., Sakai, H., Sakai, Y. & Fujii, T. An integrated microfluidic system for long-term perfusion culture and on-line monitoring of intestinal tissue models. *Lab Chip* **8,** 741–6 (2008).

35.  Ong, S.-M. M. *et al.* A gel-free 3D microfluidic cell culture system. *Biomaterials* **29,** 3237–3244 (2008).

36.  Jeon, N. L. *et al.* Neutrophil chemotaxis in linear and complex gradients of interleukin-8 formed in a microfabricated device. *Nat. Biotechnol.* **20,** 826–830 (2002).

37.  Wang, S. J., Saadi, W., Lin, F., Nguyen, C. M.-C. & Jeon, N. L. Differential effects of EGF gradient profiles on MDA-MB-231 breast cancer cell chemotaxis. *Exp. Cell Res.* **300,** 180–189 (2004).

38.  Tourovskaia, A., Figueroa-Masot, X. & Folch, A. Differentiation-on-a-chip: a microfluidic platform for long-term cell culture studies. *Lab Chip* **5,** 14–19 (2005).

39.  Leclerc, E., Sakai, Y. & Fujii, T. Cell culture in 3-dimensional microfluidic structure of PDMS (polydimenthylsiloxane). *Biomed. Microdevices* **5,** 109–114 (2003).

40.  Hung, P. J. *et al.* A novel high aspect ratio microfluidic design to provide a stable and uniform microenvironment for cell growth in a high throughput mammalian cell culture array. *Lab Chip* **5,** 44–48 (2005).

41.  Lecault, V. *et al.* High-throughput analysis of single hematopoietic stem cell proliferation in microfluidic cell culture arrays. *Nat. Methods* **8,** 581–586 (2011).

42.  Gómez-Sjöberg, R. *et al.* Versatile, Fully Automated, Microfluidic Cell Culture System. *Anal. Chem.* **79,** 8557–8563 (2007).

43.  Taylor, A. M., Rhee, S. W. & Jeon, N. L. Microfluidic chambers for cell migration and neuroscience research. *Microfluid. Tech.* **321,** 167–177 (2006).

44.  Majumdar, D., Gao, Y., Li, D. & Webb, D. J. Co-culture of neurons and glia in a novel microfluidic platform. *J. Neurosci. Methods* **196,** 38–44 (2011).

45.  Taylor, A. M. *et al.* A microfluidic culture platform for CNS axonal injury, regeneration and transport. *Nat. Methods* **2,** 599–605 (2005).

46.  Gao, Y. *et al.* A versatile valve-enabled microfluidic cell co-culture platform and demonstration of its applications to neurobiology and cancer biology. *Biomed. Microdevices* **13,** 539–548 (2011).

47.  Folch, A. & Toner, M. Cellular micropatterns on biocompatible materials. *Biotechnol. Prog.* **14,** 388–392 (1998).

48.  Folch, A., Jo, B. H., Hurtado, O., Beebe, D. J. & Toner, M. Microfabricated elastomeric stencils for micropatterning cell cultures. *J. Biomed. Mater. Res.* **52,** 346–353 (2000).

49.  Chiu, D. T. *et al.* Patterned deposition of cells and proteins onto surfaces by using three-dimensional microfluidic systems. *Proc. Natl. Acad. Sci. U. S. A.* **97,** 2408–2413 (2000).

50. Khademhosseini, A. *et al.* Cell docking inside microwells within reversibly sealed microfluidic channels for fabricating multiphenotype cell arrays. *Lab Chip* **5,** 1380–6 (2005).

51. Khetani, S. R. & Bhatia, S. N. Microscale culture of human liver cells for drug development. *Nat. Biotechnol.* **26,** 120–126 (2008).

52. Tan, W. & Desai, T. A. Layer-by-layer microfluidics for biomimetic three-dimensional structures. *Biomaterials* **25,** 1355–1364 (2004).

53. Vickerman, V., Blundo, J., Chung, S. & Kamm, R. Design, fabrication and implementation of a novel multi-parameter control microfluidic platform for three-dimensional cell culture and real-time imaging. *Lab Chip* **8,** 1468–1477 (2008).

54. Chan, Y. K. *et al.* In Vitro Modeling of Emulsification of Silicone Oil as Intraocular Tamponade Using Microengineered Eye-on-a-Chip. *Investig. Opthalmology Vis. Sci.* **56,** 3314 (2015).

55. Luo, X. *et al.* Distal modulation of bacterial cell-cell signalling in a synthetic ecosystem using partitioned microfluidics. *Lab Chip* 1485–1490 (2015). doi:10.1039/C4LC00901K

56. Jang, K.-J. & Suh, K.-Y. A multi-layer microfluidic device for efficient culture and analysis of renal tubular cells. *Lab Chip* **10,** 36–42 (2010).

57. Zhang, Y. S. *et al.* From cardiac tissue engineering to heart-on-a-chip: beating challenges. *Biomed. Mater.* **10,** 034006 (2015).

58. Yang, Y. *et al.* Evaluation of Photodynamic Therapy Efficiency Using an in vitro Three-dimensional Microfluidic Breast Cancer Tissue Model. *Lab Chip* **15,** 735–744 (2015).

59. Huh, D. *et al.* Reconstituting organ-level lung functions on a chip. *Science* **328,** 1662–1668 (2010).

60. Domansky, K. *et al.* Perfused multiwell plate for 3D liver tissue engineering. *Lab Chip* **10,** 51–58 (2010).

61. Huh, D., Hamilton, G. A. & Ingber, D. E. From 3D cell culture to organs-on-chips. *Trends Cell Biol.* **21,** 745–54 (2011).

62. Inamdar, N. K. & Borenstein, J. T. Microfluidic cell culture models for tissue engineering. *Curr. Opin. Biotechnol.* **22,** 681–689 (2011).

63. Moraes, C., Mehta, G., Lesher-Perez, S. C. & Takayama, S. Organs-on-a-chip: a focus on compartmentalized microdevices. *Ann. Biomed. Eng.* **40,** 1211–27 (2012).

64. Ghaemmaghami, A. M., Hancock, M. J., Harrington, H., Kaji, H. & Khademhosseini, A. Biomimetic tissues on a chip for drug discovery. *Drug Discov. Today* **17,** 173–81 (2012).

65. Maschmeyer, I. *et al.* A four-organ-chip for interconnected long-term co-culture of human intestine, liver, skin and kidney equivalents. *Lab Chip* **15,** 2688–2699 (2015).

66.     Materne, E.-M. *et al.* The Multi-organ Chip - A Microfluidic Platform for Long-term Multi-tissue Coculture. *J. Vis. Exp.* 1–11 (2015).

67.     Wikswo, J. P. *et al.* Scaling and systems biology for integrating multiple organs-on-a-chip. *Lab Chip* **13,** 3496–3511 (2013).

68.     Bonassar, L. J. & Vacanti, C. A. Tissue engineering: the first decade and beyond. *J. Cell. Biochem. Suppl.* **30-31,** 297–303 (1998).

69.     Desai, T. A. Micro- and nanoscale structures for tissue engineering constructs. *Med. Eng. Phys.* **22,** 595–606 (2001).

70.     Sung, J. H. *et al.* Microfabricated mammalian organ systems and their integration into models of whole animals and humans. *Lab Chip* **13,** 1201–12 (2013).

71.     Smith, Q. & Gerecht, S. Going with the flow: Microfluidic platforms in vascular tissue engineering. *Curr. Opin. Chem. Eng.* **3,** 42–50 (2014).

72.     Stroock, A. D. & Fischbach, C. Microfluidic culture models of tumor angiogenesis. *Tissue Eng. Part A* **16,** 2143–6 (2010).

73.     Bellan, L. M. *et al.* Fabrication of an artificial 3-dimensional vascular network using sacrificial sugar structures. *Soft Matter* **5,** 1354 (2009).

74.     Tien, J. Microfluidic approaches for engineering vasculature. *Curr. Opin. Chem. Eng.* **3,** 36–41 (2014).

75.     Folch, A. *et al.* Stacks of Microfabricated Structures as Scaffolds for Cell Culture and Tissue Engineering. *Biomed. Microdevices* **2,** 207–214 (2000).

76.     Andersson, H. & van den Berg, A. Microfabrication and microfluidics for tissue engineering: state of the art and future opportunities. *Lab Chip* **4,** 98–103 (2004).

77.     Harrison, R. G. Observations on the living developing nerve fiber. *Proc. Soc. Exp. Biol. Med.* **4,** 140–143 (1907).

78.     Del Turco, D. & Deller, T. Organotypic entorhino-hippocampal slice cultures--a tool to study the molecular and cellular regulation of axonal regeneration and collateral sprouting in vitro. *Methods Mol. Biol.* **399,** 55–66 (2007).

79.     Voutilainen, M., Lindfors, P. H. & Mikkola, M. L. Protocol: Ex vivo culture of mouse embryonic mammary buds. *J. Mammary Gland Biol. Neoplasia* **18,** 239–245 (2013).

80.     Gahwiler, B. H. Organotypic Monolayer Cultures of Nervous Tissue. *J. Neurosci. Methods* **4,** 329–342 (1981).

81.     Stoppini, L., Buchs, P.-A. & Muller, D. A simple method for organotypic cultures of nervous tissue. *J. Neurosci. Methods* **37,** 173–182 (1991).

82.     Youm, H. W. *et al.* Optimal vitrification protocol for mouse ovarian tissue cryopreservation: effect of cryoprotective agents and in vitro culture on vitrified-warmed

ovarian tissue survival. *Hum. Reprod.* **29,** 720–30 (2014).

83.    Passeraub, P. A., Almeida, A. C. & Thakor, N. V. Design, Microfabrication and Analysis of a Microfluidic Chamber for the Perfusion of Brain Tissue Slices. *Biomed. Microdevices* **5,** 147–155 (2003).

84.    Wittig, J. H., Ryan, A. F. & Asbeck, P. M. A reusable microfluidic plate with alternate-choice architecture for assessing growth preference in tissue culture. *J. Neurosci. Methods* **144,** 79–89 (2005).

85.    Blake, A. J., Pearce, T. M., Rao, N. S., Johnson, S. M. & Williams, J. C. Multilayer PDMS microfluidic chamber for controlling brain slice microenvironment. *Lab Chip* **7,** 842–849 (2007).

86.    Choi, Y., McClain, M. A., LaPlaca, M. C., Frazier, A. B. & Allen, M. G. Three dimensional MEMS microfluidic perfusion system for thick brain slice cultures. *Biomed. Microdevices* **9,** 7–13 (2007).

87.    Bakmand, T. *et al.* Fluidic system for long-term in vitro culturing and monitoring of organotypic brain slices. *Biomed. Microdevices* **17,** 71 (2015).

88.    Berdichevsky, Y., Staley, K. J. & Yarmush, M. L. Building and manipulating neural pathways with microfluidics. *Lab Chip* **10,** 999–1004 (2010).

89.    Choudhury, D. *et al.* Fish and Chips: a microfluidic perfusion platform for monitoring zebrafish development. *Lab Chip* **12,** 892–900 (2012).

90.    Sip, C. G., Bhattacharjee, N. & Folch, A. Microfluidic transwell inserts for generation of tissue culture-friendly gradients in well plates. *Lab Chip* **14,** 302–14 (2014).

91.    Barkefors, I., Thorslund, S., Nikolajeff, F. & Kreuger, J. A fluidic device to study directional angiogenesis in complex tissue and organ culture models. *Lab Chip* **9,** 529–535 (2009).

92.    Sivashankar, S. *et al.* Culturing of transgenic mice liver tissue slices in three-dimensional microfluidic structures of PEG-DA (poly(ethylene glycol) diacrylate). *Sensors Actuators, B Chem.* **176,** 1081–1089 (2013).

93.    Kim, M. S. *et al.* Breast cancer diagnosis using a microfluidic multiplexed immunohistochemistry platform. *PLoS One* **5,** e10441 (2010).

94.    Günther, A. *et al.* A microfluidic platform for probing small artery structure and function. *Lab Chip* **10,** 2341–9 (2010).

95.    Mauleon, G., Fall, C. P. & Eddington, D. T. Precise spatial and temporal control of oxygen within in vitro brain slices via microfluidic gas channels. *PLoS One* **7,** (2012).

96.    Abaci, H. E., Gledhill, K., Guo, Z., Christiano, A. M. & Shuler, M. L. Pumpless microfluidic platform for drug testing on human skin equivalents. *Lab Chip* **15,** 882–888 (2015).

97. Wightman, R. M. Probing Cellular Chemistry in Biological Systems with Microelectrodes. *Science* **311,** 1570–1574 (2006).

98. Neher, E. & Sakmann, B. Single-channel currents recorded from membrane of denervated frog muscle fibres. *Nature* **260,** 799–802 (1976).

99. Hamill, O. P., Marty, A., Neher, E., Sakmann, B. & Sigworth, F. J. Improved patch-clamp techniques for high-resolution current recording from cells and cell-free membrane patches. *Pflugers Arch.* **391,** 85–100 (1981).

100. Park, T. H. & Shuler, M. L. Integration of cell culture and microfabrication technology. *Biotechnol. Prog.* **19,** 243–253 (2003).

101. Timko, B. P., Cohen-Karni, T., Qing, Q., Tian, B. & Lieber, C. M. Design and implementation of functional nanoelectronic interfaces with biomolecules, cells, and tissue using nanowire device arrays. *IEEE Trans. Nanotechnol.* **9,** 269–280 (2010).

102. Picollet-D'hahan, N. Live Cell Analysis: When Electric Detection Interfaces Microfluidics. *J. Biochips Tissue Chips* **01,** 1–9 (2011).

103. Tian, B. & Lieber, C. M. Synthetic Nanoelectric Probes for Biological Cells and Tissue. *Annu. Rev. Anal. Chem.* **6,** 31–51 (2013).

104. Wilson, G. S. & Gifford, R. Biosensors for real-time in vivo measurements. *Biosens. Bioelectron.* **20,** 2388–2403 (2005).

105. Pearce, T. M. & Williams, J. C. Microtechnology: meet neurobiology. *Lab Chip* **7,** 30–40 (2007).

106. Robinson, J. T., Jorgolli, M. & Park, H. Nanowire electrodes for high-density stimulation and measurement of neural circuits. *Front. Neural Circuits* **7,** 38 (2013).

107. Park, J. W., Kim, H. J., Kang, M. W. & Jeon, N. L. Advances in microfluidics-based experimental methods for neuroscience research. *Lab Chip* **13,** 509–21 (2013).

108. Saltzman, W. M. & Olbricht, W. L. Building drug delivery into tissue engineering. *Nat. Rev. Drug Discov.* **1,** 177–86 (2002).

109. Mohammed, J. S., Caicedo, H. H., Fall, C. P. & Eddington, D. T. Microfluidic add-on for standard electrophysiology chambers. *Lab Chip* **8,** 1048 (2008).

110. Sip, C. G. & Folch, A. An Open-Surface Micro-Dispenser Valve for the Local Stimulation of Conventional Tissue Cultures. *14th Int. Conf. Miniaturized Syst. Chem. Life Sci.* 1778–1780 (2010).

111. Tang, Y. T., Kim, J., Lopez-Valdes, H. E., Brennan, K. C. & Ju, Y. S. Development and characterization of a microfluidic chamber incorporating fluid ports with active suction for localized chemical stimulation of brain slices. *Lab Chip* **11,** 2247–2254 (2011).

112. HajjHassan, M., Chodavarapu, V. & Musallam, S. NeuroMEMS: Neural probe microtechnologies. *Sensors* **8,** 6704–6726 (2008).

113. Morin, F. *et al.* Constraining the connectivity of neuronal networks cultured on microelectrode arrays with microfluidic techniques: A step towards neuron-based functional chips. *Biosens. Bioelectron.* **21,** 1093–1100 (2006).

114. Pearce, T. M., Wilson, J. A., Oakes, S. G., Chiu, S.-Y. & Williams, J. C. Integrated microelectrode array and microfluidics for temperature clamp of sensory neurons in culture. *Lab Chip* **5,** 97–101 (2005).

115. Egert, U. *et al.* A novel organotypic long-term culture of the rat hippocampus on substrate-integrated multielectrode arrays. *Brain Res. Protoc.* **2,** 229–242 (1998).

116. Berdichevsky, Y., Sabolek, H., Levine, J. B., Staley, K. J. & Yarmush, M. L. Microfluidics and multielectrode array-compatible organotypic slice culture method. *J. Neurosci. Methods* **178,** 59–64 (2009).

117. Scott, A. *et al.* A microfluidic microelectrode array for simultaneous electrophysiology, chemical stimulation, and imaging of brain slices. *Lab Chip* 527–535 (2013).

118. Cheah, L.-T. *et al.* Microfluidic perfusion system for maintaining viable heart tissue with real-time electrochemical monitoring of reactive oxygen species. *Lab Chip* **10,** 2720–6 (2010).

119. Blake, A. J. *et al.* A microfluidic brain slice perfusion chamber for multisite recording using penetrating electrodes. *J. Neurosci. Methods* **189,** 5–13 (2010).

120. Ahnood, A. *et al.* Ultrananocrystalline diamond-CMOS device integration route for high acuity retinal prostheses. *Biomed. Microdevices* **17,** 1–11 (2015).

121. Ganesan, K. *et al.* An all-diamond, hermetic electrical feedthrough array for a retinal prosthesis. *Biomaterials* **35,** 908–915 (2014).

122. David-Pur, M., Bareket-Keren, L., Beit-Yaakov, G., Raz-Prag, D. & Hanein, Y. All-carbon-nanotube flexible multi-electrode array for neuronal recording and stimulation. *Biomed. Microdevices* **16,** 43–53 (2014).

123. Chen, C. H. *et al.* A flexible hydrophilic-modified graphene microprobe for neural and cardiac recording. *Nanomedicine Nanotechnology, Biol. Med.* **9,** 600–604 (2013).

124. Inayat, S., Rountree, C. M., Troy, J. B. & Saggere, L. Chemical stimulation of rat retinal neurons: feasibility of an epiretinal neurotransmitter-based prosthesis. *J. Neural Eng.* **12,** 016010 (2014).

125. Gao, K. *et al.* Fabrication of flexible microelectrode arrays integrated with microfluidic channels for stable neural interfaces. *Sensors Actuators, A Phys.* **197,** 9–14 (2013).

126. Mcallister, D. V, Allen, M. G. & Prausnitz, M. R. Microfabricated Microneedles for Gene and Drug Delivery. *Annu. Rev. Biomed. Eng.* **2,** 289–313 (2000).

127. Sarkar, A., Kolitz, S., Lauffenburger, D. A. & Han, J. Microfluidic probe for single-cell analysis in adherent tissue culture. *Nat. Commun.* **5,** 3421 (2014).

128. Queval, A. *et al.* Chamber and microfluidic probe for microperfusion of organotypic brain slices. *Lab Chip* **10,** 326–34 (2010).

129. Du, J., Blanche, T. J., Harrison, R. R., Lester, H. A. & Masmanidis, S. C. Multiplexed, high density electrophysiology with nanofabricated neural probes. *PLoS One* **6,** (2011).

130. Lee, H. J. *et al.* A multichannel neural probe with embedded microfluidic channels for simultaneous in vivo neural recording and drug delivery. *Lab Chip* **15,** 1590–1597 (2015).

131. Desai, S. P., Freeman, D. M. & Voldman, J. Plastic masters-rigid templates for soft lithography. *Lab Chip* **9,** 1631–1637 (2009).

132. Jo, B., Lerberghe, L. M. Van, Motsegood, K. M. & Beebe, D. J. Three-Dimensional Micro-Channel Fabrication in Polydimethylsiloxane (PDMS) Elastomer. *J. Microelectromechanical Syst.* **9,** 76–81 (2000).

133. Hsu, C.-H., Chen, C. & Folch, A. 'Microcanals' for micropipette access to single cells in microfluidic environments. *Lab Chip* **4,** 420–4 (2004).

134. Crish, S. D., Sappington, R. M., Inman, D. M., Horner, P. J. & Calkins, D. J. Distal axonopathy with structural persistence in glaucomatous neurodegeneration. *Proc. Natl. Acad. Sci. U. S. A.* **107,** 5196–5201 (2010).

135. Kang, M., Day, C. A., Kenworthy, A. K. & DiBenedetto, E. Simplified equation to extract diffusion coefficients from confocal FRAP data. *Traffic* **13,** 1589–1600 (2012).

136. Beurel, E. & Jope, R. S. Lipopolysaccharide-induced interleukin-6 production is controlled by glycogen synthase kinase-3 and STAT3 in the brain. *J. Neuroinflammation* **6,** 9 (2009).

137. Lee, S. C., Liu, W., Dickson, D. W., Brosnan, C. F. & Berman, J. W. Cytokine production by human fetal microglia and astrocytes. Differential induction by lipopolysaccharide and IL-1 beta. *J. Immunol.* **150,** 2659–2667 (1993).

138. Sébire, G. *et al.* In vitro production of IL-6, IL-1 beta, and tumor necrosis factor-alpha by human embryonic microglial and neural cells. *J. Immunol.* **150,** 1517–1523 (1993).

139. Buttini, M., Limonta, S. & Boddeke, H. W. G. M. Peripheral administration of lipopolysaccharide induces activation of microglial cells in rat brain. *Neurochem. Int.* **29,** 25–35 (1996).

140. Horvath, R. J., Nutile-McMenemy, N., Alkaitis, M. S. & DeLeo, J. A. Differential migration, LPS-induced cytokine, chemokine, and NO expression in immortalized BV-2 and HAPI cell lines and primary microglial cultures. *J. Neurochem.* **107,** 557–569 (2008).

141. Kloss, C. U., Bohatschek, M., Kreutzberg, G. W. & Raivich, G. Effect of lipopolysaccharide on the morphology and integrin immunoreactivity of ramified microglia in the mouse brain and in cell culture. *Exp. Neurol.* **168,** 32–46 (2001).

142. Cui, Y.-H. *et al.* Bacterial lipopolysaccharide selectively up-regulates the function of the

chemotactic peptide receptor formyl peptide receptor 2 in murine microglial cells. *J. Immunol.* **168,** 434–442 (2002).

143. Lee, J. C. *et al.* Accelerated cerebral ischemic injury by activated macrophages/microglia after lipopolysaccharide microinjection into rat corpus callosum. *Glia* **50,** 168–181 (2005).

144. Castro Neto, A. H., Guinea, F., Peres, N. M. R., Novoselov, K. S. & Geim, A. K. The electronic properties of graphene. *Rev. Mod. Phys.* **81,** 109–162 (2009).

145. Geim, A. K. & Novoselov, K. S. The rise of graphene. *Nat. Mater.* 183–191 (2007).

146. Zhang, Y., Nayak, T. R., Hong, H. & Cai, W. Graphene: a versatile nanoplatform for biomedical applications. *Nanoscale* **4,** 3833 (2012).

147. Lee, S. K., Kim, H. & Shim, B. S. Graphene: an emerging material for biological tissue engineering. *Carbon Lett.* **14,** 63–75 (2013).

148. Hess, L. H., Seifert, M. & Garrido, J. A. Graphene transistors for bioelectronics. *Proc. IEEE* **101,** 1780–1792 (2013).

149. Heo, C. *et al.* The control of neural cell-to-cell interactions through non-contact electrical field stimulation using graphene electrodes. *Biomaterials* **32,** 19–27 (2011).

150. Cohen-Karni, T., Qing, Q., Li, Q., Fang, Y. & Lieber, C. M. Graphene and nanowire transistors for cellular interfaces and electrical recording. *Nano Lett.* **10,** 1098–1102 (2010).

151. Ye, J. H. & Goo, Y. S. The slow wave component of retinal activity in rd/rd mice recorded with a multi-electrode array. *Physiol. Meas.* **28,** 1079–1088 (2007).

152. Tian, N. & Copenhagen, D. R. Visual stimulation is required for refinement of ON and OFF pathways in postnatal retina. *Neuron* **39,** 85–96 (2003).

153. Meister, M., Pine, J. & Baylor, D. A. Multi-neuronal signals from the retina: Acquisition and analysis. *J. Neurosci. Methods* **51,** 95–106 (1994).

154. Cohen, L. B. *et al.* Changes in axon fluorescence during activity: Molecular probes of membrane potential. *J. Membr. Biol.* **19,** 1–36 (1974).

155. Grinvald, A., Anglister, L., Freeman, J. A., Hildesheim, R. & Manker, A. Real-time optical imaging of naturally evoked electrical activity in intact frog brain. *Nature* **308,** 848–850 (1984).

156. González, J. E. & Tsien, R. Y. Voltage sensing by fluorescence resonance energy transfer in single cells. *Biophys. J.* **69,** 1272–1280 (1995).

157. Ferezou, I., Bolea, S. & Petersen, C. C. H. Visualizing the Cortical Representation of Whisker Touch: Voltage-Sensitive Dye Imaging in Freely Moving Mice. *Neuron* **50,** 617–629 (2006).

158. Candiello, J. *et al.* Biomechanical properties of native basement membranes. *FEBS J.* **274,**

2897–2908 (2007).

159. Pinzón-Duarte, G., Daly, G., Li, Y. N., Koch, M. & Brunken, W. J. Defective formation of the inner limiting membrane in laminin beta2- and gamma3-null mice produces retinal dysplasia. *Invest. Ophthalmol. Vis. Sci.* **51,** 1773–82 (2010).

160. Schmidt, T. M. & Kofuji, P. An isolated retinal preparation to record light response from genetically labeled retinal ganglion cells. *J. Vis. Exp.* 2–5 (2011).

161. Bockris, J. O., Devanthan, M. A. V. & Muller, K. On the structure of charged interfaces. *Proc. R. Soc. Lond. A. Math. Phys. Sci.* (1963).

162. Grahame, D. C. The electrical double layer and the theory of electrocapillarity. *Chem. Rev.* 441–501 (1947).

163. Park, J., Ahn, Y. H. & Ruiz-Vargas, C. Imaging of photocurrent generation and collection in single-layer graphene. *Nano Lett.* **9,** 1742–1746 (2009).

164. Hartline, H. K. The response of single optic nerve fibers of the vertebrate eye to illumination of the retina. *Am. J. Physiol.* 400–415 (1938).

165. Devries, S. H. & Baylor, D. A. Mosaic arrangement of ganglion cell receptive fields in rabbit retina. *J. Neurophysiol.* **78,** 2048–2060 (1997).

166. Wyk, M. van, Taylor, W. R. & Vaney, D. I. Local Edge Detectors: A Substrate for Fine Spatial Vision at Low Temporal Frequencies in Rabbit Retina. *J. Neurosci.* **26,** 13250–13263 (2006).

167. Jacobs, G. H., Williams, G. A. & Fenwick, J. A. Influence of cone pigment coexpression on spectral sensitivity and color vision in the mouse. *Vision Res.* **44,** 1615–1622 (2004).

168. Wagner, H., Macnichol, E. & Wolbarsht, M. The Response Properties of Single Ganglion Cells in the Goldfish Retina. *J. Gen. Physiol.* **43,** 45–62 (1960).

169. Werblin, F. S. & Dowling, J. E. Organization of the retina of the mudpuppy, Neturus maculosis. II. Intracellular recording. *J. Neurophysiol.* **32,** 339–355 (1969).

170. Wong, K. Y. A Retinal Ganglion Cell That Can Signal Irradiance Continuously for Ten Hours. *J. Neurosci.* **32,** 11478–11485 (2012).

171. Weng, S., Sun, W. & He, S. Identification of ON-OFF direction-selective ganglion cells in the mouse retina. *J. Physiol.* **562,** 915–923 (2005).

172. Sun, W., Li, N. & He, S. Large-scale morphological survey of mouse retinal ganglion cells. *J. Comp. Neurol.* **451,** 115–126 (2002).

173. Coombs, J., van der List, D., Wang, G.-Y. & Chalupa, L. M. Morphological properties of mouse retinal ganglion cells. *Neuroscience* **140,** 123–136 (2006).

174. Barres, B. A., Silverstein, B. E., Corey, D. P. & Chun, L. L. Immunological, morphological, and electrophysiological variation among retinal ganglion cells purified by

panning. *Neuron* **1,** 791–803 (1988).

175. Nelson, R., Famiglietti, E. V & Kolb, H. Intracellular staining reveals different levels of stratification for on- and off-center ganglion cells in cat retina. *J. Neurophysiol.* **41,** 472–483 (1978).

176. Balkema, G. W. & Pinto, L. H. Electrophysiology of retinal ganglion cells in the mouse: a study of a normally pigmented mouse and a congenic hypopigmentation mutant, pearl. *J. Neurophysiol.* **48,** 968–80 (1982).

177. Schmidt, T. M., Taniguchi, K. & Kofuji, P. Intrinsic and extrinsic light responses in melanopsin-expressing ganglion cells during mouse development. *J. Neurophysiol.* **100,** 371–384 (2008).

178. Pang, J.-J., Gao, F. & Wu, S. M. Light-evoked excitatory and inhibitory synaptic inputs to ON and OFF alpha ganglion cells in the mouse retina. *J. Neurosci.* **23,** 6063–6073 (2003).

179. Luo, J., Boosalis, B. J., Thoreson, W. B. & Margalit, E. A Comparison of Optical and Electrophysiological Methods for Recording Retinal Ganglion Cells during Electrical Stimulation. *Curr. Eye Res.* **37,** 218–227 (2012).

180. Pang, J. J., Gao, F. & Wu, S. M. Relative contributions of bipolar cell and amacrine cell inputs to light responses of ON, OFF and ON-OFF retinal ganglion cells. *Vision Res.* **42,** 19–27 (2002).

181. Fiscella, M. *et al.* Recording from defined populations of retinal ganglion cells using a high-density CMOS-integrated microelectrode array with real-time switchable electrode selection. *J. Neurosci. Methods* **211,** 103–113 (2012).

182. Jones, I. L. *et al.* A method for electrophysiological characterization of hamster retinal ganglion cells using a high-density CMOS microelectrode array. *Front. Neurosci.* **9,** 1–16 (2015).

183. Kiernan, J. Formaldehyde, formalin, paraformaldehyde and glutaraldehyde: what they are and what they do. *Micros. Today* **12,** 8–12 (2000).

184. Anderson, J. R. *et al.* Fabrication of topologically complex three-dimensional microfluidic systems in PDMS by rapid prototyping. *Anal. Chem.* **72,** 3158–3164 (2000).

185. Kartalov, E. P., Walker, C., Taylor, C. R., Anderson, W. F. & Scherer, A. Microfluidic vias enable nested bioarrays and autoregulatory devices in Newtonian fluids. *Proc. Natl. Acad. Sci. U. S. A.* **103,** 12280–4 (2006).

186. Luo, Y. & Zare, R. N. Perforated membrane method for fabricating three-dimensional polydimethylsiloxane microfluidic devices. *Lab Chip* **8,** 1688–1694 (2008).

187. Kang, J. H., Um, E. & Park, J.-K. Fabrication of a poly(dimethylsiloxane) membrane with well-defined through-holes for three-dimensional microfluidic networks. *J. Micromechanics Microengineering* **19,** 045027 (2009).

188. Childs, W. R. & Nuzzo, R. G. Decal Transfer Microlithography : A New Soft-Lithographic Patterning Method. 13583–13596 (2002).

189. Thangawng, A. L., Swartz, M. A., Glucksberg, M. R. & Ruoff, R. S. Bond-detach lithography: A method for micro/nanolithography by precision PDMS patterning. *Small* **3,** 132–138 (2007).

190. Mosadegh, B., Agarwal, M., Torisawa, Y. & Takayama, S. Simultaneous fabrication of PDMS through-holes for three-dimensional microfluidic applications. *Lab Chip* **10,** 1983–1986 (2010).

191. Jeon, N. L. *et al.* Design and Fabrication of Integrated Passive Valves and Pumps for Flexible Polymer 3-Dimensional Microfluidic Systems. *Biomed. Microdevices* 117–121 (2002).

192. Szeri, A. Z. *Fluid Film Lubrication*. (Cambridge University Press, 2010).

193. Andres, L. S. *Modern Lubrication Theory*. (2010).

194. Kosinski, L. E. & Caruthers, J. M. The effect of molecular weight on the rheological properties of poly(dimethylsiloxane) filled with fumed silica. *Rheol. Acta* **25,** 153–160 (1986).

195. The Mathworks, Inc. MATLAB and Statistics Toolbox Release R2015a.

196. Liu, H.-B. & Gong, H.-Q. Templateless prototyping of polydimethylsiloxane microfluidic structures using a pulsed CO2 laser. *J. Micromechanics Microengineering* **19,** 037002 (2009).

197. Li, M. *et al.* A simple and cost-effective method for fabrication of integrated electronic-microfluidic devices using a laser-patterned PDMS layer. *Microfluid. Nanofluidics* 751–760 (2012).